University of South Bohemia in České Budějovice

Faculty of Science

State trajectory approach to the interpretation of self-organization in the Belousov-Zhabotinsky reaction

Ph.D. Thesis

Anna Zhyrova, MSc

Supervisor: Prof. RNDr. Dalibor Štys, CSc.

University of South Bohemia in České Budějovice,

Faculty of Fisheries and Protection of Waters

České Budějovice 2017

This thesis should be cited as:

Zhyrova A., 2017: State trajectory approach for the interpretation of the self-organization in the Belousov-Zhabotinsky reaction. Ph.D. Thesis Series, No. 14. University of South Bohemia, Faculty of Science, České Budějovice, Czech Republic, 127 pp.

Annotation

The Belousov-Zhabotinsky reaction is a well-known model for investigating the self-organization manifestations in nature. The chemical reaction cascade is easy to control and measure in laboratory conditions, which makes the investigation of diverse scenarios of the system behavior possible. The aim of this thesis was to evaluate the course of the reaction under the assumption of multifractality of observed chemical patterns. The approach of the information entropy theory was applied to image analysis to assess the visible changes in the reaction oscillation. Furthermore, the new characteristics - point information gain entropy and point information gain entropy density - were also introduced. These values were used to construct the state trajectory of the complex system with unique oscillation states recognition by multivariate stochastic data analysis.

The reliability of the developed approach was tested on numerous experiments, including the insufficiently-studied BZ reaction wave formation under the space constriction and distortion by re-shaking effect. It has been confirmed that each of the system states has its own characteristic spectrum of information entropy. The obtained state-trajectories for the BZ reaction allows researchers to study the changing system behavior in response to variation of the initial conditions and to make a prediction about state-trajectory evolution in the imminent future. It was showed that the information entropy calculation is an effective and cheap tool for non-invasive analysis of a wide range of self-organized systems. Finally, it may be implemented also to automate laborious tasks for different cell stage recognition in medicine and biology.

Anotace

Reakce Bělousova-Žabotinskyho je dobře známý model pro zkoumání projevů samoorganizace v přírodě. Kaskádu chemické reakce je snadné ovládat a měřit v laboratorních podmínkách, což umožňuje zkoumání různých scénářů chování systému. Cílem této disertační práce bylo zhodnotit průběh reakce za předpokladu multifractality sledovaných chemických vzorců. Pro zhodnocení viditelných změn v průběhu oscilace BZ reakce během analýzy obrazu byly použity přístupy teorie informační entropie a byly zavedeny nové charakteristiky: informační příspěvek jednoho bodu a entropie informačního příspěvku. Konečným výsledkem navrhovaného přístupu je vytvoření trajektorie stavů komplexního systému s unikátním zaznamenáním oscilačních stavů, které bylo dosaženo pomocí multivariační stochastické analýzy dat.

Spolehlivost vyvinutého algoritmu byla testována prostřednictvím rozmanitých experimentů včetně nedostatečně prozkoumané tvorby vln v BZ reakci v rámci prostorové konstrikce a narušení efektem opětovného otřesu. Byla potvrzená hypotéza, že každý ze stavů systému má své charakteristické spektrum informační entropie. Získané trajektorie stavů BZ reakce umožňují posuzovat měnící se chování systému v návaznosti na změnu počátečních podmínek a předpovídat o evoluci trajektorií stavů v blízké budoucnosti. Bylo prokázáno, že výpočet informační entropie jé účinný a levný nástroj pro neinvazivní analýzu širokého spektra samoorganizovaných systémů a může být použitý pro automatizaci laboratorních analýz například při identifikaci různých buněčných stavů v medicíně a biologii.

Declaration [in Czech]

Prohlašuji, že svoji disertační práci jsem vypracoval samostatně pouze s použitím pramenů a literatury uvedených v seznamu citované literatury.

Prohlašuji, že v souladu s § 47b zákona č. 111/1998 Sb. v platném znění souhlasím se zveřejněním své disertační práce, a to v úpravě vzniklé vypuštěním vyznačených částí archivovaných Přírodovědeckou fakultou elektronickou cestou ve veřejně přístupné části databáze STAG provozované Jihočeskou univerzitou v Českých Budějovicích na jejích internetových stránkách, a to se zachováním mého autorského práva k odevzdanému textu této kvalifikační práce. Souhlasím dále s tím, aby toutéž elektronickou cestou byly v souladu s uvedeným ustanovením zákona č. 111/1998 Sb. zveřejněny posudky školitele a oponentů práce i záznam o průběhu a výsledku obhajoby kvalifikační práce. Rovněž souhlasím s porovnáním textu mé kvalifikační práce s databází kvalifikačních prací Theses.cz provozovanou Národním registrem vysokoškolských kvalifikačních prací a systémem na odhalování plagiátů.

České Budějovice, 1.09.2017 ……..

Anna Zhyrova

This thesis originated at the Faculty of Science, University of South Bohemia, supporting doctoral studies in the Biophysics study program.

Financial Support

The research presented in this thesis was supported by the Ministry of Education, Youth and Sports of Czech Republic - projects CENAKVA (No. CZ.1.05/2.1.00/01.0024) and CENAKVA II (No. LO1205 under the NPU I program), GAJU (134/2013/Z) and the EEA and Norway grants (No. NF-CZ07-INS-3-028-2014).

List of Papers and Author's Contribution

I. **Zhyrova, A**., Štys, D., Císař, P., 2013. Information entropy approach as a method of analysing Belousov-Zhabotinsky reaction wave formation, *Chemicke Listy,* 107 (Suppl. 3): S341-S342. (Print). (IF 2013 = 0.196; SJR 2013 = 0.201).
Anna Zhyrova participated in Belousov-Zhabotinsky experiments and data analysis. She also wrote the manuscript and was responsible for revision of the manuscript.

II. **Zhyrova, A.**, Štys, D., 2014. Construction of the phenomenological model of Belousov-Zhabotinsky reaction state trajectory. *International Journal of Computer Mathematics*, 91 (1): 4–13. doi: 10.1080/00207160.2013.766332. (Print). (IF 2014 = 0.824; SJR 2014 = 0.453).
Anna Zhyrova made all experiments, measurements, image analysis and entropy calculation of images. She also made the graphs and cluster analysis of the entropy data, wrote the manuscript and was responsible for revision of the manuscript.

III. **Zhyrova, A.**, Rychtáriková, R., Náhlík, T., 2016. Effect of Spatial Constrain on the Self-Organizing Behavior of the Belousov-Zhabotinsky Reaction*, IWBBIO 2016: Proceedings Extended Abstracts on Bioinformatics and Biomedical Engineering*, pp. 246-258, ISBN: 978-84-16478-75-0 (Print). (no IF; no SJR).
Anna Zhyrova performed the measurements, entropy calculation of Belousov-Zhabotinsky reaction images, made the graphs and was responsible for revision of the manuscript.

IV. **Zhyrova A.**, Rychtáriková R., Štys D., 2017. Recognition of Stages in the Belousov-Zhabotinsky Reaction Using Information Entropy. *IWBBIO 2017, Proceedings, Part I, Lecture Notes in Computer Science*, 10208, Springer, Switzerland, 2017, pp. 335–346, ISBN: 978-3-319-56147-9 (Print). (no IF; SJR 2016 = 0.315).
Anna Zhyrova participated in measurements, image analysis, writing and revising of the manuscript.

Dedicated to my parents

ACKNOWLEDGEMENTS

Firstly, I would like to thank my scientific advisor Prof. RNDr. Dalibor Štys, CSc. who taught me not to be afraid of challenged scientific projects and inspired me through all these years.

I greatly appreciate Ing. Bc. Renata Štysová Rychtáriková, Ph.D. for bringing many outstanding ideas to my diploma project and helping with the analysis of the data. I would like to express my gratitude to whole our programming team (Ing. Petr Císař, Ph.D.; Ing. Jan Urban Ph.D.; Ing. Petr Macháček) for developing the Information Entropy Calculation package. I am sincerely grateful my senior colleagues Aliaksandr Pautsina and Tomáš Náhlík for shearing their knowledge with me and patiently supported through whole my study.

I would like to express special thanks to my scientific consultant Prof. Harald Martens who discovered for me the world of multivariate analysis. I appreciate as well all our Norwegian collaborators (Prof. Bjørn Kåre Alsberg and Prof. Lise Lyngsnes Randeberg) for providing me a great opportunity to work in Norwegian University of Science and Technology and help me during the project realization.
I want to thank all my friends and colleagues from Nové Hrady, České Budějovice and Trondheim Tatsyana Holubeva, Vitali Bialevich, Katsiaryna Shamaeva, Hanna Huryna, Karina Romanova, Valentina Kuznetsova, Gürkan Keşan, Daria Malakhova, Dmytro Soloviov, Julia Ermak and Savis Gohari with whom I have experienced many unforgettable moments.

I am also thankful to all the technical and administrative stuff of the Institute of Complex Systems and the chateau in Nové Hrady for making my life and studies pleasant and productive. Especially, I would like to acknowledge our technician Vladimír Kotal who offered not only high-quality technical assistance in the implementation of the project, but also his friendship with a lot of joint adventures.

Finally, I thank my parents, my father Zhyrov Pavel Alekseevich, my mother Zhyrova Tatyana Fedorovna who believed in me and supported till their last breath and my brother Pavel whose delicate care for them has allowed me to continue my PhD study. I also grateful my husband Martin Klíma and his family that supported me in my intention to graduate.

Motto

Our best inventions arise not as a result of a majestic flight to the shining peaks of thought, but as a result of a slow myopic search of endless variants

(Original: Наши лучшие изобретения возникают не в результате величественного полета к сияющим вершинам мысли, а в результате медленного близорукого поиска бесконечных вариантов)

(Carl Zimmer, "Microcosm: E. Coli and the New Science of Life")

TABLE OF CONTENTS

LIST OF ABBREVIATIONS AND NOTATIONS

BZ	Belousov-Zhabotinsky (reaction)
$Fe(phen)_3^{2+}$	reduced form of redox indicator ferrion (formula $C_{36}H_{24}FeN_6^{2+}$)
$Fe(phen)_3^{3+}$	oxidized form of redox indicator ferroin
FKN	the complex chemical mechanism of the B-Z reaction suggested by Field, Korös and Noyes in 1974
ODE	ordinary differential equation
CA	cellular automata model
PIG	the point information gain
PIE	the point information gain entropy
PIED	the point information gain entropy density

INTRODUCTION

1.1. History of the Belousov-Zhabotinsky Reaction

The recipe of the Belousov-Zhabotinsky (BZ) reaction was discovered by chance, when Russian chemist Boris Belousov, in attempt to devise a primitive model of citric acid cycle, employed cerium ions instead of an enzyme as a catalyst (*Belousov, 1959*) and found that his test tube contained a biochemical oscillator. The discovered chemical oscillator has some of the fundamental features of the metabolism of aerobic organisms (*Shanks, 2001*). That makes the Belousov-Zhabotinsky oscillations and accompanying self-organisation (*Taylor, Tinsley, 2009*) a very interesting phenomenon for investigating principles of self-organisation in nature. Belousov's work has not received proper recognition in the scientific community because the reversibility of the chemical process contradicted the postulates of the second law of thermodynamics.

A few years after the first discovery, Russian postgraduate student biophysicist Anatol Zhabotinsky not only rediscovered the phenomenon but also suggested the first interpretation of its reaction dynamics (*Zhabotinsky, 1964*). Zhabotinsky improved the components involved in the reaction by using ferroin $C_{36}H_{24}FeN_6^{2+}$, a blood-red complex of Fe^{2+} ion with 1,10-phenanthroline that catalyzes the reaction, instead of cerium Ce^{4+} to enhance contrast during chemical oscillation. He was the first person to observe the reaction dynamics in a thin layer of solution in a Petri dish where the chemical waves produced were organized in a pattern with an impressive variety of shapes and sizes. He also made the first system description which did not contradict the second law of thermodynamics and charted a mathematical model of the chemical reaction dynamics (*Rovinsky et al., 1984*). Due to the foundation-laying work of these two scientists, the reaction was named after them as the Belousov-Zhabotinsky reaction and was introduced to the world's scientists at the "Conference on Biological and Biochemical Oscillators" in Prague (*Vavilin, 1968*).

Basic principles of non-equilibrium thermodynamics were honored with the Nobel Prize in 1977 (*Nicolis and Prigogine, 1977*) and the BZ reaction was the cornerstone of this theory.

1.2. The Main Features of the Chemical Waves

The result of performing the BZ reaction in a thin layer of reaction mixture in a Petri dish is the formation of two-dimensional space structures of the ferric/ferrous concentration gradient that migrate and evolve over time. These are the so-called chemical waves or BZ patterns, first described in the work by *Zaikin et al., 1970*. Up to now, it is not known what serves as the initiation points of the waves. According to some researchers (*Amemiya et al., 1996; Taylor et al., 1996*), the circular and spiral-like waves could arise from local excitability perturbation (by an increase in the excitability of the medium in the foci region). The chemical waves phenomenon represents itself not only through the concentration changes of $Fe(phen)_3^{3+}$ and related reaction components (malonic acid, bromomalonic acid, and BrO_3^-), but also through density changes (*Kasuya et al., 2005*) and a temperature gradient (*Böckmann et al., 1996*). There are several types of waves (*Cross et al., 1983*), generated by the BZ system.

1.2.1. The Travelling Waves' Properties

There are the following types of travelling waves: wave trains (the wave profile V (ξ) is periodic); wave fronts (V (−∞) and V (∞) exist and are unequal); pulses (V (−∞) and V (∞) exist, are equal, but V (ξ) is not constant); radially symmetric wave or circular waves; and their combinations (*Kuttler, 2011*). The wave trains in the initial reaction phase tend to keep an equal distance from each other and produce circles. Mikhailov et al., *(2006*) claims that the wave propagates according to Huygens's principle, where each point on a wave front became a source of wavelets, and wavelets spread out in the forward direction at the same speed as the source wave, forming a new wave front in a tangent line to all of the wavelets. This opinion is clearly challenged by the experiments (Fig. 1.1.), where we show that the chemical waves do not cross each other as Huygens-type waves, e.g., those observed upon throwing two stones into the water. The variability of the wave velocity, mainly acceleration of the wave trains registered in *Pojman et al., 1990*, was explained by the convection effect (*Wu et al., 1995*), whereas the wave front's diversity, namely the existence of big waves compared to the normal trigger wave, is attributed to an unequal concentration distribution of ferriin caused by the Marangoni effect (*Inomoto et al., 2012*) – the flow between two fluids' interface is

caused by the surface tension gradient, but the authors do not rule out the influence of the temperature effect.

1.2.2. The Spiral Waves' Properties

The spiral waves (so-called Archimedean spirals), according to work in *Agladze et al., 1982*, could be generated as open wave ends that evolve from a breaking-down continuous wave front, or, according to *Tóth et al., 2000,* from the refractory tail of another wave. The breaking of wave fronts was often shown to be induced by microbubbles evolving in the reaction solution. The Winfree turbulence *(Winfree 1994a,b)* also credited for the appearance and further development of spiral waves in the BZ reaction medium (*Alonso et al., 2003*). The spiral tips, as it was shown in theoretical and experimental studies (*Skinner et al., 1991; Jahnke, 1989*), have different types of motion: from rigid around a small circular core to compound rotation along epicycle-like patterns. This drift could be caused by inhomogeneity of the reaction medium (*Pertsov et al., 1988*) or wave interaction with a boundary (*Ermakova et al., 1986*). For example, an interesting effect of the spiral lateral drift along a straight line in conditions where the forcing frequency is equal to the spiral frequency was observed by *Agladze et al., 1987*. Also, single and double so-called "ram's horns" spirals, which exhibit different dynamics drift, were identified during the reaction (*Rovinskii, 1986; Steinbock et al., 1993; Jensen et al., 2002*). In addition, there were reported feedback phenomena found in the BZ system, which automatically correct unstable waves (waves with free ends) by changing the particular size and shape of the unstable wave segment (*Mihaliuk et al., 2002*). When waves collide with the boundaries of the container or with other waves, they vanish upon annihilation.

The final step of the damping non-stirred BZ reaction is the transition from space-arranged spiral waves to the chaos (random orientation of the reaction surface wave front's fragments mixed with spiral waves and blank spaces), which develop from the propagating waves interaction with stationary dissipative structures (presumably the bubbles generated during the organic substrate consumption) (*Agladze et al., 1984*).

I was able to reproduce many of the waves, including the spiral types of waves (Fig. 1.1a) but their identification with structures described in the literature is often complicated by the lack of original data for comparison. Typically there are observed circular waves (target patterns) of three frequencies: dense irregular waves which, by formation of "ram's horns", break into a system of dense waves and spirals. These patterns are observed in gently-mixed circular vessels (i.e. a Petri dish mixed by hand or by the orbital mixer). In experiments with vigorous mixing (magnetic mixer) the system collapsed into dense waves much faster, and additional patterns were observed in square vessels (Fig, 1.1 b).

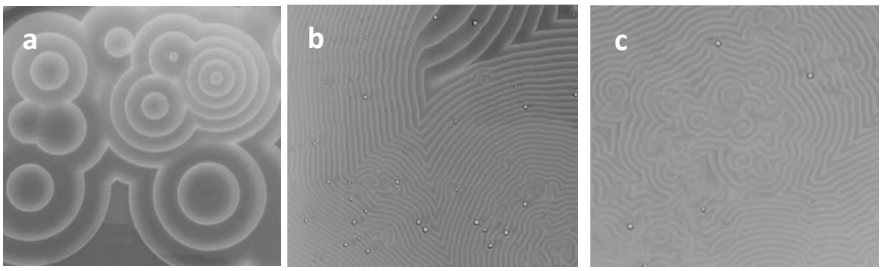

Figure 1.1. The time-lapse shots (at the 75 sec, 8575 sec and 19525 sec after the start of the reaction) of the chemical wave's evolution during the Belousov-Zhabotinsky reaction in a thin layer (1.3 mm) of liquid: (a) circular waves, (b) wave trains' interaction, (c) spiral waves. The surface area is 40x40 mm.

The constant build-up of these varying and often conflicting hypotheses indicates that the existence of spatial segregation driven by the chemical reaction remains an unresolved problem.

1.2.3. Chemical Waves' Parameters Estimations

Visualization of the BZ reaction is based on the optical property of the redox indicator ferroin whose absorption maxima in the reduced state $Fe(phen)_3^{2+}$ is 510 nm, and is 630 nm in the oxidized state $Fe(phen)_3^{3+}$ (*Kinoshita, 2013*). This makes the chemical waves available for visual perception, recording by common RGB photo cameras, and analysis by commonly available image processing approaches. In other words, it is generally believed (1) that the color change by which the progress of the BZ reaction is monitored is solely the reflection of the redox potential,

which is instantly reflected in the change of the redox state of the $Fe(phen)_3^{2+/3+}$ in that particular region of the Petri dish and (2) that there is no other significant light-absorbing compound (and perhaps (3) that there is a constant concentration of $Fe(phen)_3^{2+/3+}$).

In our experiments, the speed of the wave fronts was estimated by measuring the shift of the intensity profile curve from blue color channel for two subsequent frames using the MATLAB image tool box (*The MathWork Inc., 2014*). Even one frame of the BZ reaction scene presents a combination of a variety of wave fronts spreading with different velocities (see Fig. 1.2.). As it may be seen---although in most cases the increase in the absorbance recorded in the red camera channel was accompanied by the decrease in the blue camera channel---there were cases of asynchronicity. This indicates that even the most basic assumption on which the observation of the course of the BZ reaction is based should be re-examined. Indeed a prime candidate for the additional light-absorbing compound is molecular bromine, which is present in all reaction schemes and has a strong absorption in the far red region of the spectrum.

It should also be mentioned that (1) the $Fe(phen)_3^{2+/3+}$ is itself part of the complicated redox process, it is part of many chemical reactions (as described in chapter 1.3) which cause changes in the redox state and thus $Fe(phen)_3^{2+/3+}$ does not necessarily "per se" have to be in a redox equilibrium with the environment in all places in the reaction vessel and (2) the true end of the redox process is observed after a long period of time and results in precipitation of Fe_2O_3 or some of its hydrated forms. Thus neither of the assumptions about the chemical basis of the observation of the BZ process may be taken for granted.

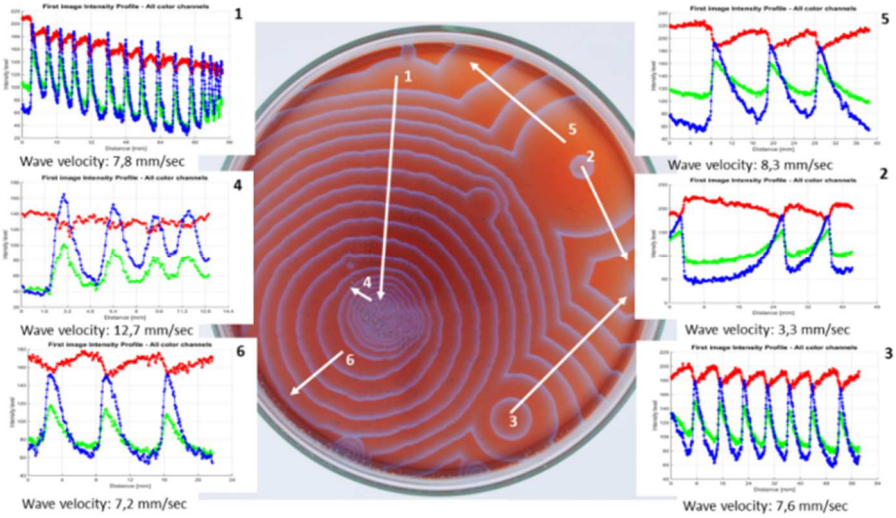

Figure 1.2. BZ wave fronts intensity profiles, calculated from red, green and blue color channels (the profile colors correspond the colors of the RGB channels), and taken from the image place marked by the vector with consecutive number. The estimates for wave velocities are given below under the profile scheme.

1.3. Chemical Mechanism

A detailed BZ reaction chemical description was proposed by Field and coworkers (*Field et al. 1972*). This kinetic model is known as FKN mechanism and contains 80 elementary reactions and 26 concentration variables which provide quite a precise explanation of the chemical transformations of the reactants. The 16% of reaction chains accounts for the inorganic part, i.e., the interaction between bromate $HBrO_3^-$ and bromide Br^-. The remaining 84% of the reaction chain includes the organic substances, mainly malonic acid $C_3H_4O_4$ and its derivatives. The majority of the organic reactions chain consists of reactions with the participation of radicals and the products of radical reactions: malonil radical, peroxymalonil radical, oxymalonil radical, tartronic acid, oxalic acid and mesoxalic acid (*Hegedús et al., 2001*). In the core of the reaction process is a reduction-oxidation loop branching into a tree-like scheme process. Process A consists of bromate BrO_3^- reduction to bromine *Br* by the reducing agent bromide Br^- in the presence of a ferroin $Fe(phen)_3^{2+}$ catalyst and results in production of bromomalonic

acid $BrCH(COOH)_2$ and hypobromous acid $HBrO_2$, which is included in process B (model adopted by *Zhabotinsky and colleagues, 1984*):

$H^+ + Br^- + HBrO_2 \leftrightarrow 2HOBr$ ($k_1 = 10^6\ M^{-2}s^{-1}$)

$H^+ + Br^- + HOBr \leftrightarrow Br_2 + H_2O$ ($k_2 = 8^x10^6\ M^{-2}s^{-1}$)

$H^+ + Br^- + HBrO_3 \leftrightarrow HBrO_2 + HOBr$ ($k_3 = 2\ M^{-3}s^{-1}$)

In process B, the hypobromous acid begins to compete with the bromide Br^- to reduce the bromate BrO_3^-. $Fe(phen)_3^{3+}$ is produced in this autocatalytic sequence. The solution color changes from red to blue:

$H^+ + HBrO_3 + HBrO_2 \leftrightarrow HBrO_2^+ + BrO_2^{\cdot} + H_2O$ ($k_4 = 10\ M^{-2}s^{-1}$)

$BrO_2^{\cdot} + H^+ \leftrightarrow HBrO_2^+$ ($k_5 = 2\ ^x10^{-5}\ M^{-2}s^{-1}$)

$Fe(phen)_3^{2+} + HBrO_2^+ \leftrightarrow Fe(phen)_3^{3+} + HBrO_2$ ($k_6 = 6^x10^5\ M^{-2}s^{-1}$)

$2HBrO_2 \leftrightarrow HBrO + HBrO_3$ ($k_7 = 10\ M^{-2}s^{-1}$)

The organic reactionsin process C consist of concurrent oxidation of bromomalonic acid and other organic species, in which the $Fe(phen)_3^{3+}$ reduces to the $Fe(phen)_3^{2+}$, restoring the original red color to the BZ solution. Bromide Br^- that is released during the process pushes the system to a reduction loop after reaching some critical level and the entire reaction sequence repeats itself again until the main reaction components, mainly bromine and malonic acid, will not be consumed by the oscillating system:

$Fe(phen)_3^{3+} + CHBr(COOH)_2 + HBrO \leftrightarrow$

$Fe(phen)_3^{2+} + H^+ + {}^{\cdot}CBr(COOH)_2$ ($k_8 = 2\ M^{-2}s^{-1}$; $k_{-8} = 2^x10^6 M^{-2}s^{-1}$)

${}^{\cdot}CBr(COOH)_2 + H_2O + HBrO \leftrightarrow$

$H^+ + Br^- + {}^{\cdot}COH(COOH)_2$ ($k_9 = 2^x10^3\ M^{-2}s^{-1}$)

$HOBr + CHBr(COOH)_2 \leftrightarrow$

$CBr_2(COOH)_2 + H_2O$ ($k_{10} = 7.5^x10^{-3}\ M^{-2}s^{-1}$)

$Br_2 + CHBr(COOH)_2 \leftrightarrow$

$CBr_2(COOH)_2 + H^+ + Br^-$ $(k_{11} = 10^{-2}\ M^{-2}s^{-1})$

According to prevalent opinion, the oscillation process in the BZ reaction is guided by the chemistry of bromine oxoacids $HBrO_x$. A more detailed study in *Glaser et al., 2012* shows that the rate-limiting effect could be caused by a bromous acid disproportionation reaction: $2HOBrO \rightleftarrows HOBr + HBrO_3$ with the generation of $(HOBr)(HOBr_2)$, which aggregates as the products of disproportionation. In support of this theory also is the fact that hypobromous acid and bromous acid are not dissociated at pH values typical for the reaction (*Glaser et al., 2013*). The reaction cascade resulting in $Fe(phen)_3^{3+}$ reduction occurs at a much slower rate than the inverse to it---$Fe(phen)_3^{2+}$ oxidation process---since that $Fe(phen)_3^{3+}$ complex is unstable itself (*Jamal et al., 2008*), breaking into $Fe(phen)_3^{2+}$ and colorless intermediate derivatives $[Fe(II)(phen)_2(L')]^{n+}$ that could conjugate with Br^- to form the BZ reaction products. So far the final product of the reaction is not clear. Previously, *Hegedüs et al., 2006* claimed that the main organic oxidation product of bromomalonic acid is bromo-ethene-tricarboxylic acid, but the authors were not able to find any oxidation product of malonic acid in the ferriin-malonic acid and stood on the opinion that Fe^{3+} oxidizes mostly by its phenantroline ligand. In the Ce^{4+}-catalyzed BZ reaction, the following products of the Ce^{4+}-malonic acid reaction were found: ethane-tetracarboxylic acid, malonyl malonate, and CO_2 (*Gao et al., 1994*). The schematic view of the BZ reaction cascade is presented in Figure 1.3.

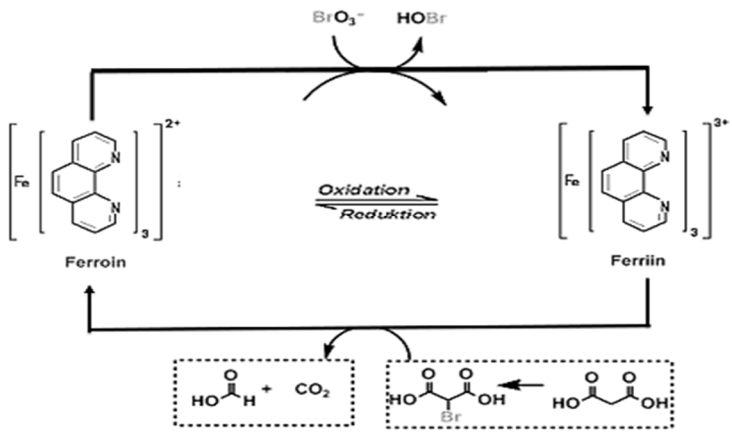

Figure 1.3. The schematic draw of the ferroine-type Belousov-Zhabotinsky reaction oxidation-reduction loop (adopted from *Hiro, 2009*).

The existence of different waves and sometimes counteracting velocities discussed in 1.3. is an experimental indication of a rather complicated reaction scheme. The observable color changes of the redox state of the $Fe(phen)_3^{2+}$/ $Fe(phen)_3^{3+}$ complex (chapter 1.2) may not be a response to the overall redox potential since the redox indicator is involved in a few processes which may not be in instant equilibrium with the surroundings. If this were true, we lack a good measure of the local state in the reaction vessel. The only study which considers the elementary bottleneck reaction is based exactly on the assumption that the change of bromine redox state and not that of the $Fe(phen)_3^{2+}$/ $Fe(phen)_3^{3+}$ complex is the rate limiting process (*Glaser et al., 2012, Glaser et al., 2013*). In this case, the spectrum of the $Fe(phen)_3^{2+}$/ $Fe(phen)_3^{3+}$ complex would be a good measure of the local redox state.

The only effect which is included in the real reaction's course beyond any doubt is the oxidative breakage of brominated malonic acid, which gives rise to carbon dioxide. The evolution of CO_2 is sparsely discussed in articles that focus on the reaction mechanisms. This energy-driving mechanism likely requires the existence of certain redox conditions (i.e. potential) but details of the mechanism at the level of chemical bond re-structuring are not known. In addition, it is known that it is possible to

re-start the wave formation by re-shaking the reaction vessel (Cohen 2011). This is evidence that the formation of chemical waves is not directly related to the course of the depletion of chemicals.

1.4. Models of the BZ Reaction

1.4.1. The Reaction-Diffusion Model: Concepts and Existing Mathematical Models of the BZ Reaction

The reaction schemes presented in Fig. 1.3. do not directly explain why there are oscillations, spatial dynamics and/or segregation, and other observed phenomena. In order to solve this issue, the current reaction scheme has been modified. The new model is called Oregonator (*Gyorgyi et. al. 1990),* which is the first known oscillatory chemical dynamics model of BZ. This network (Fig. 1.4) is obtained by reduction of the complex chemical mechanism of the BZ reaction to a few processes and consideration of the rate-determining-step of a reaction unit (*Espenson, 1995*). Another variant of such BZ system model are Brusselator (*Prigogine et al., 1968*) and three-variable Györgyi-Field (*Györgyi et al., 1992*) models with characteristic oscillating BZ reaction chaotic behavior. The negative feedback BZ reaction loop involving a fast reaction between malonyl and bromine dioxide radicals was described by *Försterling et al., 1990* in the Radicalator model. The Marburg-Budapest-Missoula (MBM) model, a compromising model that combines both bromous acid-bromide ion and bromine dioxide-organic free radicals BZ reaction feedback with some additions and also considers the newly discovered radical-radical recombination reactions, was proposed by *Hegedus et al.* in 2001.

The work of these scientists is based on a reaction-diffusion theory (*Fisher, 1937; Kolmogorov et. al., 1937; Grindord, 1996*) - the most popular explanation of the phenomenon of chemical oscillations in the BZ reaction up to the present day.

The assumptions of the reaction-diffusion theory are:

- the reaction–diffusion system approximates the observed phenomenon by the mathematical model which exhibits the

same properties as the studied physical phenomena in continuous space;

- spatial elements – cells -- are dealt with indirectly through their vector function *q(x, t)*;
- the final model describes the local chemical reactions in which the substances are transformed into each other; and
- the chemical reaction occurs instantly in comparison to the diffusive events.

Changes in concentrations of the components of the system during its evolution may be expressed in general form by the partial differential equation:

$$\partial_t q(x,t) = D\nabla^2 q(x,t) + R(q(x,t)) \qquad (1)$$

where *q(x, t)* represents the unknown vector function (corresponding to a concentration variable in our case), *D* is a diagonal matrix of diffusion coefficients, and *R* accounts for all local reactions. In the case of the BZ reaction (activator-inhibitor system class), we are dealing with a two-component system and according to *Rovinsky et al., 1984*, the ODE equation for BZ system has the following final form:

$$\varepsilon \frac{dx}{d\tau} = x(1-x) - 2q\alpha \frac{z}{1-z} \frac{x-\mu}{x+\mu} = g(x,z) \qquad (2)$$

$$\frac{dz}{d\tau} = x - \alpha \frac{z}{1-z} = h(x,z) \qquad (3)$$

where $x = \frac{2k_4[HBrO_2]}{k_1[HBrO_3]}$;

$z = \frac{[Fe(phen)_3^{3+}]}{[Fe(phen)_3^{2+}] + [Fe(phen)_3^{3+}]}$;

$\varepsilon = \frac{k_1[HBrO_3]}{k_4[Fe(phen)_3^{2+}] + [Fe(phen)_3^{3+}]}$; $\alpha = \frac{k_4 k_8 k_9 [CHBr(COOH)_2]}{k_{-8} {k_1}^2 [HBrO_3]^2 {h_0}^2}$;

$\mu = \frac{2k_4k_7}{k_1k_5}$; $\tau = \frac{{k_1}^2[HBrO_3]^2{h_0}^2}{k_4[Fe(phen)_3^{2+}]}t$;

h_0 is the acidity function (*Igh, = - Ho*); q is the stoichiometric factor. $k_{1\text{-}7}$ are rate constants determined in 1.4. *x, z,* ε, μ, α, and τ are variables which are introduced to simplify the form of the final equation and indicate the nature of the dependence of the corresponding components of the reaction among themselves. Indeed, each of the reaction schemes leads to a different set of differential equations.

Solution of such a system of ordinary first order differential equations (ODEs) can be shown as the 3-dimensional attractor (see subfigure (b) in Fig. 1.4.), the vertical intersection of which represents a Poincare plane: a limited cycle that reproduces the periodic behavior of the oscillating reaction (subfigure (a) in Fig. 1.4.). The BZ reaction contains various nonlinear dynamic behaviors such as period-1, period-2, quasi-periodic oscillations, chaotic attractor, and period-doubling bifurcation. It is well known that if chaotic behavior should occur in continuous systems (i.e. ODE), the dimensions of the system must be 3 or higher (*Györgyi et al., 1992*). With the application of an external periodic force, the BZ system could switch its behavior from periodic to chaotic and vice versa as a bifurcation switch (*Petrov et al., 1993; Zhang et al., 1993*). According to the hypothesis presented in *Li et al., 2003*, the transition observed as oscillations is caused by resonance between the main frequency of the chaos and the frequency of the external periodic perturbations. In this way, just a very narrow range of the perturbation frequencies (mainly those that caused the resonance effect) are appropriate to force the reaction oscillation to change its regime. The periodic perturbation in this case has the double-face structure: i.e., the transitions from periodicity to chaos in the periodic window and the transitions from chaos to periodicity in the chaotic window.

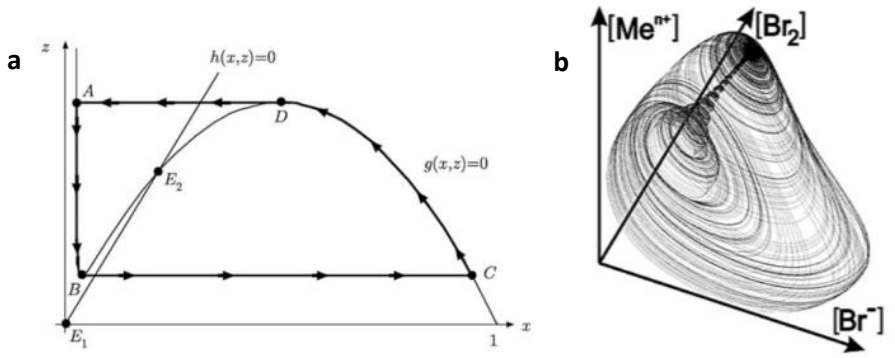

Figure 1.4. The BZ system limit-cycle with periodic behavior as an Oregonator-type system solution and strange attractor in 3-dimensional concentration coordinates as a BZ process phase. (a) The BZ reaction $x - z$ phase plane with nullclines $g(x,z) = 0$ and $h(x,z) = 0$, the reaction curse vector and critical points that system pass depended on parameters h_0 and q (for more details see *Gray, 2002)*; (b) a three-dimensional phase portrait of fractal tore, represented the manifold of concentration distributions during BZ reaction process (according to *Ryzhkov, 2000*).

With the addition of the second component, the system acquires new properties: a state that is stable can become unstable in the presence of diffusion (*Turing, 1952*). When such a system undergoes a change of parameters (so-called bifurcation), one may pass from conditions under which a homogeneous ground state is stable to conditions under which it is linearly unstable. The corresponding bifurcation may be a Hopf bifurcation (a qualitative change in the phase portrait that occurs as the real parts of eigenvalues of the Jacobian matrix for the system (evaluated at a fixed point) change from negative to positive) whose parameters depend on the stirring rate. This bifurcation type, according to authors in *Gang, 2000* and *Kalishyn et al., 2010*, is prevalent in the oscillation process in the BZ reaction. The alternative proposal is a Turing bifurcation, for which the diffusion coefficients of both components of the system must be very different to each other, which results in a globally patterned state which is not observed in the BZ reaction. The majority of spatial structures in BZ reaction patterns (fronts, spirals, targets, etc.) can be obtained as particular solutions for types of reaction-diffusion systems in spite of large variety of border conditions and input arguments (for more details see *Gray et. al., 1994*; *Taylor, et. al., 1999*; *Alonso et. al., 2006*). But no theory predicts the sequence of patterns observed in the experiment.

1.4.2. Disadvantages of the Reaction-Diffusion Theory

The reaction-diffusion theory describes the cause of the oscillations in the system and some of the factors influencing the oscillation parameters well, explaining the presence of migrating chemical waves in the environment. It does not give explanations for the spatial variation in wave patterns produced by the changing chemical process. Moreover, the stoichiometric relations between ferric reduction and Br^- production that had been obtained in continuous-time simulation of FKN model (*Fields et al. 1974)* were not confirmed by direct discrete-time experimental measurements and thus the FKN model was strongly criticized because such simple model could not account for the complexity of real systems (*Tyson, 1984*). The FKN scheme could not be applied to the ferroine-catalyst BZ reaction category because, unlike cerium, the phase of ferroin oxidation is very fast while the phase of ferriin reduction is rather slow (*Rovinsky et al., 1984*). In addition, ODEs based on Oregonator models are not chaotic, and are valid only for certain values of a variable's parameters (*Connolly et al., 2011*).

Description based on the reaction-diffusion theory obviously needs many very specific conditions to be valid. Any of its postulates still are not able to create a robust explanation of observed waves' diversity effect. We (*Stys et al., 2016a*) suggested that if the spatial segregation and state quantisation is included, the specific model does not have to be sought or – in another words – the freedom of choice of available chemical models is much higher.

First the assumption that the reaction occurs "instantly" in comparison to the diffusion-based events should be discussed. This certainly is not the case in all chemical reactions, namely in organic chemistry. Consideration of several reactants which have to be involved in the process leading to the evolution of carbon dioxide invokes a need for an extensive local re-structuration upon the critical bond breakage and active complex restoration. To this local process the assumption of "instant-to-be chemical reaction" or a lengthy "general" diffusive process cannot be applied. This somewhat-detailed analysis clearly questions the foundation of the reaction-diffusion theory.

We suggest a version of a Bénard-Marangoni type of spatial segregation as discussed in section 1.2.1., which challenges the fundamental

component of the reaction-diffusion theory, the spatial continuum. The principles of quantum mechanics assume the existence of discrete excitation states of the chemical bond and the maximal energy needed for the bond breakage neglects the state continuity assumption of the reaction-diffusion approach. Finally, any numerical calculation of the ODE system is implemented in the computer and is thus performed always in a discrete way. Therefore, if there is a strict qualitative difference between the discrete and continuous model, the validity of all computer simulations should be re-examined.

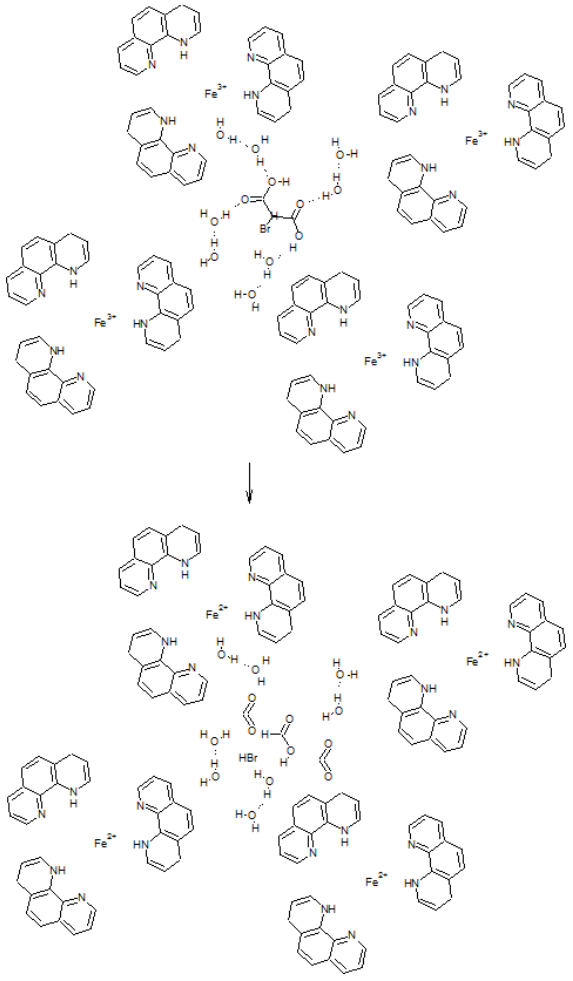

Figure. 1.5. A handful of individual molecules involved in the process which leads to the carbon dioxide evolution, a key observable process in the BZ reaction.

1.4.3. The Cellular Automata Model of the BZ Reaction

In discrete systems, complex spatial phenomena including chaotic behavior may be observed already in a one dimensional case (*Poincare 1901, Bendixson 1901,* in essence *Schröder, 1870* who first examined the logistic equation*)*. As an alternative to the existing FKN model of the BZ reaction, but aimed primarily at understanding the causes of spatial patterns orientation within the BZ reaction, the cellular automata (CA) model was designed (*Dewndey 1988*). In contrast to the reaction-diffusion theory, it does not aim to explain particular chemical reactions but focuses on explaining observed spatial phenomena.

The cell space or lattice that comprises the CA model is defined as:

$$L = \{(i,j)|i,j \in N: 0 \leq i < n, 0 \leq j < m\} \quad (4)$$

where *i, j* is the number of columns and rows, and, correspondently, *n,m* is the maximal amount of columns and rows.

Each subsequent cell state at time *t* ($a_{n,t}$) is determined from the previous one:

$$a_{n,t=m+1} = f(a_{n,t=m}, a \in N_{t=m}) \quad (5)$$

where N_t are neighborhoods of the considered cell.

In the simplest version, each cell has two possible values, 0 or 1, and evolves according to deterministic or stochastic rules that depend only on the values of the cell itself and of its nearest neighbors (*Wolfram, 1983*). The behavior of each cell in response to changing external conditions makes a complete picture of the behavior of the automata and expresses the model's response in its effort to adapt to the outside environment. The theory of two state cellular automata is still under development; the theoretical foundation of multilevel cellular automata, i.e., when the cell may achieve many states (i.e. *Wuensche, 2011*), is a matter of extensive research of many research groups.

By applying different transitions rules and initial/boundary conditions, multilevel CA could be developed into the complex system with unique

evolution trajectory into discrete space (*Vanag, 1999*). Any reaction-diffusion system may be modelled by a multilevel cellular automaton.

The BZ-like CA type of model is called an excitable system and is characterized by a steady increase of the cell state level and dropping of the cell state level to zero when the maximal level is reached (*Zhao et al., 2005*). The dynamics of individual elements in such media are not chaotic and spatiotemporal chaos can develop only as a result of interactions between the elements. Relatively simple rules in the CA pattern pictures are near-identical to those found in BZ reaction experiments (see Fig. 1.6. below).

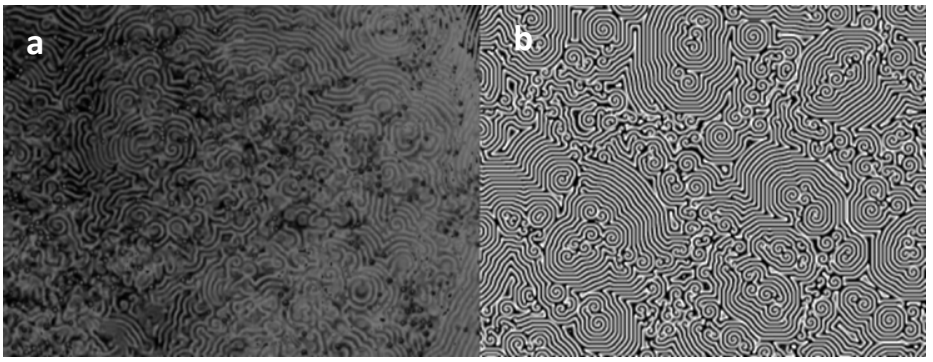

Figure 1.6. Snapshot of spiral waves' formation during the BZ reaction course in a blue color channel on a 30×50 mm cell (a) and CA simulation results performed on a canvas of 1000 x 1000 cells (b) (according to *Stys et al., 2016a*).

This stunningly good agreement in the structure of spiral waves between the experiment and the simulation by multilevel cellular automata was reported by ourselves (*Stys et al., 2016a; Stys et al., 2016b; Stys et al., 2016c*), but has been, in essence, observed already by Dewndey in 1988 (*Dewndey, 1988*). Any CA model so far was not able to mimic anything like target waves until a small number of ignition points was introduced (*Stys et al., 2016a; Stys et al., 2016b*).

The noise that was originally introduced to compensate for the lack of precise knowledge about internal mechanism was considered (*Horsthemke et al., 1984; Kádár, 1998*).

We have shown that for the successful observation of waves, an asymmetric rule for ignition points and noise within a certain interval of

levels is needed (*Stys et al., 2016c*). This model is the only one which is qualitatively equivalent to the experimental observations; it starts with circular structures that break into dense waves evolving around the proto-spirals, and irregularities in dense waves give rise to the final spirals' and waves' coexistence in which spirals and waves are in the same ratio as that found in the experiment.

The correctness of the description of the final stage of the B-Z reaction is outside any discussion (for 30 years). For that reason, the mathematical and technical basis of the model should be examined from the point of view of its realization in nature. In our opinion, this model may easily be translated into chemical reality based on these principles:

(1) Nature is in part discrete. At least, the molecules in the vast majority experiments behave as discrete units. These units, to some extent, interact. Discrete elements repeat in nature at all levels, from microcrystals up to galaxies, and the discrete description of the nature is natural – but, to many extents, resistant to smooth mathematical analysis. Thus it is more than acceptable to assume a discrete unit to be the element of the proper model of the natural process.

(2) The energy levels are discrete and have a maximum. Anyone familiar with the quantum mechanical description of chemical bonds and with molecular spectroscopy understands that the chemical bond behaves as quantized string which, when the upper limit of the vibrational energy is exceeded, breaks. It is thus natural to assume a countable number of discrete levels of energy in any model including chemical bond breakage. This assumption is a basis of the textbook model of the transition state complex of Eyring *(Eyring and Polányi 1931)*.

(3) A simple ionic reaction in inorganic chemistry likely occurs much faster than the diffusion of compounds. Yet, when there is a significant contribution from solvation/re-solvation of ions and bond re-arrangements, already this elementary reaction may contain a few diffusive processes. Thus, the chemical change does not necessarily occur at negligible speeds. Even more so, the diffusive process may not be spatially symmetrical.

In summary of the arguments (2) and (3), the breakage of the bond and re-formation of the Eyring complex is quantized and includes the specific re-distribution of many molecules. Its duration may be comparable with the diffusion "outside" the broken and newly restored Eyring complex. There is no reason to prefer the continuous model over the discrete one--and the discrete model gives proper results.

1.4.4. Disadvantages of the Cellular Automata BZ Model

Technical disadvantages of the cellular automata model (*Wolfram, 1985*) include that the modeling accuracy depends on the number of cells in the model, which is restricted by computer power, and the limits of the periodic boundary condition have been reported *(Stys et al. 2016c)*.

Objections against the CA model were cast against the assumed homogeneity (each cell is updated according to the same rules related to some logic formulas), when there are some doubts about BZ system homogeneousness (*Menzinger et al., 1986; Ali et al., 1997; Kasuya et al., 2005*). We have, however, shown, that the inhomogeneity naturally arises in the properly chosen CA model (*Stys et al., 2016c*).

The arguments that the elementary unit is the Eyring-complex-at-large, which we gave in the previous chapter, is questioned by our own observation (*Stys et al., 2016a*) that the elementary cell is rather big, with an estimated size of 10^{10}molecules. On the other hand, we have shown that as long as the number of energy levels is countable, it is only the ratio of the two processes which determines the behavior. In other words, in the chemical explanation proposed by us, we accept the *a priori* spatial separation in the reaction vessel as it was suggested in some articles mentioned in chapter 1.2.1. and assume a critical maximal value of the excitation within one spatial element. Some suggestions about the chemical identity of the compounds involved in the reaction are included (Fig. 1.3.), but their exact identity is not critical for the explanation. The two assumptions, *a priori* spatial segregation and existence of a maximal critical value of the state of the cell, allowed us to map the experimental observation on the cellular automaton model.

1.4.5. Combining the Models

Interesting solutions from combinations of partial differential equations with the cellular automata model were presented in previous work (*Méndez et al., 2004*). Such models are widely used for modeling the processes of tumor dissemination (*Swanson et al., 2002*). The authors propose to express the wave front transport equation through substituting the *q(x, t)* vector function on the probability density function *P(x, t)* of finding a random walker at time t at distance x from its starting point:

$$P(x,t) \sim \exp[-c\,(\frac{x}{\frac{1}{t^{\overline{d_w}}}})^{\frac{d_w d_{min}}{d_w - d_{min}}}] \qquad (6)$$

where d_w is the random-walk dimension of the fractal, and d_{min} is the fractal dimension of the minimum distance between points of the fractal. Although a mean-square displacement in a fractal object at time *t* depends on the d_w as: $\langle x^2 \rangle \sim t^{2/d_w}$, the wave front speed depends on d_{min} as: $v \sim t^{(1/d_{min})-1}$. The transport takes place through the "chemical distance" space, which is defined as the shortest path between two points belong to the fractal, not their Euclidian space. This approach may be valid in respect to the Belousov-Zhabotinsky reaction. It explains the acceleration of fractal fronts phenomena that were observed in BZ reaction wave dynamics (*Miike et al., 1993*).

1.5. Sensitivity to the Operating Environment

The chemical oscillation observed in the BZ reaction is very sensitive, not only to changes in reaction compound concentrations (*Menzinger et al., 1990*), but also to variation of the external factors, like temperature (*Vinson et. al, 1997*), illumination (*Toth et. al., 2000*), mechanical mixing (*Menzinger et al., 1986; Kalishyn et al., 2010*), reaction medium size and shapes (*Liveri et al., 2003*), air composition in the reactor (*Steinbock et. al, 2000; Kalishyn et al., 2005*), the presence of electrical (*Ševčíková et al., 1983*) or magnetic (*Nishikiori et al., 2011*) field, etc.

In order to examine the simplest influence, the spatial constraint, we have done a few experiments in dishes of various shapes. Indeed, the nearly free evolution was found only in the largest circular dish (20 cm in diameter). The influence of mixing was also rigorously examined. It was found that it is only the gentlest mixing method which leads to free evolution of the system.

1.6. Applied Examples of the BZ Reaction for Complex-System Dynamic Investigations

The similarity of the reaction with other oscillatory processes in nature (such as growth pattern of *Dictyostelium discoideum*, a soil-dwelling amoeba colony (*Lee et al., 1996*), the catalytic surface reaction of *CO* oxidation on platinum (*Nettesheim et al., 1993*), the oscillation regulation mechanism was found in the gene network (*Zhang et al., 2012*), etc.) prompted scientists (*Adamatzky, 2002*) to come up with the idea of a computer using a chemically-active environment of the BZ reaction as the main structural memory cell to mimic certain properties of neurons (*Hodgkin et al., 1952*). In other works (*Rambidi et.al., 1997; Rambidi, 2004; Gorecki et. al., 2015*) the possibilities of using the BZ reaction-diffusion system as a low cost and effective information processing device had been discussed. The reaction particles generated by the BZ reaction are a primary mechanism for carrying information over long space-time distances. Logical operations on the signals are performed when the particles interact (*Crutchfield, et al., 1995*). Understanding of the mechanisms of life's self-organization at the molecular level should enable us to approximate laws on the complexity observed in various biological species.

Under certain conditions, it is possible to achieve the transformation of flat 2D waves into complex spatial structures or 3D waves in the BZ reaction space (see example in Fig. 1.7.). This type of pattern is similar to ones generated by nerve impulses into the cardiac muscle (*Davidenko et al., 1992*) or into the chicken retina (*Gorelova et al., 1983*), which makes the BZ reaction an irreplaceable phenomenon for modeling abnormal states in many internal organs.

Figure 1.7. 3D waves' formation in the Belousov-Zhabotinsky reaction, which was observed in a test tube of 1 cm in diameter (reaction volume is 2.5 ml) and after 5 minutes' continuous mixing of components by a magnetic stirrer (Fisher Scientific Isotemp Magnetic Stirrer 60-1200 Rpm) with 150 rot/min.

The frequency of the finding of BZ-like patterns in nature increases scientific interest in finding a unifying mathematical concept. We have shown (*Stys et al., 2016a*) that in the simplest possible rule of the cellular automaton, i.e. where the evolution rule is that (a) a new state is an average of non-zero states in the closest neighborhood and a constant, and, (b) upon achievement of the maximum state, the state drops to zero, then the final structure of spirals and waves is highly similar in a certain range of ratios of total number of levels to constants. At a too-high ratio, diffusive structures are observed, and at low ratio, very small spirals are observed. This model is very natural for a colony of living cells which grow in time and divide upon achievement of certain size. It looks like this simplest CA model called the hodgepodge machine (*Dewndey, 1988*) may be one of the unifying models in nature.

1.7. Global Analysis of the BZ Reaction Experiment

The comparison of BZ reaction experiments with the model is complicated by the (1) absence of good characteristics of observed structure and (2) obvious and observable mixtures of structures in various stages of evolution of the system.

1.7.1. The General Stochastic Systems Theory Concepts

For the analysis of the *observed (measured)* trajectory we used the theory of Žampa (*Žampa et al., 2004*), which is, to our knowledge, the best breakdown of the factual process of measuring an experimental dynamic system. The main features of the theory are the inclusion of the input and output into the description of the system, and the acknowledgment of the fact that measureable parameters of the system – system variables – are aspects of the system model and are distinct from the system's internal variables. In other words, due to the limitation of existing laboratory techniques, only the system parameters recorded for a certain short time window t_k (camera shot) are available, and state trajectory is composed from a set of consecutive ($t_k < t_{k+1}$) experimental records of an examined event in a given time window:

$$t_k \in T, k \in K, K = \{0, 1, 2, \dots F\} \tag{7}$$

where *T* is non-empty set of all time events, and *K* is the appropriate index set.

Due to technical limitations, it is not possible to measure all of the system parameters (authors call it system attributes a_i):

$$A = \{a_i | i \in I\} \tag{8}$$

where *I* is an appropriate non-empty index set.

The *i*-th variable of the *i*-th attribute ($v_i \in V_i, i \in I$) only could be measured to map the examined system state trajectory (z) using the mathematical equations reflecting our knowledge about relations between attributes and variables:

$$z: T \times I \rightarrow \bigcup_{i \in I} V_i \ such\ that\ z(t,i) \in V_i, i \in I \tag{9}$$

The state of the system (i.e. Petri dish in which the BZ reaction is performed, organism, etc.) is known when a complete set of possible trajectories (Ω) is known:

$$\Omega = \{z|\ z: T \times I\ \rightarrow \bigcup_{i \in I} V_i\ such\ that\ z(t,i) \in\ V_i, i \in I\} \quad (10)$$

The system state trajectory z may be mapped through the definition set D:

$$D = T \times I \quad (11)$$

The system is measured at certain time intervals, but it also evolves between them. Thus the entire trajectory of the evolution of the system z can be drawn by means of its individual segments $z|D_{k,l}$, which could be used in mathematical modelling to adequately relate the measured points and the behavior of the system under the influence of intense external factors (Fig. 1.8.).

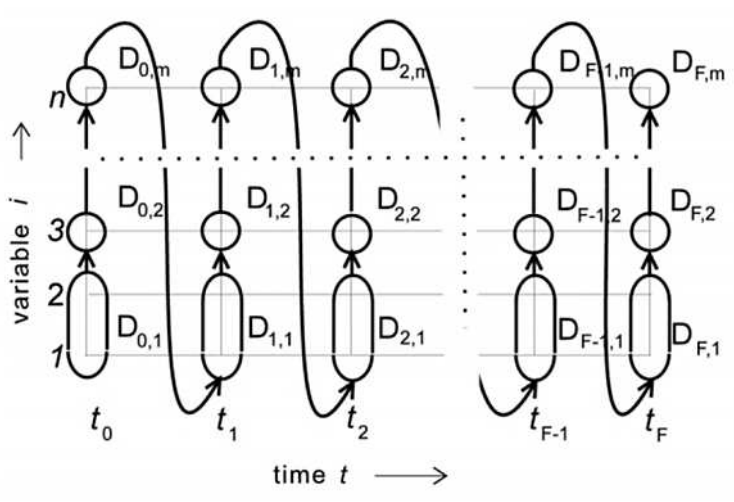

Figure 1.8. The set of variables measured at a time instant (represented by circles and ovals) and causal relations in the behavior between measuring times (adopted from *Žampa et al., 2004* handouts for the lecture).

The complete set of trajectories may not be determined and the system may be replaced by the probabilistic system mapping instead of the deterministic one.

Irrespective to the deterministic or probabilistic definition of the model, the causality relation in the system is preserved. In this way, the

complete immediate cause $C_{k,l}$ of the consequence $D_{i,j}$ should be considered to express the system trajectory while considering the causality within the measurement time intervals:

$$C_{k,l} \subset \bigcup_{(i,j)<(k,l)} D_{i,j} \tag{12}$$

The state trajectory thus depends on as many previous time events as the model predicts. In discrete dynamic systems (*Štys et al., 2015, Wuensche 2011*) for a given attractor only the basin of attraction may be identical for all the trajectories and the trajectories themselves may be widely different. A complete description of the system trajectory may include even the starting conditions which may not be known (*Štys et al., 2015*). The discrete dynamic systems, on the other hand, predict the existence only of a certain number of avenues towards the basin of attraction, i.e. there may be anticipated a natural classification of system events defined by eq. 9.

The basis of the analysis of the BZ reaction trajectories given in this thesis is the search for statistically-most-appropriate set of variables which describe the observed phenomena.

1.7.2. Phenomenological Analysis Using Information Theory Assumptions

As mentioned by the authors of *Žampa et al., 2004*, we must accept the technical limitation of the information. The Shannon information entropy theory may be easily adopted to these concepts of measurements (*Shannon, 1948*). Let us consider the information process in the example of the BZ experiment recording via the charge-coupled device (CCD, see *Hainaut, 2016* for details). Each element of such an experiment could be represented as the operating unit in the Shannon communication scheme (see Fig. 1.9.).

The CCD-chip is divided into cells (pixels) that are covered by a Bayer mask to translate them into color (the most common Bayer mask represent the square of four pixels has one filtered red, one blue, and two green corresponding to the human eye's color perception abilities).

Each pixel should be considered as a unique information source, and the final image that we see on the screen consists of the sum of signals from each pixel (see the work of *Nakamura, 2006* for details).

The light transmitted through the investigated object was modified to conduct information about the object (like object color, the position of its borders, coordinates of patterns on the object surface, dynamics of its shape changes, etc.). This message from the object is in a standard software transformed by the CCD into a digital signal by the image processing, which was performed in the PC core (GPU, CPU): linearization, white balance correction, demosaicing, color space correction, brightness and contrast control, and compression (see i.e. work by *Sumner, 2014* for the details).

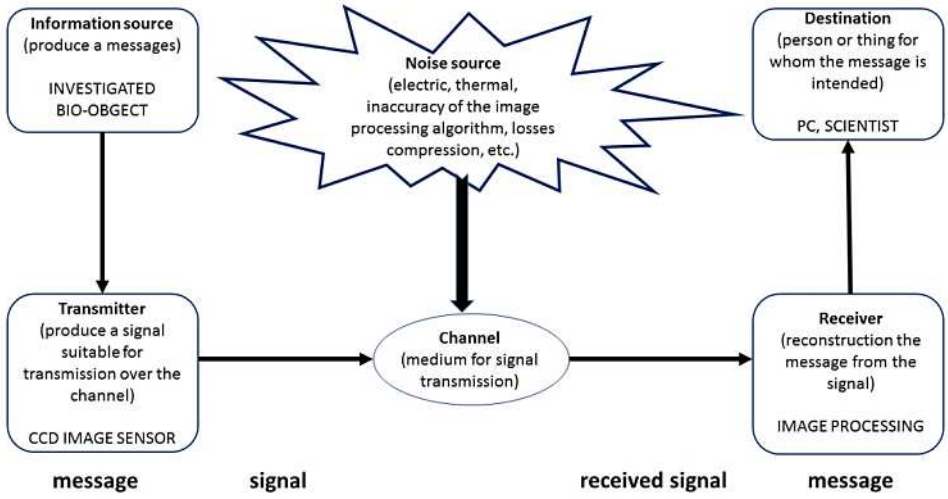

Figure 1.9. Schematic diagram of the signal transmission during the process recording by CCD photo camera (adopted from *Shannon, 1948*)

In the final step, only part of the initial information will reach the receiver. The percentage of correctly transmitted information can be measured by the Shannon information entropy:

$$H(p_i) = -K \sum_{i=1}^{n} p_i \ln p_i \qquad (13)$$

where p_i is the probability of *i*-th event occurrence, K is the positive constant, and $\ln a$ is the most natural and practically suitable choice of the logarithmic function (time, bandwidth, etc. tend to vary linearly with the logarithm of the number of possibilities).

In the standard camera capture approach, the noise source, namely the processing algorithms, distorts the signal in an uncontrollable way. In order to use the digital camera as, in fact, a three-channel spatially resolved colorimeter, we have developed a whole set of software procedures, data compression standards, etc. which enable us to preserve the maximum original information and correct the visual inspection of data *(Štys et al. 2016, Macháček et al. 2016)*. In the final data processing, we deal with the original dataset and the noise observed should be attributed to the electrical responses of the camera and to the properties of the optical system.

Among the Shannon information entropy disadvantages is the following: it was designed to process non-stationary signals coming from the stochastic process obeying the central limit theorem. The biological or BZ-like processes could hardly be assigned as having normal distribution. The information entropy by Shannon is not associated with information content or message meaning, but with the amount of information generated by source per symbol or per second (so-called entropy rate); it is scale-dependent and has special problems when applied to continuous variables, etc.

Restrictions of the Shannon entropy can be avoided by using the more general Rényi entropy (*Rényi, 1961*), which extends Shannon entropy to a continuous family of entropy measures and connects them with the information content (*Bromiley et al., 2004*):

$$I_\alpha(p_i) = \frac{1}{1-\alpha} \ln \sum_{i=1}^{N} p_i^\alpha \qquad (14)$$

where α is Rényi coefficient. The Rényi entropy becomes Shannon entropy as $\alpha \to 1$. (*Rényi, 1961*). The formula proposed by Rényi allows scientists to calculate quantitatively the amount of undistorted information for some *i*-th event from *N* possible events with the probability of occurrence p_i in space order determined by α.

Any complex structure may be assumed to be of a multifractal character. That by no means constraints the possibility that the object is not unifractal or that it does not have a whole number dimension. The generalized dimension of a multifractal object (*Grassberger and Procaccia, 1983)* may be defined using the Rényi entropy as:

$$D_\alpha(p_i) = \frac{1}{\alpha - 1}\lim_{r\to 0}\frac{\ln\sum_i p_i^\alpha}{\ln r} = \lim_{r\to 0}\frac{-I_\alpha(p_i)}{\ln r} \qquad (15)$$

where p_i is the probability of a system being in cell *i* with the side size *r* of its phase space, and α is the order of generalized dimension. For α = 1, the generalized average is the geometric average; for α = 2, it is the ordinary arithmetic average, when for α = 3 it is a root mean square (according the work by *Theiler, 1989*). $I_\alpha(p_i)$ – the Rényi entropy – is the average information needed to specify one cell (or pixel in our case) to a given accuracy p_i under the assumption of distribution appropriate to the α coefficient. There is thus a direct relation between the information variable – entropy – and the generalized dimension of the fractal system. The multifractal system has a spectrum of fractal dimensions.

Thus, the use of Rényi information entropy not only extends the range for information theory action objects, including the ability to describe the properties of the multi-fractal objects (*Sporring et al., 1997*), but also provides a complete set of data for a more detailed representation for the mathematical modelling of a process exhibiting spatial structures like a BZ reaction or many biological processes (*Phillips et al., 2006; Thalheim et al., 2014*).

In the article *Rychtáriková et al., 2016,* there were defined new information variables: the point information gain (PIG), point information gain entropy (PIE) and point information gain entropy density (PIED).

The point information gain ($\gamma_{\alpha,i}(x,y)$) is defined as:

$$\gamma_{\alpha,i}(x,y) = \frac{1}{1-\alpha}\ln\sum_{i=1}^{k} p_{i,x,y}^\alpha - \frac{1}{1-\alpha}\ln\sum_{i=1}^{k} p_i^\alpha \qquad (16)$$

where k is the number of elements in the discrete distribution, and p_i and $p_{i,x,y}$ are the probabilities of the occurrence of a given intensity for a given point *x, y* coordinate of a camera pixel without and with the examined point.

Point information gain entropy (H_α) is calculated using the formula:

$$H_\alpha = \sum_{i=1}^{k} n_i \gamma_{\alpha,i}\,(x,y) \tag{17}$$

And H_α is a cumulative variable in which all $\gamma_{\alpha,i}(x,y)$ values are summed. Finally, the point information gain entropy density (Ξ_α) is defined by the formula:

$$\Xi_\alpha = \sum_{i=1}^{k} \gamma_{\alpha,i}\,(x,y) \tag{18}$$

where n_i is the total number of pixels in the examined data array. PIE and PIED can be understood, respectively, as a multiple of the average point information gain (H_α) and as an average gain of the phenomenon i (Ξ_α).

These variables enable us to combine the calculation of information content with a certain algorithm-assumption about the structure of the valid surrounding components of the element of the set. In case that the element is classified in the context of the whole set, i.e. image, the same classification is used for the case of any standard entropy or from other point of view, generalized dimension. In this way, we can obtain many new information measures which may be used for particular purposes. Thus, any structured dataset may be represented by one unique number or by a vector of numbers and these numbers may be used for classifying the data, as similar objects give similar PIE/PIED values.

1.8. Summary

In summary, the Belousov-Zhabotinsky reaction is a process with a complex behavior consisting of many potential feedback loops which are extremely sensitive to any variations in the external conditions and can change the oscillatory mode or chemical waves' geometry. The BZ process has more than 60 years' investigation history. Despite the many works which are summarized in this thesis' theoretical introduction, many of the properties of the system are left without explanation (for

example the nature of the ignition point, what defines the spatial geometry in BZ patterns, how it is possible that the system 'remembers' to come back into its previous state after the application of some external force, etc.). Existing methods of modelling (ODE, cellular automata or their combinations) did not give a complete description of all these details and therefore it became necessary to apply an alternative approach to the construction of an adequate BZ reaction model.

As a first step, before introducing a new model and assuming certain chemical process, we decided to analyze in detail all technical settings in the BZ process and classify them using PIE and PIED.

Aims of the thesis:

The aim of this thesis is

1) to complete a detailed experimental series of the BZ reaction that would allow us to analyze the course of the evolution of individual structures;
2) to evaluate the course of the reaction under the assumption of multifractality of observed structures;
3) to test the possibility of the usage of multivariate stochastic modelling for analysis to estimate the system behavior at the most probable orthogonal internal coordinates.

Together these goals gave us the experimental basis for other analyses of structured dynamic systems in which the starting conditions are less controllable and the trajectory is more difficult to measure.

REFERENCES

Adamatzky, A., Benjamin D. L. C. (2002) Experimental logical gates in a reaction-diffusion medium: The XOR gate and beyond, *Physical Review,* E 66 (4): 046112.

Agladze, K. I., Krinsky, V. I. (1982). Multi-armed vortices in an active chemical medium, *Nature*, 296:424–426.

Agladze, K. I., Krinsky, V. I., Petrsov, A. M. (1984). Chaos in the non-stirred Belousov-Zhabotinsky reaction is induced by interaction of waves and stationary dissipative structures, *Lett. to Nature*, 308: 834-835.

Agladze, K., Keener, J. P., Müller, S. C., Panfilov A. (1994). Rotating spiral waves created by geometry, *Science*: 264(5166), 1746-1750.

Agladze, K.I., Davydov, V.A., Mikhailov, A.S. (1987). Observation of a helical-wave resonance in an excitable distributed medium, *Sov. Phys. JETP Lett.,* 45 (12): 767–770.

Ali, F., Menzinger, M. (1997). Stirring Effects and Phase-Dependent Inhomogeneity in Chemical Oscillations: The Belousov−Zhabotinsky Reaction in a CSTR, *J. Phys. Chem. A,* 101 (12): 2304–2309. DOI: 10.1021/jp9624515.

Alonso, S., Sagués, F., Mikhailov, A. S. (2006). Negative-tension instability of scroll waves and winfree turbulence in the oregonator model, *J. Phys. Chem.* A., 110(43): 12063-71. DOI: 10.1021/jp064155q.

Alonso, S., Sagues, F., Mikhailov. A. S. (2003). Taming Winfree turbulence of scroll waves in excitable media, *Science* 299(5613):1722-5. DOI: 10.1126/science.1080207.

Amemiya, T., Kádár, S., Kettunen, P., Showalter, K., (1996). Spiral Wave Formation in Three-Dimensional Excitable Media, *Phys. Rev. Lett.*, 77: 3244-3247.

Argoul, F., Richetti, P., Arneodo, A., Roux, J. C. (1987). From quasiperiodicity to chaos in the Belousov-Zhabotinsky reaction I. Experiment, *J. Chem. Phys.*, 86: 3325-3338. DOI: 10.1063/1.452751.

Belousov, B. P. (1959). Batch reaction and its mechanism. Collection of abstracts on radiation medicine, *Medgiz*, 147: 145.

Bendixson, I. (1901), Sur les courbes définies par des équations différentielles, *Acta Mathematica* (Springer Netherlands) 24 (1): 1–88, DOI: 10.1007/BF02403068.

Birdi, K.S. (2013). Fractals in Chemistry, Geochemistry, and Biophysics: An Introduction, *Springer Science*, 264 pp.

Böckmann, M., Hess, B., Müller, S. C. (1996). Temperature gradients traveling with chemical waves, *Phys. Rev. E*., 53(5): 5498-5501.

Bromiley, P.A., Thacker, N.A., Bouhova-Thacker, E. (2004). Shannon Entropy, Renyi Entropy, and Information, *Tina Memo,* 2004-004, 8 pp. On-line source: http://www.tina-vision.net/docs/memos/2004-004.pdf.

Connolly, D., Nelson, B. (2011). Chaos in the Belousov-Zhabotinsky Reaction, Dartmouth College archive, 12 pp. On-line source: https://math.dartmouth.edu/archive/m53f11/public_html/proj/ConnollyConnol.pdf.

Cross, M. C., Hohenberg, P. C. (1983). Pattern formation outside of equilibrium, *Rev. Mod. Phys*., 65(3): 854-1112.

Crutchfield, J. P., Mitchell, M. (1995). The evolution of emergent computation, *Proc. Nat. Acad. Scien*., 92(23): 10742-10746.

Davidenko, J. M., Pertsov, A. V., Salomonsz, R., Baxter, W., Jalife, J. (1992). Stationary and drifting spiral waves of excitation in isolated cardiac muscle. *Nature 355(6358)*, 349-351. DOI: 10.1038/355349a0.

Dewdney, A. K. (1988). Computer Recreations: The hodge-podge machine makes waves. *Sci Am., 225:104–107*. DOI: 10.1038/scientificamerican0888-104.

Ermakova, E.A., Pertsov, A.M. (1986). Interaction of rotating spiral waves with a boundary, *Biofizika*, 31(5): 855-861.

Eyring, H.; Polanyi M. (1931). "Über Einfache Gasreaktionen". Z. Phys. Chem. B. 12: 279–311.

Espenson, J. A. (1995) Chemical Kinetics and Reaction Mechanisms, 2nd Edition, *McGraw-Hill, Inc*., New York, N.Y., 296 pp.

Field, R.J., Koros, E. and Noyes, R.M. (1972). Oscillations in chemical systems. II. Thorough analysis of temporal oscillation in the bromate-cerium-malonic acid system, *J. Am. Chem. Soc.* 94, 8649-8664. DOI: 10.1021/ja00780a001.

Fisher R. A. (1937). The wave of advance of advantageous genes. *Annals of Human Genetics 7(4):353–369*. DOI: 10.1111/j.1469-1809.1937.tb02153.x.

Försterling, H.-D., Murányi, S., Noszticzius, Z. (1990). The role of radicals in the Belousov-Zhabotinsky reaction, *React. Kinet. Catal. Lett.*, 42: 217. DOI: 10.1007/BF02065357.

Gang, Ch. (2000). A mathematical model for bifurcations in a Belousov-Zhabotinsky reaction, *Physica D: Nonlinear Phenomena*, 145(3-4): 309-329. DOI: 10.1016/S0167-2789(00)00113-5.

Gao, Y., Foersterling, H.-D., Noszticzius, Z., Meyer, B. (1994). HPLC Studies on the Organic Subset of the Oscillatory BZ Reaction. 1. Products of the Ce^{4+}-Malonic Acid Reaction, *J. Phys. Chem.,* 98: 8377-8380. DOI: 10.1021/j100085a018.

Gerhardt, M., Schuster, H., Tyson, J. J. (1990). A Cellular Automata Model of Excitable Media Including Curvature and Dispersion, *Science Reports*, 247: 1563-1566.

Glaser, R., Delarosa, M., Salau, A. O. (2013). Why the Acidity of Bromic Acid Really Matters for Kinetic Models of Belousov-Zhabotinsky Oscillating Chemical Reactions, *J. Thermodyn. Catal*, 4:e115. DOI: 10.4172/2157-7544.1000e115.

Glaser, Rainer, Jost, M. (2012). Disproportionation of Bromous Acid HOBrO by Direct O-Transfer and via Anhydrides $O(BrO)_2$ and $BrO–BrO_2$. An Ab Initio Study of the Mechanism of a Key Step of the Belousov–Zhabotinsky Oscillating Reaction, *J. Phys. Chem. A*, 116 (32): 8352–8365. DOI: 10.1021/jp301329g.

Gorecki, J., Gizynski, K., Guzowski, J., Gorecka, J.N., Garstecki P., Gruenert G., Dittrich, P. (2015). Chemical computing with reaction-diffusion processes, *Philosoph. Trans. of The Royal Soc.: A Math. Phys. and Engin. Sc*., 373(2046). DOI: 10.1098/rsta.2014.0219.

Gorelova, N. A., Bures, J. (1983). Spiral waves of spreading depression in the isolated chicken retina. *J. Neurobiol. 14(5)*, 353-63. DOI:10.1002/neu.480140503.

Grassberger, P., Procaccia, I. (1983). Measuring the strangeness of strange attractors. *Physica D: Nonlin. Phen., 9 (1-2)*: 189-208. DOI: 10.1016/0167-2789(83)90298-1.

Gray C. R. (2002). An Analysis of the Belousov-Zhabotinskii Reaction. *The High School Summer Science Research Program*, Baylor University Waco, 15 pp.

Gray P., Scott S.K. (1990). Chemical oscillations and instabilities: Non-linear chemical kinetics, Oxford University Press, New York, 453 pp.

Grindrod P. (1996). The theory and applications of reaction-diffusion equations: Patterns and waves. Oxford Applied Mathematics and Computing Science Series. The Clarendon Press Oxford University Press, New York, second edition, 275 p. ISBN 0-19-859676-6; ISBN 0-19-859692-8.

Gyorgyi L., Turanyi T., Field R. J. (1990). Mechanistic details of the oscillatory Belousov-Zhabotinskii reaction, *J. Phys. Chem*., 94 (18): 7162–7170. DOI: 10.1021/j100381a039.

Györgyi, L., Field, R.J. (1992). A Three-Variable Model of Deterministic Chaos in the Belousov-Zhabotinsky Reaction, *Nature*, 355: 808-810. DOI: 10.1038/355808a0.

Hainaut, O. R. (December, 2006). Basic CCD image processing [Web source]. Available at: http://www.sc.eso.org/~ohainaut/ccd.

Hegedüs, L., Försterling, H. D., Onel, L., Wittmann, M., Noszticzius, Z. (2006). Contribution to the chemistry of the Belousov-Zhabotinsky reaction. Products of the Ferriin-Bromomalonic acid and the Ferriin-Malonic acid reactions, *J. Phys. Chem. A*, 110(47): 12839-44. DOI: 10.1021/jp064708x.

Hegedús, L., Wittmann, M., Noszticzius, Z., Yan, S., Sirimungkala, A., Försterling, H. D., Field, R. J. (2001). HPLC analysis of complete BZ systems. Evolution of the chemical composition in cerium and ferroin catalysed batch oscillators: experiments and model calculations, *Faraday Discuss*, 120: 21-38. DOI: 10.1039/b103432b.

Hiro (2009/9/11). Belousov-Zabotinski (BZ) reaction [Web source]. Available at: http://www.chem-station.com/odos/2009/09/-belousov-zhabotinskybz-reacti.html.

Hodgkin, A., and Huxley, A. (1952): A quantitative description of membrane current and its application to conduction and excitation in nerve. *J. Physiol*, 117:500—544.

Horsthemke, W., Lefever, R. (1984). Noise-Induced Transitions: Theory and Applications in Physics, Chemistry, and Biology, *Springer*, Berlin, 322 pp.

Inomoto, O., Sakaguchi, A., Kai, S. (2012). Experimental Evidence of Marangoni Convection Rolls in Belousov-Zhabotinsky Reaction, in book: Complexity and Diversity, *Springer Mathematics*, 135-137.

Jahnke, W., Skaggs, W.E., Winfree, A.T. (1989). Chemical vortex dynamics in the Belousov-Zhabotinsky reaction and in the two-variable Oregonator Model, *J. Phys. Chem*., 93: 740-749.

Jamal, M. M. El., Hammud, H. H. (2008). About the instability of $[Fe(III)(phen)_3]^{3+}$, *J. Univ. Chem. Technol. Metall*., 43(3): 349-356.

Jensen, F. G., Sporring, J., Nielsen, M., Sørensen, P. G. (2002). Tracking target and spiral waves, *Chaos*., 12(1):16-26. DOI: 10.1063/1.1429968.

Kádár, S., Wang, J., Showalter, K. (1998). Noise Supported Traveling Waves in Subexcitable Media, *Nature,* 391: 770-772.

Kalishyn, Y. Y., Rachwalska, M., Khavrus, V. O., Strizhak, P. E. (2005). The effect of oxygen on time-dependent bifurcations in the Belousov-Zhabotinsky oscillating chemical reaction in a batch, *Phys. Chem. Chem. Phys*., 7(8):1680-1686.

Kalishyn, Y. Y., Rachwalska, M., Strizhak, P. E. (2010). Stirring effect on the Belousov-Zhabotinsky oscillating chamical reactions in a batch. Experimental and modelling, *Z. Naturforsch*. 65a: 132-140.

Kasuya, M., Hatanaka, K., Hobley, J., Fukumura, H., Sevcíkova, H. (2005). Density Changes Accompanying Wave Propagation in the Cerium-Catalyzed Belousov-Zhabotinsky Reaction, *J. Phys. Chem. A*, 109: 1405-1410.

Kinoshita, S. (2013). Pattern Formations and Oscillatory Phenomena, 1st Edition, *Print book*, p.280. ISBN-9780123970145.

Kolmogorov A., Petrovskii I., Piskunov N. (1937). A study of the diffusion equation with increase in the amount of substance, and its application to a biological problem. In V. M. Tikhomirov (ed.), *Selected Works of A. N. Kolmogorov*, pp. 248–270. Kluwer 1991, ISBN 90-277-2796-1.

Kolmogorov, A. (1998). On Tables of Random Numbers, *Theor. Comp. Science,* 207(2): 387–395. DOI: 10.1016/S0304-3975(98)00075-9.

Kuttler, C. (2011). Reaction-Diffusion equations with applications, *Sommersemester*, 50 pp.

Lee, K., Cox, E., Goldstein, R. (1996). Competing patterns of signaling activity in Dictyostelium Discoideum, *Phys. Rev. Lett*., 76: 1174–1177. DOI: 10.1103/PhysRevLett.76.1174.

Lee, K., J. (1997). Wave Pattern Selection in an Excitable System, *Phys. Rev. Lett.*, 79(15): 2907-2910.

Li, Q., S., Zhu, R. (2003). Chaos to periodicity and periodicity to chaos by periodic perturbations in the Belousov–Zhabotinsky reaction, *Chaos, Solitons and Fractals,* 19: 195–201. DOI: 10.1016/S0960-0779(03)00103-6.

Liveri, M. L. T., Lombardo, R., Masia, M., Calvaruso, G., Rustici, M. (2003). Role of the Reactor Geometry in the Onset of Transient Chaos in an Unstirred Belousov−Zhabotinsky System*, J. Phys. Chem. A*, 107: 4834-4837. DOI: 10.1021/jp027213q.

Méndez, V., Campos, D., Fort, J. (2004). Dynamical features of reaction-diffusion fronts in fractals, *Phys. Rev. E.,* 69, 016613: 1-6. DOI: 10.1103.

Menzinger, M., Jankowski, P. (1986). Heterogeneities and stirring effects in the Belousov-Zhabotinsky reaction, *J. Phys. Chem. Lett.*, 90(7): 1271-1291.

Menzinger, M., Jankowski, P. (1990). Concentration fluctuations and stirring effects in the Belousov-Zhabotinskii reaction, *J. Phys. Chem*., 94 (10): 4123–4126. DOI: 10.1021/j100373a045.

Mihaliuk, E., Sakurai, T., Chirila, F., Showalter, K., (2002). Feedback Stabilization of Unstable Propagating Waves, *Phys. Rev. E*, 65: 0656021-4. DOI: 10.1103/PhysRevE.65.065602.

Miike, H., Yamamoto, H., Kai, S., Müller S. C. (1993). Accelerating chemical waves accompanied by traveling hydrodynamic motion and surface deformation, *Phys. Rev. E* 48, R1627(R). DOI: http://dx.doi.org/10.1103/PhysRevE.48.R1627.

Mikhailov A. S., Showalter, K. (2006). Control of waves, patterns and turbulence in chemical systems, *Phys. Rep*., 425(2–3): 79–194. DOI: 10.1016/j.physrep.2005.11.003.

Nakamura, J. (2005). Image Sensors and Signal Processing for Digital Still Cameras, *CRC Press is an imprint of Taylor & Francis Group*, 350 pp.

Nettesheim, S., von Oertzen, A., Rotermund, H.H., Ertl, G. (1993). Reaction diffusion patterns in the catalytic CO-oxidation on Pt (110): Front propagation and spiral waves, *J. Chem. Phys*., 98 (12): 9977-9985.

Nicolis, G. and Prigogine, I. (1977) Self-Organization in Non-equilibrium Systems. Wiley, New York, 491 pp.

Nishikiori, R., Morimoto, S., Fujiwara, Y. (2011). Magnetic Field Effect on Chemical Wave Propagation from the BelousovZhabotinsky Reaction, J. Phys. Chem. A, 115: 4592–4597. DOI: 10.1021/jp200985j.

Peitgen, H. O. (2012). Newton's Method and Dynamical Systems, *Springer Science*, 226 pp.

Pertsov, A.M., Ermakova, E.A. (1988). Mechanism of the drift of a spiral wave in an inhomogeneous medium, *Biofizika*, 33(2): 338-342.

Petrov, V., Gaspar, V., Masere, J., Showalter, K. (1993). Controlling chaos in the Belousov-Zhabotinsky reaction, *Lett. To Nature*, 361: 240-243.

Phillips, S. J., Anderson, R. P., Schapire, R. E. (2006). Maximum entropy modeling of species geographic distributions, Ecol. Modell., 190(3–4): 231–259. DOI: 10.1016/j.ecolmodel.2005.03.026.

Poincaré, H. (1892). Sur les courbes définies par une équation différentielle, Oeuvres 1, Paris.

Pojman, J. A., Epstein, I. R. (1990). Convective Effects on Chemical Waves. 1: Mechanisms and Stability Criteria, *J. Phys. Chem.*, *94*: 4966-4972.

Prigogine, I., Lefever, R. (1968). Symmetry Breaking Instabilities in Dissipative Systems, *J. Chem. Phys.*, 48, 1695, http://dx.doi.org/10.1063/1.1668896.

Rambidi, N. G. (2004) Biologically Inspired Information Processing Technologies: Reaction-Diffusion Paradigm, *Int. Journ. Unconv. Comp*., Vol. 1: 101-121.

Rambidi, N. G., Maximychev, A. V. (1997). Towards a biomolecular computer. Informationprocessing capabilities of biomolecular nonlinear dynamic media. *BioSystems,* 41, 195–211. DOI: 10.1016/S0303-2647(96)01678-4.

Rényi, A. (1961). On measures of entropy and information, *In Proc. Fourth Berkeley Symp. Math. Stat. Prob.,* 1: 547.

Rovinskii A. B. (1986). Spiral waves in a model of the ferroin catalyzed Belousov-Zhabotinskii reaction, *J. Phys. Chem*. Lett., 90 (2): 217–219. DOI: 10.1021/j100274a001.

Rovinsky, A. B., Zhabotinsky, A. M. (1984). Mechanism and Mathematical Model of the Oscillating Bromate-Ferroin-Bromomalonic Acid Reaction, *Journ. of Phys. Chem*., 88(25): 6081-6084. DOI: 10.1021/j150669a001.

Rychtáriková, R., Korbel, J., Macháček, P., Císař, P., Urban, J., Štys, D. (2016). Point Information Gain and Multidimensional Data Analysis, *Entropy 2016*, 18: 372. DOI: 10.3390/e18100372.

Rychtáriková, R.; Korbel, J.; Macháček, P.; Císař, P.; Urban, J.; Štys, D. (2016). Point Information Gain and Multidimensional Data Analysis. *Entropy, 18(10), 372*. DOI: 10.3390/e18100372.

Ryzhkov A. B. (2000). An investigation of complex dynamics of chemical systems by the mathematical modeling methods, *Dissertations on competition of a scientific degree (PhD in Chemistry)*, Ufa Research Centre of the Russian Academy of Sciences. On-line source: http://redandr.ca/diss/index.computer.translated.htm.

Schröder, E. (1870). Ueber iterirte Functionen. *Math. Ann. 3 (2): 296–322*. DOI: 10.1007/BF01443992.

Ševčíková, H., Marek, M. (1983). Chemical waves in electric field, *Physica D: Nonlinear Phenomena*, 9(1–2): 140–156. DOI: 10.1016/0167-2789(83)90296-8.

Shanks, N. (2001) Modeling biological systems: the Belousov-Zhabotinsky reaction, *Foundations of Chemistry.* 3: 33–53. DOI: 10.1023/A:1011434929814.

Shannon, C. E. (1948). A Mathematical Theory of Communication, *Bell Syst. Tech. J.*, 27 (3): 379–423. DOI:10.1002/j.1538-7305.1948.tb01338.x.

Skinner, G. S., Swinney, H. L. (1991). Periodic to quasiperiodic transition of chemical spiral rotation, *Physica D: Nonlinear Phenomena*, 48(1), 1-16. DOI: 10.1016/0167-2789(91)90048-E.

Sporring, J., Weickert, J. (1997). On Generalized Entropies and Scale-Space, First Int. Conf. Proc., Scale-Space '97, *Springer Science,* 53-64.

Steinbock, O. Müller, S.C. (1993). Multi-armed spirals in a light-controlled reaction, *Int. J. Bifurcation Chaos,* 03, 437. DOI: http://dx.doi.org/10.1142/S0218127493000325.

Steinbock, O., Hamik, C. T., Steinbock, B. (2000). Oxygen Inhibition of Oscillations in the Belousov−Zhabotinsky Reaction, *J. Phys. Chem. A*, 104 (27): 6411–6415. DOI: 10.1021/jp000531.

Štys, D., Náhlík, T., Zhyrova, A., Rychtáriková, R., Papáček, Š., Císař, P. (2016). Model of the Belousov-Zhabotinsky reaction, *Lec. Not. In Comp. Science*, V.: 9611, pp.: 171-185.

Stys, D., Rychtarikova, R., Nahlik, T., Zhyrova, A. and Papacek, S. (2015). Model of the Belousov Zhabotinsky reaction part 1: Influence of the ignition constants, *ArXiv*, 11 pp. Article ID on ArXiv: 1507.08783.

Štys, D., Urban, J., Rychtáriková, R., Zhyrova, A., and Císař, P. (2015). Measurement in biological systems from the self-organization point of view, *Bioinformatics and Biomedical Engineering: Third International Conference, IWBBIO 2015, Granada, Spain, Proceedings, Part 2*: 431-443.

Sumner R. (2014). Processing RAW Images in MATLAB, *Department of Electrical Engineering, UC Santa Cruz.*, 15 pp. On-line source: http://www.cnba.it/contenuti/uploads/2016/03/Processing-RAW-Images-in-MATLAB-Sumner.pdf.

Swanson, K. R., Alvord, E. C., Murray, J. D. (2002). Virtual brain tumors (gliomas) enhance the reality of medical imaging and highlight inadequacies of current therapy, *Br J Cancer*, 86(1): 14–18. DOI: 10.1038/sj.bjc.6600021.

Taylor, A. F., Gáspár, V., Johnson, B. R., Scott, S. K. (1999). Analysis of reaction–diffusion waves in the ferroin-catalysed Belousov–Zhabotinsky reaction, *Phys. Chem. Chem. Phys.*, 1, 4595.

Taylor, A. F., Tinsley, M. R. (2009). Chemical self-organization: A path to patterns, *Nature Chemistry 1: 340 – 341.* DOI: 10.1038/nchem.310.

Thalheim, B., Jaakkola, H., Kiyoki Y. (2014). Information Modelling and Knowledge Bases XXVI, *IOS Press*, 484 pp.

The MathWorks Inc., 2014. MATLAB 2014b, The MathWorks – MATLAB and Simulink for technical computing. Official site: http://www.mathworks.com/products/matlab.

Theiler, J. (1990). Estimating fractal dimension, *J. Opt. Soc. Am. A,* 7(6): 1055-1073. DOI: 0740-3232/90/061055-19$02.00.

Tóth, R., Gáspár, V., Belmonte, A., O'Connell, M. C., Taylor, A., Scott, S. K. (2000). Wave initiation in the ferroin-catalysed Belousov–Zhabotinsky reaction with visible light, *Phys. Chem. Chem. Phys.*: 2, 413-416.

Turing, A. M. (1952). The Chemical Basis of Morphogenesis, Philosophical Transactions of the Royal Society of London. Series B, *Biological Sciences*, 237(641): 37-72.

Tyson, J. J. (1984). Relaxation oscillations in the revised oregonator. *Journ. Chem. Phys*. 80: 6079–6082.

Vanag, V.K. (1999). Study of the Spatially Distributed Dynamic Systems by the Methods of Probabilistic Cellular Automaton, *Usp. Phys. Nauk*, 169(5): 481-505.

Vavilin, V. A., Zhabotinsky, A. M., and Zaikin, A. N. (1968). A study of a self-oscillatory chemical reaction I. The autonomous system, in Biological and biochemical oscillators, Proceedings of a Conference on Biological and Biochemical Oscillators, Prague, 522 pp.

Vavilin, V. A., Zhabotinsky, A. M., Zaikin, A. N. (1968). A study of a self-oscillatory chemical reaction I. The autonomous system, *in Biological and biochemical oscillators. Proceedings of a Conference on Biological and Biochemical Oscillators*, *Prague: 71-79*. ISBN: 978-0-12-167872-2.

Vinson, M., Mironov S., Mulvey S., Pertsov A. (1997). Control of spatial orientation and lifetime of scroll rings in excitable media, *Nature,* 386(6624):477-80. DOI: 10.1038/386477a0.

von Neumann, J. Burks, A. W. (1966). Theory of Self-Reproducing Automata. University of Illinois Press, 388 pp.

Winfree, A. T. (1994a). Persistent tangled vortex rings in generic excitable media. *Nature 371: 233-236*. DOI: 10.1038/371233a0.

Winfree, A. T. (1994b). Electrical turbulence in three-dimensional heart muscle. *Science 266(5187): 1003-1006*. DOI: 10.1126/science.7973648.

Wolfram, S. (1983). Statistical Mechanics of Cellular Automata, *Rev. Mod. Phys.*, 55: 601-644. DOI: http://dx.doi.org/10.1103/RevModPhys.55.601.

Wolfram, S. (1985). Twenty Problems in the Theory of Cellular Automata, *Phys. Scripta*, T9: 170-183.

Wu, Y., Vasquez, D. A., Edwards, B. F., Wilder, J. W. (1995). Convective chemical-wave propagation in the Belousov-Zhabotinsky reaction, *Phys. Rev. E*., Stat. Phys. Plasmas. Fluids. Relat. Interdiscip. Topics, 51(2): 1119-1127.

Wuensche, A. (2011). Exploring Discrete Dynamics; The DDLab Manual. *Luniver Press*, UK, 538 pp.

Zaikin, A. N., Zhabotinsky, A. M., (1970). Concentration wave propagation in two-dimensional liquid phase self-oscillating system, *Nature*, 225: 535-537. DOI: 10.1038/225535b0.

Žampa, P., Arnošt, R. (2004). Alternative Approach to Continuous Time Stochastic Systems Definition, *Proc. of the 4th WSEAS conference*, 3(10): 2228.

Zhabotinsky, A.M. (1964). Periodic processes of malonic acid oxidation in a liquid phase. *Biophysics*, 9: 306 – 311.

Zhang, D., Gyorgyi, L., Peltier, W. R. (1993). Deterministic chaos in the Belousov-Zhabotinsky reaction: Experiments and simulations, *Chaos*, 3(4):723-745. DOI: 10.1063/1.165933.

Zhang, Z., Ye, W., Qian, Y., Zheng, Z., Huang, X., Hu, G. (2012). Chaotic Motifs in Gene Regulatory Networks, *PLoS ONE*, 7(7): e39355. DOI: 10.1371/journal.pone.0039355.

Zhao, Y., Billings, S. A., Routh, A. (2005). Identification of Excitable Media using Cellular Automata, *Reports of department of Automatic Control and Systems Engineering, University of Sheffield*, 897.

MATERIALS AND METHODS

2.1. Belousov-Zhabotinsky Reaction Composition and Compound Mixing Conditions

The oscillating and self-organizing bromated-ferroin-bromomalonic acid system, known as the Belousov-Zhabotinsky reaction (BZ), was chosen for our experiments. The BZ reaction was performed as instructed by the commercially available reaction kit (*Cohen, 2009*). The reaction mixture include 0.34 M sodium bromate (manufactured by Penta), 0.2 M sulfuric acid (99.9 %, manufactured by Penta), 0.057 M sodium bromide (manufactured by Penta), 0.11 M malonic acid (manufactured by Sigma-Aldrich) as substrate, and redox indicator 0.12 M 1,10-phenanthroline iron(II) complex (ferroine, manufactured by Penta). All the solutions were prepared with distilled water.

The structure formation in the chemical system was initiated by consistent mixing of the reaction compounds and reagents in the order described above. After adding the last one (the redox indicator), the reaction mixture was stirred for another 2 minutes by different methods (detailed below). The reaction dish was kept at a constant temperature of 26 °C.

The development of the BZ system was examined with respect to two fundamental conditions: influence of mixing and space constriction. We applied three methods of mixing for the BZ reaction initiation: (1) commonly used dish mixing by hand with non-regulated frequency and depending only on the personal habits of the experimenter; (2) gentle reagent mixing using an orbital mixer (Edmund Buhler GmbH, TL-10) at different regimes ($14\frac{rot}{min}$ and $16\ \frac{rot}{min}$); (3) and intensive reaction mixture infusion in a chemical beaker by the magnetic stirrer (Fisher Scientific Isotemp Ceramic Hotplate 11-700-49SH) at various rotational speeds ($100\ \frac{rot}{min}$ and $200\ \frac{rot}{min}$). We modified the BZ reaction space by using vessels of different space geometry: circular, squared, rectangular and triangular. The initial component concentration was maintained through all experiments in the series. The thickness of the reaction layer was also kept constant at 3 mm.

2.2. Recorded System Setup

Two different photo-systems were used for monitoring the BZ reaction pattern evolution.

In the first system, images were captured by a Nikon D90 camera with 12.3 effective megapixels Nikon DX-format CMOS image sensor (see camera specification in Fig. 2.2. and in source provided by *Nikon Corp., 2014*). Images were stored in an un-compressed 12-bit NEF (4096 shades per channel) image format in order to store the maximum information from the original space-structure proper for further image data processing.

The photo-camera was set to time-lapse with a time interval between frames of 10 seconds. Camera settings were chosen to capture the highest resolution of BZ reaction patterns; specifically, with Exposure compensation + $\frac{2}{3}$ EV, ISO 320, Aperture $\frac{f}{18}$ and Shutter speed $\frac{1}{10}$ second. Minor fluctuations in the focal distance of the camera were compromises between the wide variation of the size of the investigated object and achieving the maximum visual clarity of recorded images.

When designing the system for the BZ reaction recording procedure, we had to take into account the optical characteristics of the investigated object, including the reflective properties of liquids, as well as the transparency of and blurring of observable chemical waves' boundaries. The recording device was placed in a fume hood and an illuminated photographic tent to control the factors of external light influence on the photographed area (the construction is presented in Fig. 2.1.).

For illumination, white light from two Spiral 5500K daylight lamps of 40 Watt oriented in 45° to both sides of the reaction surface was used. A white reflectance diffuser (type SG 3214 with 95% surface reflectivity, manufactured by the SphereOptics Company, see transmission specification in Fig. 2.2.) was placed under the vessel's bottom. To obtain the diffused light and to minimize the external stochastic light impact by the light source in the laboratory, the experimental sample photographing was conducted in the white photo tent (manufactured by Opnamebox).

The photo-system constructed in this way provides the best image quality we could reach in our experimental setup with uniform light

distribution throughout the whole photographed area and a lack of glare on the surface of the BZ reaction.

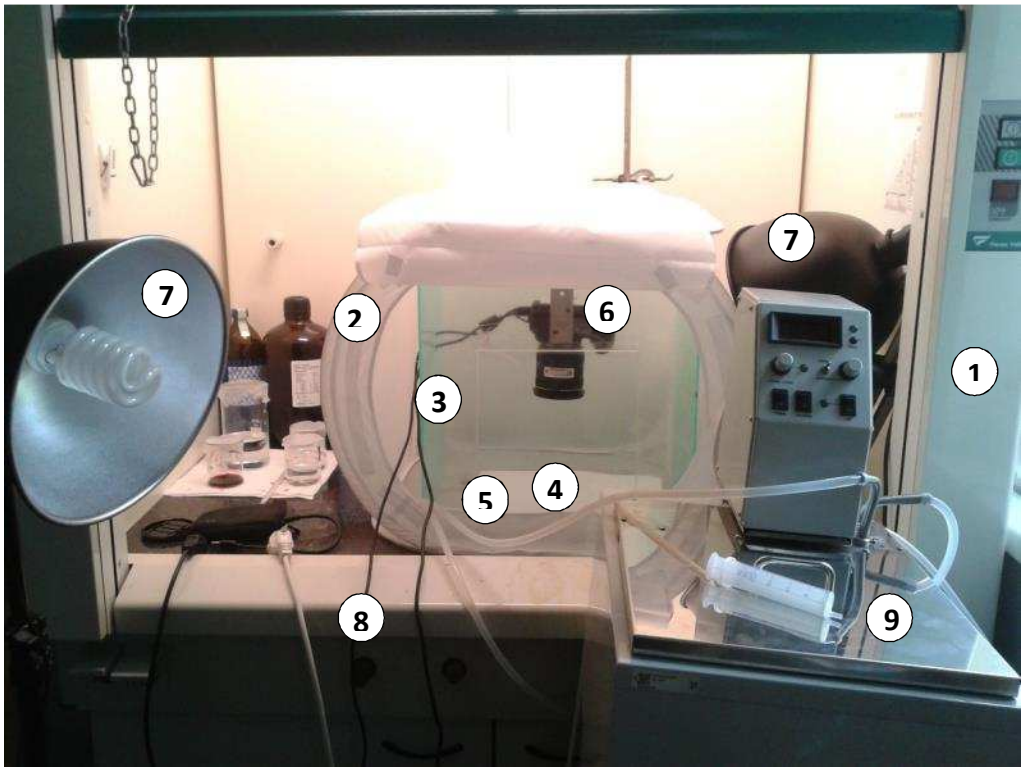

Figure 2.1. Photo of the experimental installation for Belousov-Zhabotinsky reaction pattern monitoring: (1) laboratory hoods corps; (2) photo-tent; (3) thermostat; (4) position of investigated object (vessel with BZ reaction); (5) optical diffuser plate; (6) Nikon D90 photo-camera; (7) light sources; (8) connection with PC; (9) water bath.

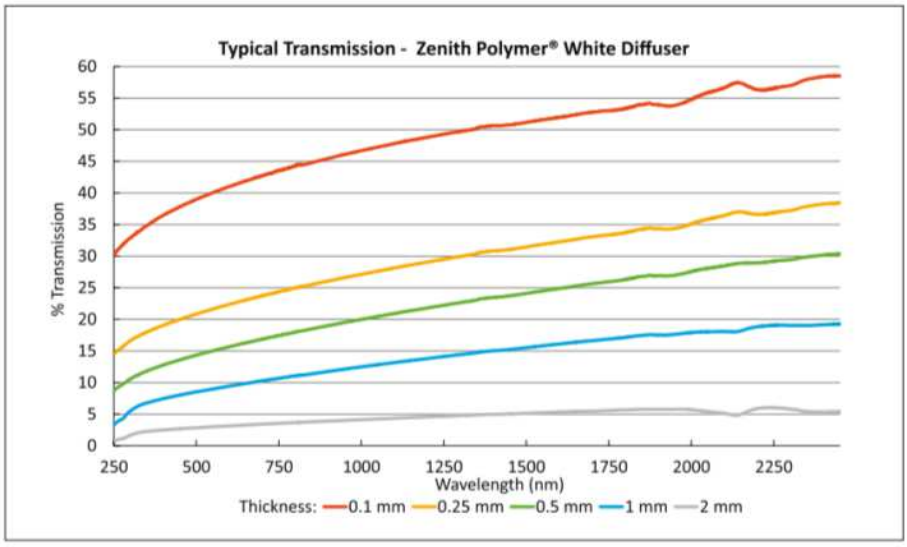

Figure 2.2. The typical transmission of the Zenith Diffusion Material through the entire wavelength range of 250 nm to 2500 nm (according to *Zenith Specification Datasheet*).

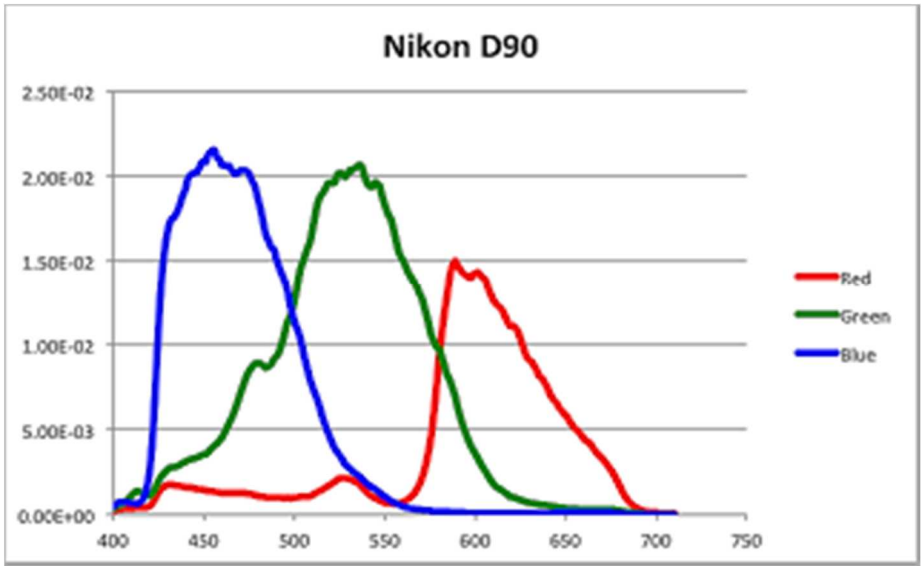

Figure 2.3. The spectral response of Nikon D90 camera to red (in red color), green (in green color) and blue (in blue color) color channels. The X-axis is a wavelength in nm and the Y-axis shows the relative signal response (according to *Vitabin, 2013*).

In the case of the second photo-system, a JAI Spark SP-5000-USB rapid high-resolution camera (manufactured by JAI, see specification for more details) was used. The best image quality was reached with the following camera adjustments: exposure 170; gain 100; shutter: 1.8; gamma: 0.45; gamma raw 7; pulse generator clock 0.72; acquisition frame 30.9943 Hz; acquisition raw 32264. The recorded images were stored in 16-bit grayscale PNG format (resolution: 2048^{x}2560). The Delay between shots was 1000 ms, which, in comparison with Nikon D90 results, obtains more data for plotting more precise BZ reaction state-trajectories from more segments.

Like the case of the first photo-system, the second photo-system was constructed in a way to prevent the reflection of the camera and of light patches on the photographed surface of the reaction (see Fig. 2.4.). To isolate the experimental system from the laboratory light sources and to provide homogenous sample lighting, a two-layer cube was constructed from white plastic. On surface of the sides of the outer cube, there were homogeneous light sources, which were also dispersed through the sides of the internal plastic cube. In order to avoid camera reflection on the reaction surface, the camera body was positioned in the white photo tent (Opnamebox). Additional stabilization during photography was achieved by placing the entire structure on the Anti-Vibration Optical Table (CVI Melles Griot). The air conditioning system in the laboratory room maintained a constant temperature of 24° C.

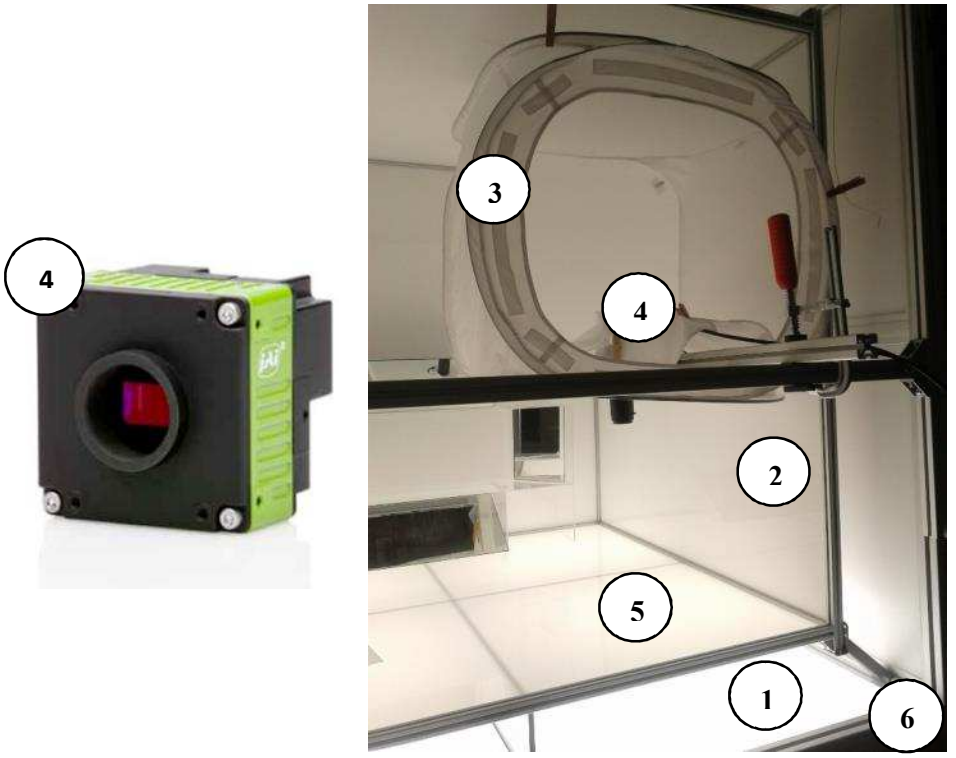

Figure 2.4. Photo of the second experimental installation for Belousov-Zhabotinsky reaction patterns monitoring: (1) outer plastic cube with homogeneous light sources; (2) internal plastic cube; (3) photo-tent; (4) JAI Spark SP-5000-USB photo-camera; (5) position of the sample (vessel with BZ reaction); (6) Optical Table.

2.3. Extracting Useful Information from the Belousov-Zhabotinsky Reaction Image Series

Considering that each camera chip producer has its own raw file format, the image preprocessing steps were different for the Nikon NEF format and the RAW image format from the JAI camera.

2.3.1. Nikon Images Preprocessing Strategy

The individual frames from the unique experimental run of the BZ oscillation process were processed in the sequence described in Fig. 2.4.

The original NEF format was transformed into a 12-bit PNG format without information loss. In the next step, the 12-bit format was transformed into the least information loss (LIL) format (*Štys et al., 2016*), where most the information was still preserved. Then the relevant region of the image was extracted by manual selection using the Expertomica cell marker software (*Císař, Štys, 2011*). The relevant part of the image was analyzed with the calculation of point information gain (PIG), point information gain entropy (PIE) and point information gain entropy density (PIED) (*Rychtarikova et al., 2016*). The resulting spectrum of values, collected from the image sequence, was subjected to multivariate analysis which resulted in objective classification of states along the BZ self-organization trajectory.

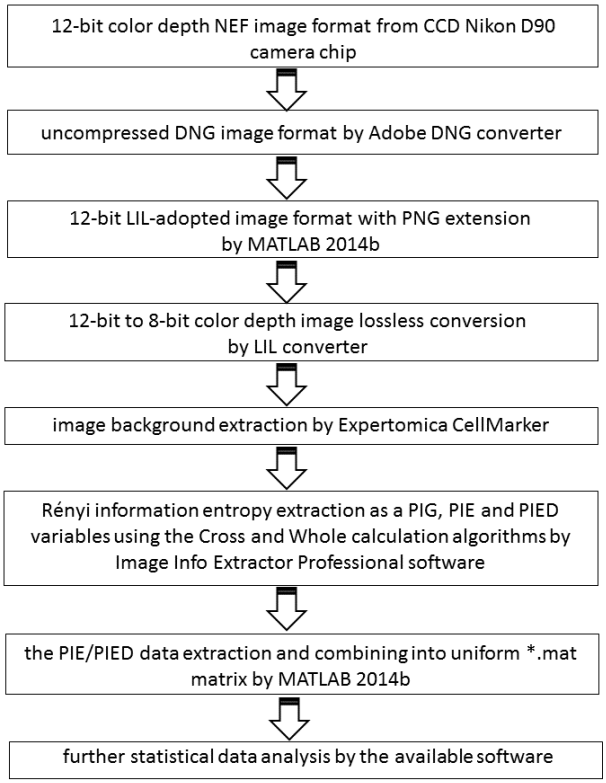

Figure 2.4. The sequence of manipulations carried out for each Belousov-Zhabotinsky reaction image for the BZ system state-trajectory construction.

Nikon Electronic Format (NEF, see *Nikon Inc. 2016* for the details), the Nikon's RAW file format, does not come directly from the camera CCD image sensor, it is transformed after the capture by the camera chip from the original 14 bit digital set. In other words, is an image format in which the unmodified data is written on the memory card was already processed in the camera and we do not have access to the original signal. The image files contain all the image information captured by the camera's sensor, along with the image's metadata (the camera's identification and its settings, the lens used and other information). Despite the high image quality, the lack of a uniform standard for the RAW data is another significant disadvantage of this format. In order to convert this specialized NEF format into the PNG image format which is necessary for further analysis, we needed to convert the NEF images to DNG, which is a specific kind of TIFF file, and transform them into MATLAB Tiff class images with PNG extensions *(Eddins, 2011)*. These conversions were done in two stages.

During the first step, the NEF image format was converted to the DNG (Digital Negative) uncompressed (bit-packed) 12-bit color depth format without demosaicing by using the commercial software Adobe DNG Converter (version 8.7.1.311, see *Adobe Systems Inc. 2015* for more detail). The second image preprocessing step consisted of the DNG image format transformation to the one adopted for the LIL conversion procedure (*Stys et al. 2016d*, see also Least Information Loss (LIL) Conversion section below for the details) that has PNG extension. The DNG to PNG image conversions were performed in MATLAB® (version 2014b, 8.4.0.260532 64-bit, developed by *MathWorks Inc., 2014)*. The conversion algorithm makes a structure which contains Exif information (metadata embedded within images) associated with the DNG version of the image file, reads the image metadata from the current image file directory (IFD) in the MATLAB Tiff class file, and stores the obtained files with new names as images with a PNG extension format.

The final product of the image transformation is the adopted PNG signature and extension for convenience to further LIL conversion with nonlinear quantization off the original 12-bit values (coming from Nikon raw sensor data compression procedure – *Martinec, 2010*) and GBRG Bayer grid that contains the same metadata information as original NEF files.

A full-color RGB image typically consists of three color channels—red, green and blue. The digital camera sensor actually captures one grayscale intensity value at each pixel location. Color filters are applied to each pixel to imitate the human perception of light (so-called Bayer masks – *Bayer, 1976*). The resulting capture still has just one full channel of information, but some of those pixels represent regions in part of the spectrum---for example, some represent green and blue spectral regions.

Least Information Loss (LIL) compression format was developed by our laboratory (*Náhlík et al., 2015*). It preserves most of the information contained in the 12/16-bit original data and creates a foundation for an objective visual evaluation of an image series, as it allows for the maintenance of scale along the whole image series.

The data conversion is performed in two ways:

- unoccupied levels are removed in all images individually and the remaining levels are expanded uniformly into 256 levels;
- only levels which are unoccupied in all images in the series are omitted and the remaining levels are expanded.

The LIL conversion does not offer any possibility to adopt the relative intensity levels to the visual perception by the human eye. Thus, the resulting images may seem strangely colored. But it should be noted that for image comparison only the intensity histogram is important. The LIL conversion is very useful when the color camera is used for technical or scientific purposes. For our purposes, when we assess the distribution of intensities in space, such a procedure is vital.

We performed LIL conversion of preliminary prepared images as described in the previous section for 12-bit color depth NEF.RAW images (Nikon D90 only provides one color depth option) with the following software set-up:

- RAW Bit Color Depth = 12 bit;
- the resulting .DNG.LIL.PNG image format has 8 bit color depth;
- the applied Bayer grid is GBRG;
- the demosaicing algorithm is Simple LIL (normalization of the all RGB color channels together);
- the calibration rows and columns were removed.

The results of the LIL conversion operation with corresponding histogram for each color channel in comparison with RAW.NEF and losses .JPEG conversion are presented in Fig 2.5.

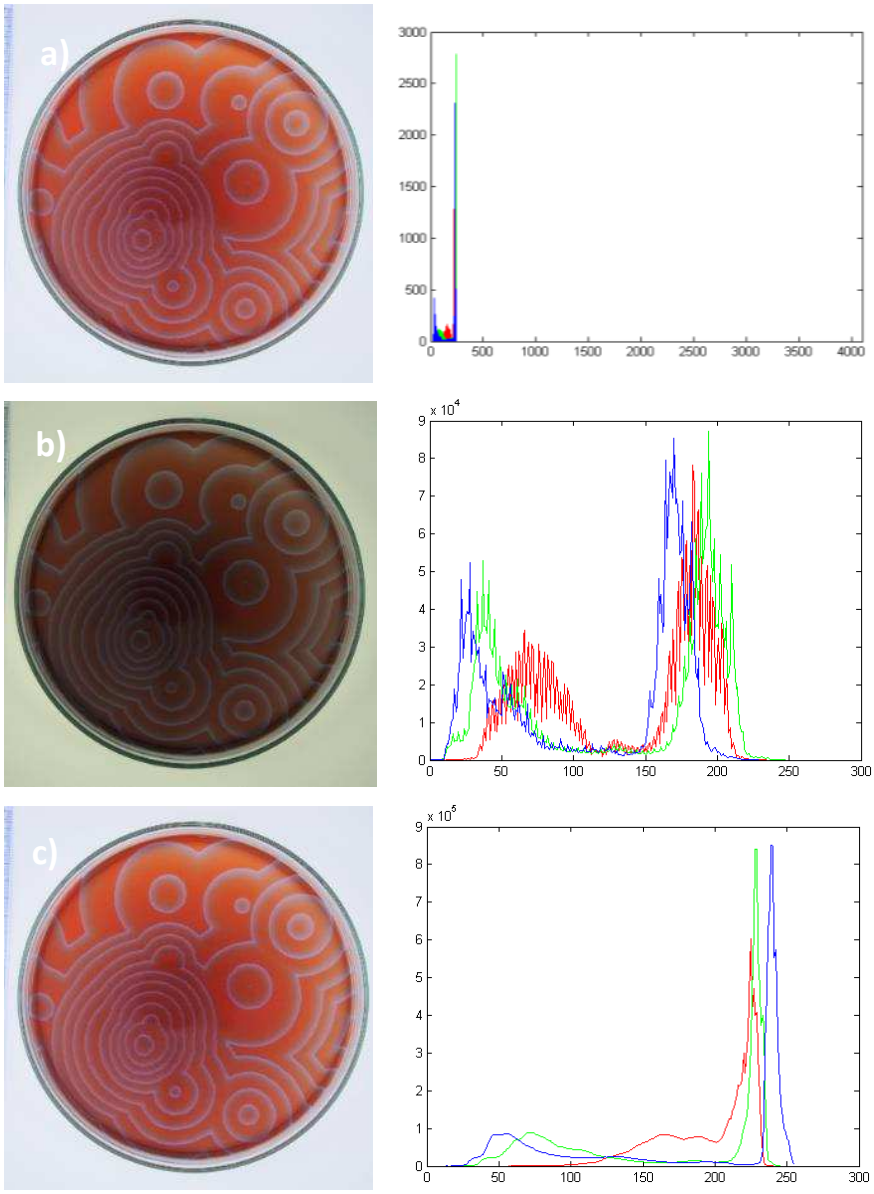

Figure 2.5. Example of the LIL conversion performance. The RGB color profiles histogram (right side) and image view (left side) represent the difference between original (a) 12-bit color depth (4096 intensity levels) NEF images, (b) images converted by the LIL algorithm 8-bit color depth format (256 levels), and (c) common JPEG 8-bit color depth format (256 levels) images. LIL conversion saved the original amount of intensity profiles for each color channel, and the JPEG conversion algorithm merges the unique intensities. Therefore, the intensity histograms of JPEG images look smoother than LIL-converted image histograms.

The image background (outside Petri dish boundaries) has been found to not be the informative part of the image and was removed by Expertomica CellMarker software (*Císař et al., 2011, 2016*). This software was originally developed for manually labeling cells in a series of microscopy images. However, it provides a wide range of possibilities, including object ID assignment, scale definition, and storing the information about labeled cells into txt file. In this work, it was used for manual definition of the borders of the object of interest, border replication into the next frame, and extraction of the defined objects by cutting at the drawn border (see subfigures (a) and (c) at the Fig. 2.6.). The software also allows for visual inspection of individual color channels as well as the extension of levels and inspection of image patterns which differ only in a few intensity levels.

We use CellMarker software for the automatic extraction of the BZ reaction scene encapsulated in the reaction vessel's interior without any contrast adjustment procedure.

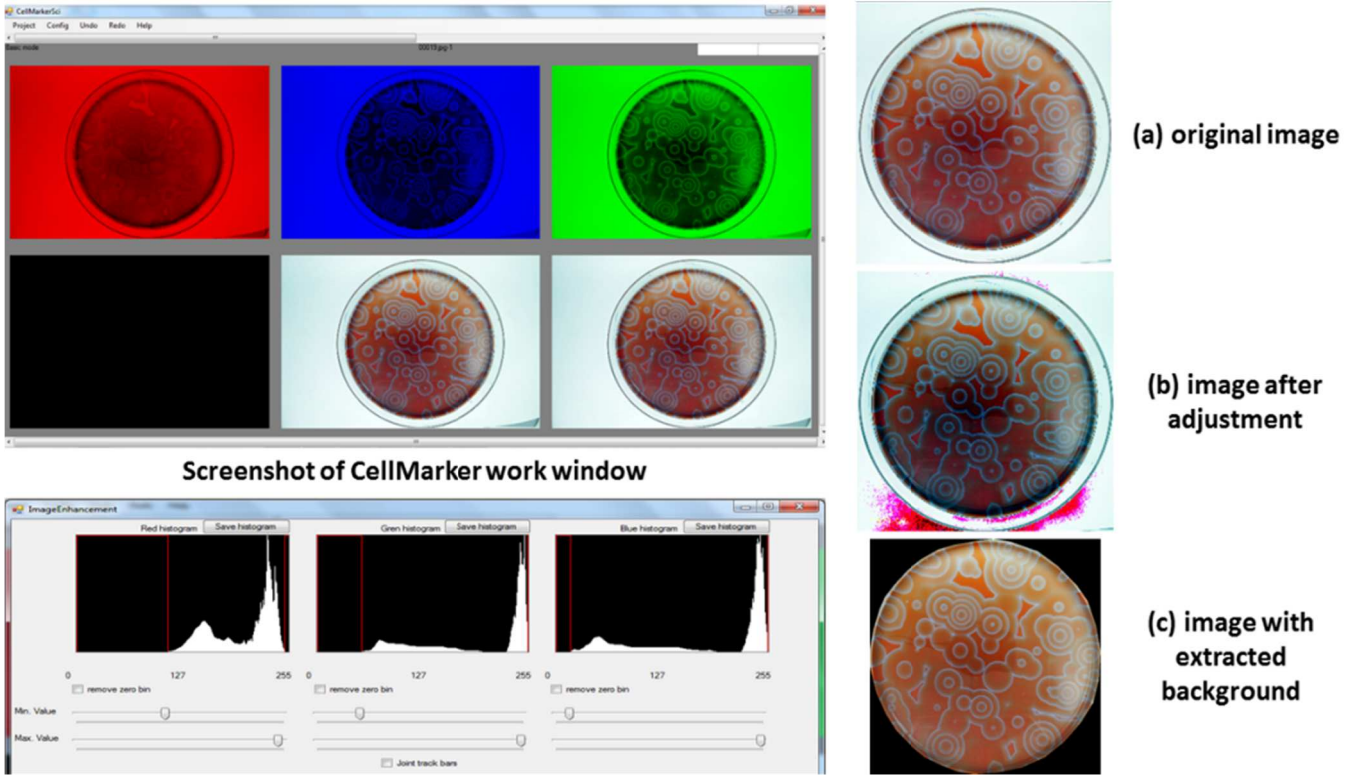

Figure 2.6. Screenshot of CellMarker work window with image view coming from each of RGB color channel with corresponded intensity distribution histograms (right column) and some software function demonstration applied on the original image (a), like contrast enhancement (b) and background extraction (c).

2.3.2. JAI Images Preprocessing Strategy

Image preparation obtained by the JAI camera was different from Nikon (see Fig. 2.8.), especially on the first-ever image processing steps. The crucial difference was that with the use of JAI camera we for the first time had access to the true primary signal captured by the camera chip.

The CMOS element in the JAI Spark SP-5000-USB camera produces the 16-bit grayscale PNG format. The object color composition and "true" curvature of the intensity profile information in each of RGB camera channel was related to spectral ranges of all three color channels (acquired by OceanOptics USB4000-VIS-NIR-ES portative spectrometer with range 350-1000 nm), measured in the same light conditions as ones applied under experiment recording. The specially developed software application – Image Corrector v. 1.2. was designed to solve the issue. The image correction was achieved by constructing a correcting matrix for the camera chip of the reference solution with a known spectrum and color. The result of the procedure is the construction of a calibration curve receiving the corrected micro-objects images with the "true colors." During the correction process, the image did not undergo any compression or conversion with smoothing algorithms where some pixels are interpolated and lost.

In the next step, the uninformative background and dish borders were dissected from the BZ reaction image by the MATLAB® (version 2014b, 8.4.0.260532 64-bit, developed by *MathWorks Inc., 2014)* tools. The software recognized the outlines of the dish borders and extracted only internal content within the vessel to the new created image, living the environment intensity signal as zero.

Processed in this way, images store the native information recorded by the chip that is corrected for all the non-idealities of the optical path.

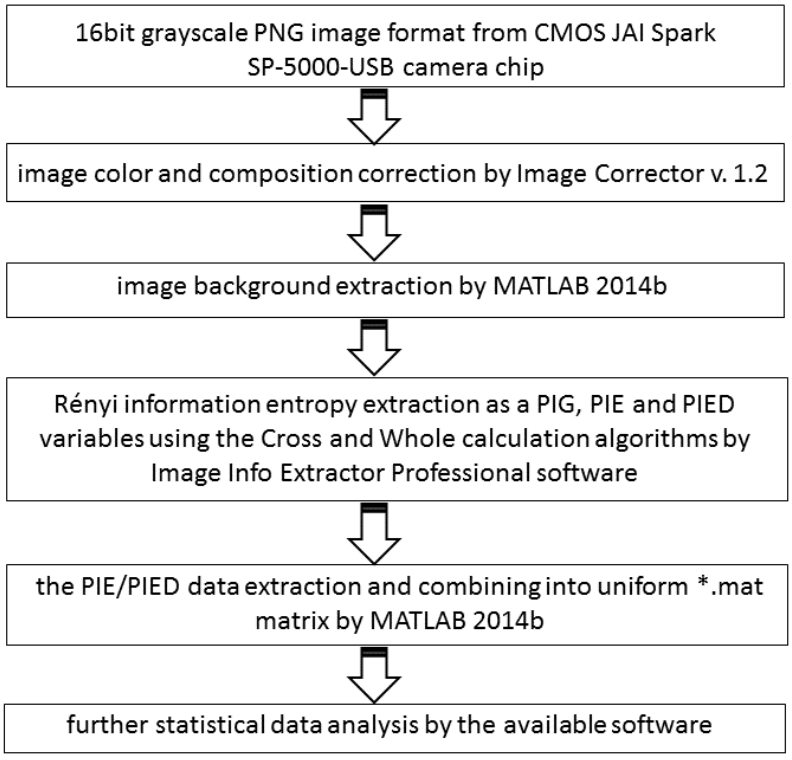

Figure 2.8. The sequence of manipulations carried out for each Belousov-Zhabotinsky reaction image from JAI Spark SP-5000-USB camera for the BZ system state-trajectory construction.

2.4. Information Entropy Extraction. Point Information Gain (PIG), Point Information Gain Entropy (PIE) and Point Information Gain Entropy Density (PIED) as Characteristics of the Structured Object State

As described in *Rychtarikova et al. (2016),* the PIG may be calculated using different assumptions about the pixel's surroundings. In this thesis, there were two approaches:

(a) No specific surrounding, i.e. the dataset from which the pixel was extracted includes all pixels in the image (the **whole** method).
(b) The dataset is formed by a cross of pixels' columns and rows whose shanks intersect in the position of the examined point (the **cross** method).

Each of these approaches is focused on certain type of information content of examined image - the former ignores any information about the pixel's surroundings, the other maps all possible surroundings at all available distances in the dataset. These two methods thus, from a certain point of view, represent the dataset completely.

Fig. 2.7. shows the dependency of PIG values of different pixels of on the value of the α parameter. The dependency of each of the values on the coefficient α is another unique characteristic of the distribution. Due to limitations of the digital precision, there is not any characteristic available over the whole range of α (in fact even the value of $\alpha \rightarrow \infty$ may be decisive). The visualization of the effect of different Rényi coefficients on the information entropy calculation output is shown in Fig. 2.8. From practical point of view, Fig. 2.8. demonstrates that a few α values must be used for the calculation of PIG, PIE and PIED to avoid the influence of digital averaging on the results. We used a selected set of 13-th values in the range from 0.1 to 4.0: 0.1; 0.3; 0.5; 0.7; 0.99 (in order to avoid $\alpha = 1.0$, the Shannon information entropy case, which would then be implemented differently in the computer); 1.3; 1.5; 1.7; 2.0; 2.5; 3.0; 3.5 and 4.0 in our calculation to cover most of the above-mentioned cases.

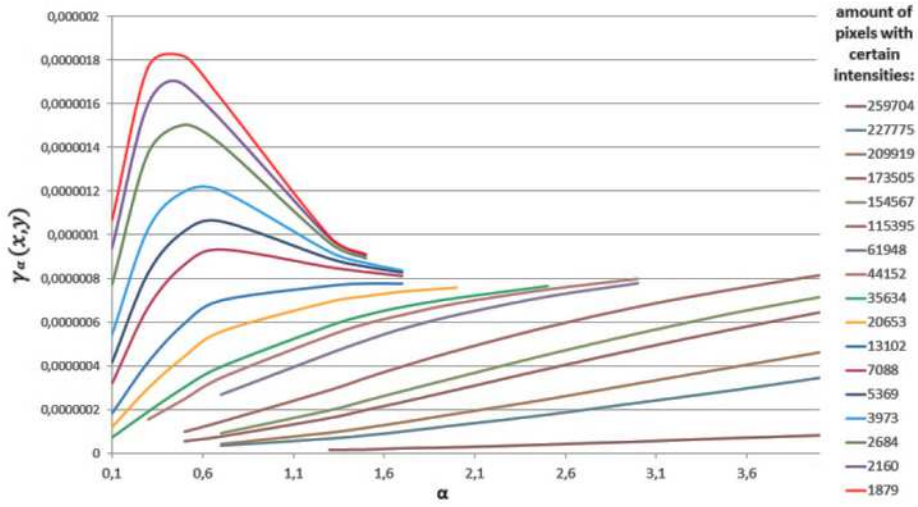

Figure 2.7. Distribution the $\gamma_\alpha(x, y)$ for different α-values for one examined image from the BZ reaction recording that collects a set of statistical characteristics of the image components (BZ particles) and is a unique feature of the BZ system state fixed by the camera at the shooting time Δt.

In the following steps, the PIG values for the single image pixels are assembled into PIE or PIED (see equations 17 and 18 in the Introduction part), which are unique characteristics of the whole set of image intensity scenes and can be understood, respectively, as a multiple of the average point information gain (H_α) and as an average gain of the phenomenon i (Ξ_α).

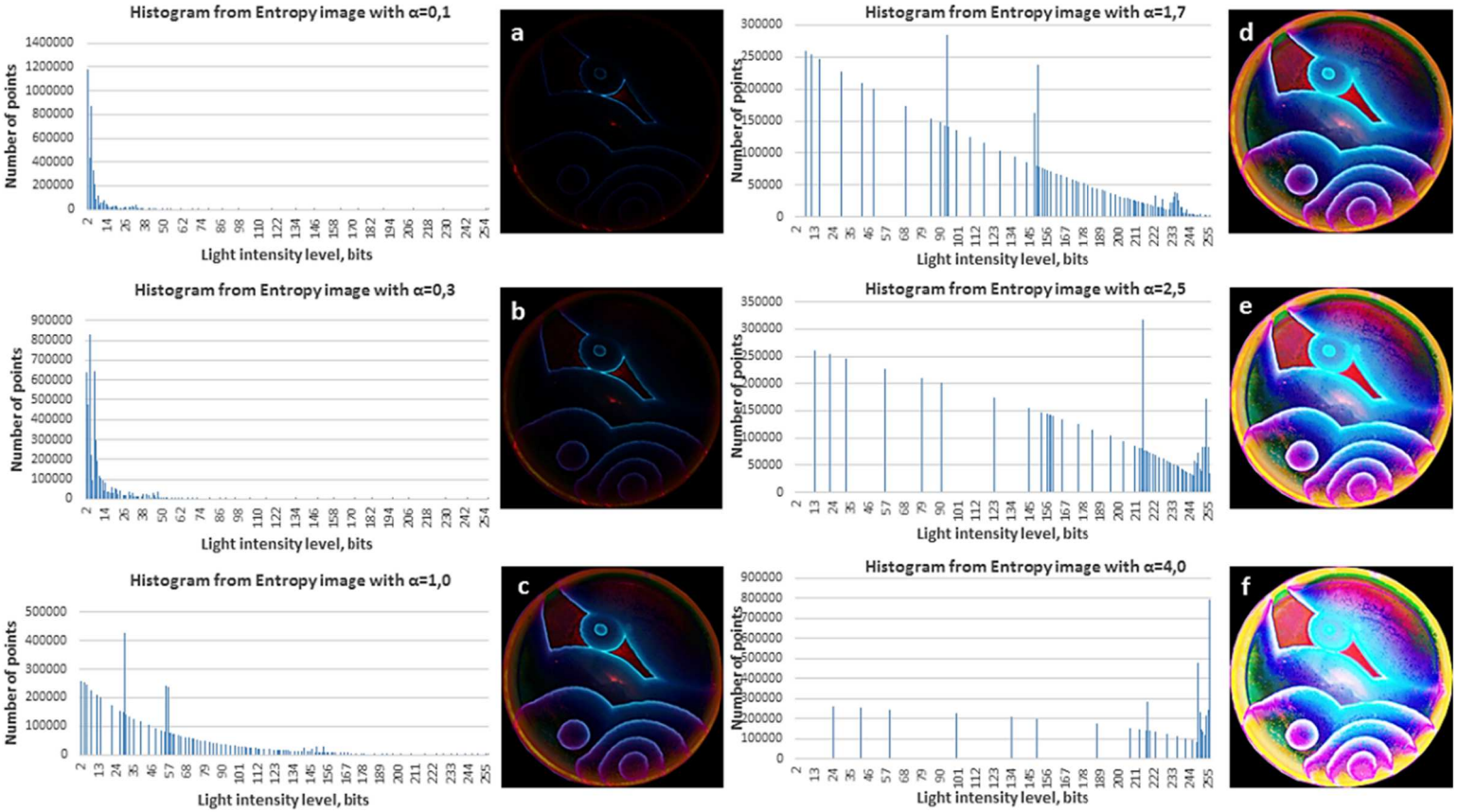

Figure 2.8. The light intensity distribution histograms for different cases of α-values for one BZ reaction Entropy image from experimental series with classical (90-mm diameter) Petri dish. For α<1, the events with rare occurrence are highlighted (a, b), when for α>1 the more eventful field of action falls into the focus of research (d, e, f), and α=1 present the intensity distribution, typical of the Shannon information entropy case (c). The intensity values are in the range from 0 to 255 (an 8-bit image).

2.5. Statistical Analysis of the Multi-dimension Data: Principal Component Analysis (PCA) and *K*-Means Clustering

After the image characteristic structure extraction as pair of H_α or Ξ_α for each image from the experimental series, we got a 39- dimensional data set, consisting of thirteen α-parameters, calculated for each RGB camera color channel. Taking into account that the number of frames taken during one full BZ reaction run is about 500, the outcome of one experiment represents a huge data matrix. Working with such a data dimension is very difficult.

We chose principle component analysis (*Pearson, 1901*) and *k*-means clustering (*Forgy, 1965*) for further statistical analysis of obtained data. The mentioned multivariate analysis was performed by using the commercial software the Unscrambler X 10.1 (*CAMO Software, 2011*).

In the orthogonal transformation, the PIE and PIED image data set---from a combination of thirteen Rényi coefficients and three (red, green and blue) color channels---is transformed into a set of values of linearly uncorrelated variables (called principal components) in a new coordinate system (orthogonal basis set). During PCA (NIPALS computation method), the initial data matrix (*X*) with *n* rows and *p* columns undergoes a decomposition into a set of empirical mean matrices ($\bar{X}$). The algorithm performs the subtraction from that sequence of *p*-dimensional vectors of weights (loadings) $w_{(k)} = (w_1, .., w_p)_{(k)}$ that map each row vector x_i of *X* to a new vector of principal component scores $t_{(i)} = (t_1, .., t_k)_{(i)}$, given by $t_{k(i)} = x_{(i)} \cdot w_{(k)}$, coming from each subsequent PC plus noise (the matrix of unmodeled residuals ε_k):

$$X = 1 \cdot \bar{X} + t_1 \cdot w_1^T + \cdots + t_{k(i)} \cdot w_{(k)}^T + \varepsilon_k \qquad (19)$$

where *1* is a vector of ones, symbol "*T*" means that matrix $w_{(k)}$ was transposed, and *k* determines the number of PC applying for the analysis. Scores describe the data structure in terms of sample patterns, which are the differences or similarities with each other, whereas loadings describe the data structure in terms of variable contributions and correlations, which are the amount of individual variable contribution to the examined PC. More details about PCA interpretation was provided in the work by *Abdi et al. (2010*).

The initial number of principal components for our data set was chosen to equal 10, but during the detailed analysis of explained variance from

obtained statistical model (see Discussion section for more details), the number of principle components (PC) was reduced to three. As a result, instead of the 39-dimension matrix we got the BZ reaction state trajectory charted in orthogonal 3D space (phase space) of the first three principal components, wherein each point (individual event that comprises a BZ patterns evolution track during individual experiment performance) is represented by projections of PIE or PIED outcomes from the combination of three color channels and 39-th α parameters for each time instant. We call the obtained plot: the individual (under the certain experimental conditions) phenomenological model of the BZ reaction.

The difficulty in the interpretation of the model arising from PCA-based dimensionality reduction (*Linsker, 1988*) is that the measurement does not give us the position of the point in a multidimensional chemo-mechanical space but only the projection of it into a fewer-dimensional space. In other words, we plotted the model not in real world (yet phenomenological) coordinates (as concentrations), but in orthogonal coordinates of projections which connected to the information entropy outcomes. These new coordinates may or may not be identical to internal orthogonal coordinates of the observed process, for example physio-chemical activities.

The obtained set itself does not represent the state of the system, which has to be determine by using other statistical analysis approach. We use the *k*-mean clustering approach to separate the BZ system state trajectory into similar points which may represent individual states that corresponds to unique phases of the chemical self-organization. We use PCA scores as inputs for the clustering procedure (*Ding et al., 2004*). The algorithm works on the principle of minimizing an objective function know as squared error function given by:

$$J(V) = \sum_{i=1}^{c} \sum_{j=1}^{c_i} (||x_i - v_i||)^2 \qquad (20)$$

where $||x_i - v_i||$ is the Euclidean distance between x_i (element in set of data points: $X = \{x_1, x_2, \dots, x_n\}$) and v_i (element in the set of centers: $V = \{v_1, v_2, \dots, v_c\}$), c_i is the number of data points in *i*-cluster, and c is the number of cluster centers.

The main goal of this approach is the objective separation of PC-space state trajectories into clusters weighted by shortest distance to cluster

core, each of which is supposed to present the one phase of system dynamics which is characterized by a set of states with similar properties. In order to determine the optimal value of *c,* we were led by the previous information about the investigated BZ system (see Introduction section) and our previous results (*Zhyrova et al., 2013, 2014, 2016*). Usage 7 clusters is the number that the best logically characterizes our system.

The output of the clustering in seven clusters more logically represents the states of the BZ reaction: chemical wave initiation, target patterns spreading through the available reaction space, the creation of the spiral wave centers and their competition with target waves, drift of the spiral wave centers and reorganization the BZ pattern picture, and chemical oscillation damping. Depending on imposed external conditions (such as reaction vessel size or geometry, or intensity of reaction component mechanical mixing), the intermediate states (coexistence target waves and spiral waves in the reaction medium) could elongate and stand out in a separate phase or, in the contrary, some stages could be eliminated during BZ system evolution (see Discussion section for details). Under these conditions, the "rule of seven clusters" is not followed and the algorithm either distributes the appropriate states into separate clusters or determines the smaller number of clusters for the investigated system.

In any case, performing *k*-mean clustering based on standard PCA of PIE(PIED)/α/color channel data gives us a quite nice logical separation of the image sequence into groups which we identify with states on the systems trajectory and gives a clear picture of BZ pattern dynamics in response to changes in initial conditions. An example of one experiment calculation, which is the BZ reaction state-trajectory with oscillating stages segmentation (by color), id shown in Fig. 2.9.

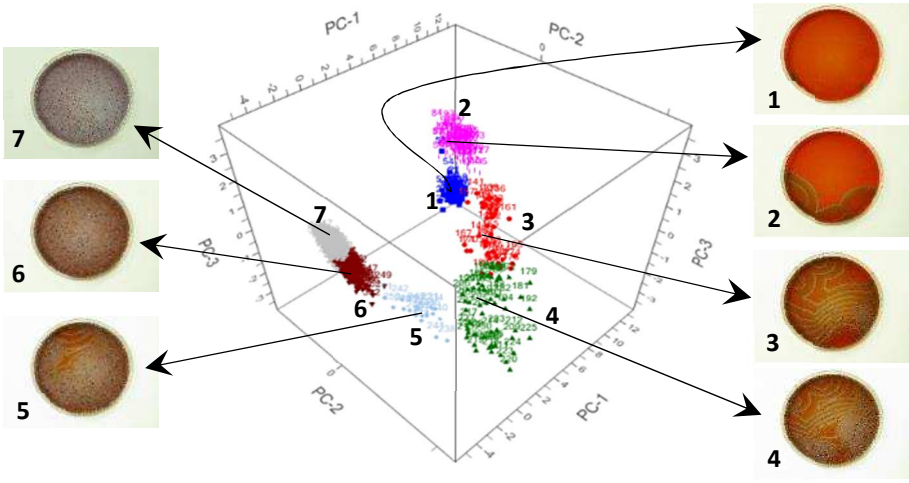

Figure 2.9. 3D model of Belousov-Zhabotinsky reaction (reaction state-trajectory) obtained by the developed information entropy calculation algorithm. The unique reaction oscillation stages highlighted by the different colors and images corresponding to them represent the reaction process time-schedule.

RESULTS AND DISCUSSION

3.1. Information Entropy Approach as a Method of Analyzing Belousov-Zhabotinsky Reaction Wave Formation

---

This chapter is based on Paper I:

Zhyrova, A., Štys, D., Císař, P., 2013. Information entropy approach as a method of analysing Belousov-Zhabotinsky reaction wave formation, *Chemicke Listy,* 107 (Suppl. 3): S341-S342. (Print). (IF 2013 = 0.196)

ABSTRACT

This work is aims to develop a method of analysis for self-organized systems such as living cell cultures or herds in native ecosystem. The Belousov-Zhabotinsky reaction (chemical clock) was chosen as a simple and appropriate model. Our proposed method is based on the information theory of mutifractal objects. We use the Renyi information entropy equation for the calculation of information gain by which a point contributes to the total information in the image, the point information gain. Obtained values present unique information about object structure. This method allows us to highlight tiny features in investigated samples' structures and characterize system behavior in dynamic systems.

1 Introduction

The Belousov-Zhabotinsky (BZ) reaction was devised as a primitive model of the citric acid cycle. When performed in a thin (few centimeters thick) layer, it creates easily observable travelling waves which may be captured by an ordinary color camera and analyzed. The system behavior in time indicates the existence of a sequence of distinct states stable for a certain period of time. The experimenter has control of mechanical constraints imposed on the system. Intermediate states in the reaction may be identified in all cases when the geometry of the experimental vessel allows the creation of travelling waves.

2 Material and Methods

Experiments were performed with the oscillating bromated-ferroin-bromomalonic acid reaction type (kits were provided by Dr. Jack Cohen) [1]. The reaction mixture was composed of the following solutions: 0.34 M sodium bromate, 0.2 M sulphuric acid, 0.057 M sodium bromide, 0.11 M malonic acid as substrate, and the redox indicator 0.12 M 1,10-phenantroline ferrous complex. All reagents were coherently mixed at the temperature of 22 ºC and added into a Petri dish. Images were captured by a Nikon D90 camera in regime time-lapse shooting with an interval of 10 seconds between snapshots.

In our practical approach [2,3], we calculated the Renyi entropy contribution of each of the points in the image. We calculated the Renyi entropy difference for the data set containing the examined point and the dataset in which the examined point was excluded. This is the Point Information Gain ($\gamma_\alpha(x,y)$) for given entropy of the order α:

$$\gamma_\alpha(x,y) = \frac{1}{1-\alpha} ln\left(\sum_{i=1}^{n} p_{i,x,y}^{\alpha}\right) - \frac{1}{1-\alpha} ln\left(\sum_{i=1}^{n} p_i^{\alpha}\right) \qquad (1)$$

where $\rho_{i,x,y}$ and ρ_i are probabilities of occurrence of given intensity for given point/*x, y* coordinate of camera pixel at a given α in the image without and with the examined point.

In the next step, the number of points of a given intensity is summed and normalized to obtain Point Information Gain Entropy (H_α):

$$H_\alpha = \sum_{x=1}^{x=n} \sum_{y=1}^{y=m} \gamma_\alpha(x,y) \qquad (2)$$

And in the final step of image processing, Point Information Gain Entropy Density (Ξ_α) was calculated:

$$\Xi_\alpha = \sum_{i=1}^{i=o} \Gamma_{\alpha,i}(x,y) \qquad (3)$$

For a given dataset, i.e. image, the ordered set of H_α and Ξ_α tuples a unique characteristic of the image, i.e. each image will have a different dataset, provided that the image is captured with infinite precision and the calculation is performed for all α values form 0 to infinity. In reality, the precision is defined by the digital camera and the set of α values is chosen arbitrarily.

Using statistical approaches such as principal component analysis (PCA) [4], we may construct orthogonal spaces which best fit the observed dataset. All data divided on the clusters depend on the value of the PCA-components. Each cluster of the trajectory presents one of the states of the BZ reaction.

3 Results and Discussion

The sets of H_α were used for describing the evolution of the system as a multi-fractal object. The state evolution is split into a logical sequence of clusters in the new orthogonal, although still phenomenological, state space. In Fig. 1 is shown the decomposition of the system trajectory of the Belousow-Zhabotinsky reaction into a series of states which are, for a distinct period of time, asymptotically stable under current conditions. Clusters (series of images) are very well separated and consistent in time, for each of group could find characteristic image represented the state of the system in their developing process. Moreover, each of the clusters' states should have its own spectrum of H_α values which characterizes it.

4 Conclusions

Applying the information entropy as the basic characteristics of the image is a promising area for further research, with the ultimate aim of creating a reliable method of automated segmentation of the self-organizing system state space obtained by a non-invasive imaging method. The trajectory segmentation may be used despite the fact that we do not know the proper manifold in the internal orthogonal coordinate space.

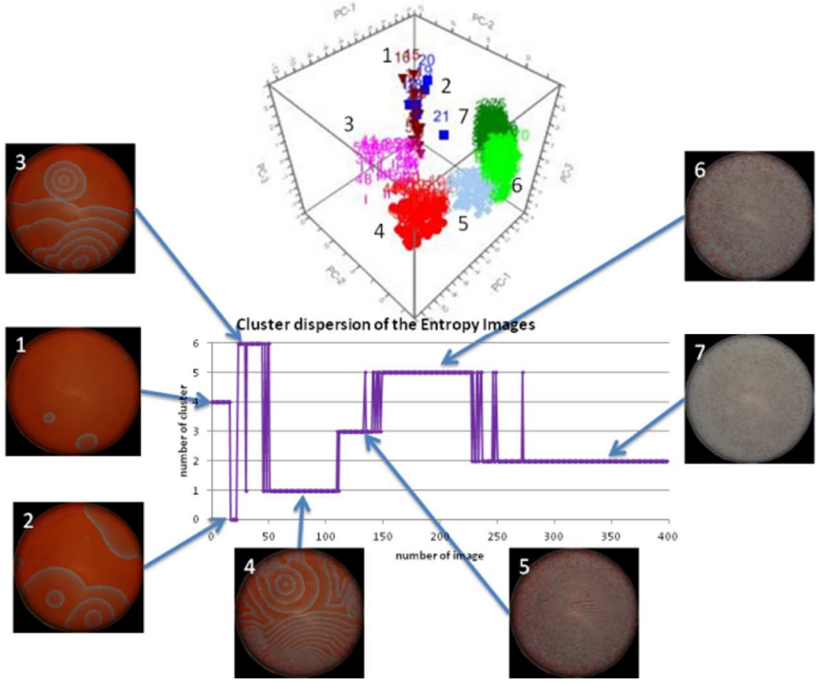

Fig. 1. The state trajectory of the BZ reaction performed in the Petri dish. Principle component analysis of the H_α allows us to designate different states of the system (changes in waves structure during the reaction evolution) from the point of view of the method clusters of points in the state space. Scores differ significantly between clusters oriented and form logical trajectory in the principal coordinates space.

References

[1] Dr. Jack Cohen at http://drjackcohen.com/BZ01.html

[2] Štys, D., Urban, J., Levitner, T., *Materials Structure in Chemistry, Biology, Physics and Technology* 2011, *18(1)*: 1211 – 5894.

[3] D. Štys at http://www.expertomica.eu/software.php

[4] http://www.camo.com/rt/Products/Unscrambler/unscrambler.html

3.2. Construction of the Phenomenological Model of Belousov-Zhabotinsky Reaction State Trajectory

---

This chapter is based on Paper II:

Zhyrova, A., Štys, D., 2014. Construction of the phenomenological model of Belousov-Zhabotinsky reaction state trajectory. *International Journal of Computer Mathematics*, 91 (1): 4–13. doi: 10.1080/00207160.2013.766332. (Print). (IF 2014 = 0.824).

ABSTRACT

The Belousov-Zhabotinsky reaction is used as an example of a self-organizing system which is easily and intelligibly observable and experimentally accessible. The analysis does not require elaborate reconstruction of series of 3D images as in the case of bird flocks or fish schools or organ behavior. The analysis of living cells' microscopic image series is even more elaborate. Moreover, the experimenter in the case of this BZ chemical clock has full control of the mechanical constraints imposed on the system.

We report both experimental and theoretical results using the Belousov-Zhabotinsky reaction as an experimental tool for analysis of the behavior of the self-organizing system.

We have created a state trajectory using several selected image identifiers (point information gain entropy – H_α). The H_α values define an approximate state space which may be analyzed using multivariate analysis. In this paper, we provide results of this analysis.

1. Introduction

The BZ reaction [1, 2] was devised as a primitive model of the citric acid cycle. To the surprise of the authors, it brought about the phenomenon of a chemical clock (in mixed systems) or spontaneous pattern formation (in still compartments). The distinct feature of the BZ reaction is that although it in fact consists of 80 chemical reactions,

relatively simple patterns arise and may be modeled by approaches such as cellular automata. Most BZ reactions are homogeneous.

For our experiments, we used a recipe for the Belousov-Zhabotinsky reaction modified by Dr. Jack Cohen [1] – bubble-type one with reagents of sodium bromate, sulphuric acid, sodium bromide, malonic acid, and 1,10 phenantroline ferrous complex as a redox indicator.

The BZ reaction makes it possible to observe the development of complex patterns in time and space with the naked eye on a very convenient human time scale of dozens of seconds and a space scale of several millimeters. The BZ reaction can generate up to several thousand oscillatory cycles in a closed system, which permits studying chemical waves and patterns without constant replenishment of reactants.

In the case of the Belousov-Zhabotinsky reaction, we can choose the form of the reaction vessel, which is impossible in living cells [4]. This approach allows us to discover whether the developed method is sensitive to changes in the shape and size of the investigated objects and how well the resulting model describes the internal changes in the self-organizing properties. Comparing the results of the study for both objects (the development of the cell cycle and the states' evolution in the reaction) makes it possible to judge the appropriateness and sensitivity of the developed method, and the impact of external factors (change of form, the formation of intercellular connections) on the state trajectories discovered by our model.

2. Preliminaries. Assumptions for model construction

The reason for developing an automatic method is that it is impossible to describe, objectively, all the features manually due to time and precision requirements. We base our analysis on the generalized stochastic systems theory [8], which is based mainly on proper description of the experimental dataset. In any real experiment, there is nothing equivalent to continuous time record. In the best scenario, the achieved time resolution is smaller than the highest time resolution that does not distort the response of the model used by us for experimental evolution. The sampling frequency must be at least double the

frequency of the fastest event. We must determine the time instants experimentally.

Let $s(t, a_u)$ represents the value of u-th variable (for example, individual values of measurement outcome i. e., spectral line intensity or molecular absorption) at a time point $t \in T$. Then the ordered n-tuple:

$$s(t) = [s(t, a_1), s(t, a_2), \ldots, s(t, a_u)] \quad (1)$$

is called the state of the system at time t. The state, $s(t)$, in our approach [3] represents the set values of recurrent objects' parameters for a given time window. The state, $s(t)$, is defined as the unique description of the system behavior at a given time instant. The state describes the system itself without knowledge of previous states. There is, however, no guarantee that the evolution of the system could be described solely based on a set of values obtained at given time instant. In reality, it is usually exactly the opposite case.

General system theory, provided by Zampa and Arnost [8], introduced the term "trajectory elements". By trajectory we mean mapping z, given by the Cartesian product:

$$z : T \times U \rightarrow \bigcup_{u \in U} V_u \text{ such that } z(t, u) \in V_u, u \in U \quad (2)$$

This minimal number of preceding and actual state variable values defines the trajectory element. Here T represents the ordered set of concrete time instants for a given experiment, U is a set of system attributes, and V_u is a set of system variables corresponding to the subset of attributes u which the system attains at time t.

In the Belousov-Zhabotinsky reaction, a variety of chemical transformations is taking place in the volume limited by the Petri dish. These reactions manifest themselves as ornate drawing of the reaction where every point is in occupied space. We must deal with the combination of a mechanical and a chemical space. Therefore, analyzing the data must clearly address this fact. The chemical space in equilibrium thermodynamic needs to be characterized with chemical potentials which are in logarithmic relation to activities a_i:

$$\mu_i = \mu_i^{\theta} + RT \ln a_i \quad (3)$$

where μ_i is the chemical potential of the species under the conditions of interest, μ_i^θ is the chemical potential of that species in the chosen standard state, R is the gas constant, and T is the thermodynamic temperature.

The chemical reaction pattern is a consequence of chemical dynamics, not a static event. Thus, the observed pattern is a reflection of the phase space rather than the state space. The problem is that we could not clearly define all the specific parameters of the system at each time evolution of the system. A key issue is the definition of system variables which may be measured at a time, although their relation to system attributes is unclear.

3. Dimension definition and multivariate analysis of the self-organized system

Self-organization arises in dissipative dynamical systems whose post-transient behavior involves fewer degrees of freedom than are nominally available. The system is attracted to a lower-dimension phase space, and the dimension of this reduced phase space represents the number of active degrees of freedom in the self-organized system. Estimating dimensions from a time series is one way to detect and quantify the self-organizational properties of natural and artificial complex system.

For our example, we consider the system as a set of chaotic attractors developing gradually in time and replacing each other.

Informally, the attractor $\mathcal{A}$ of a dynamical system is the subset of phase space toward which the system evolves. We define the phase-space volume of the attractor as $\mu(\mathcal{A})$. A measure μ is defined on the set $\mathcal{A}$ if the subsets $\mathcal{B}$ of the set $\mathcal{A}$ can be associated with real values $\mu(\mathcal{B})$ that represent how much of $\mathcal{A}$ is contained in $\mathcal{B}$ (the so called "natural measure"). Our entire fractional dimension is covered by a fixed-size grid (box-counting dimension) limited by the bounds of the investigated system. If $\mathcal{B}_i$ denotes the i-th box, let $p_i = \mu(\mathcal{B}_i)/ \mu(\mathcal{A})$ be a normalized measure of this box (the number of points in the box is taken into account). Equivalently, it is the probability of a randomly chosen point on the attractor to be in $\mathcal{B}_i$, and it is usually estimated by counting the

number of points that are in the i-th box and dividing by the total number of points.

The generalized dimension is defined by [6]:

$$\mathrm{D}_{\alpha} = \frac{1}{\alpha - 1} \lim_{r \to 0} \frac{log \sum_i p_i^{\alpha}}{\log r} \tag{4}$$

In such way D_{α} can be identified as a scaling of bulk with size:

$$\mathrm{D}_{\alpha} \sim \lim_{size \to 0} \frac{\log\ bulk}{\log\ size} \tag{5}$$

The parameter α determines the order of the generalized dimension. Limit $\alpha \to 1$ leads to a geometric average and, finally, $\alpha = 0$ corresponds to the plain box-counting dimension.

A generalized dimension is useful for quantifying the non-uniformity of the fractal or, in general, for characterizing its multifractal properties.

As an alternative to the scaling of mass with size, one can also think of the dimension of a set in terms of how many real numbers are needed to specify a point on that set. Here, dimension is something that counts the number of degrees of freedom. One way to extend this definition is to determine not how many real numbers but how many bits of information are needed to specify a point to a given accuracy. For example, for a line segment of unit length, k bits are needed to specify the position of a point to within $r = 2^{-k}$. In general, $S(r) = -d\ log_2(r)$ bits of information are needed to specify the position of the unit d-dimensional hypercube to an accuracy of r.

Consider partitioning the fractal into boxes $\mathcal{B}_i$ of size r. To specify the position of a point to an accuracy r requires that one specify in which box the point is. The average information needed to specify the box is given by Shannon's formula:

$$S(r) = -\sum_i p_i \log_2 p_i \tag{6}$$

Where p_i is the probability measure of the i-th box: $p_i = \mu(\mathcal{B}_i)/\ \mu(\mathcal{A})$. This relation leads directly to an expression for the information dimension of the attractor:

$$D_I = \lim_{r\to 0} \frac{-S(r)}{\log_2 r} = \lim_{r\to 0} \frac{\sum_i p_i \log_2 p_i}{\log_2 r} \quad (7)$$

Is necessary to stipulate that the Shannon entropy is a limiting case of the Renyi entropy:

$$I_\alpha(r) = \frac{1}{\alpha-1} log \sum_i p_i^\alpha \ , \quad (8)$$

which reduces to Shannon's formula in the limit $\alpha \to 0$. The generalized information dimension associated with the Renyi entropy is just the generalized dimension that has been defined:

$$D_\alpha = \lim_{r\to 0} \frac{-I_\alpha(r)}{\log r} = \frac{1}{\alpha-1} \lim_{r\to 0} \frac{\log \sum_i p_i^\alpha}{\log r} \quad (9)$$

The practical estimation of dimension begins with a finite description of the fractal object. In the model calculation, we have only the limit of the digital precision. In reality, we analyzed the representation of the multifractal object, i.e. a digitized photograph with finite resolution, as an aggregation with a finite number of aggregates, or a finite sample of points from the trajectory of a dynamical system.

In our case, we worked with images (initial form of our data). This is a two-dimensional representation of the spatial distribution of concentrations of chemicals giving rise to image color. In other words, the images are reflections of the position of the system in a two-dimensional chemo-mechanical phase space. It may be a reflection of a higher dimensional chemical space but such an assumption is not very likely to be true. In other words, the dimensionality of the systems in the Belousov-Zhabotinsky reaction shrinks from the observed over-80 chemical-individuals into a smaller number, perhaps even one chemical dimension. Our intention should be to find the most intelligible representation of the movement of the system in the phase space, a dynamic model which would allow the comparison of experiments of different types.

Obviously if the only source of information is the intensity of the signal in the given color channel at given image point, the only measure which may be examined is the multifractality of the object at the image. The intention of this article is not to discuss in depth the theoretical

background of our method but to show its practical use in the case of an image series of objects of changing structure.

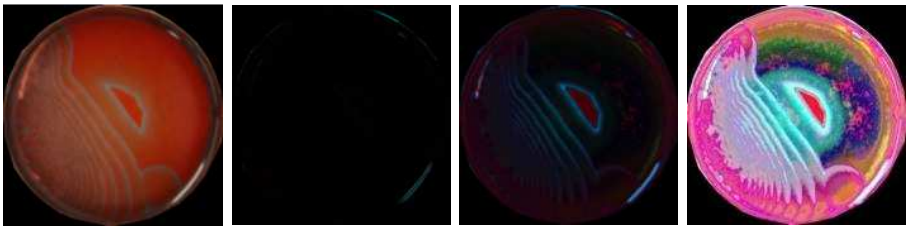

original image α = 0.1 α = 1.0 α = 2.5

Figure 1. Examples of the influence α parameter on the value of Point Information Gain ($\gamma_\alpha(x,y)$). The color and intensity is the result of projection of the $\gamma_\alpha(x,y)$ for the given color channel and image point into the RGB space. In contrast to the original image at the left side, where the colors are given by true coloration of the reaction vessel, the $\gamma_\alpha(x,y)$ - based images represent pseudo-colors used for visualization of the information structure of the image. Due to the multifractal structure of the image, there is no single α value which would be appropriate for proper representation of the intensity distribution in the whole image. With changing α value, different occurrences are emphasized. At low α the rare points are emphasized; at high α, points with higher occurrence are emphasized.

We chose the Belousov-Zhabotinsky reaction because we believe that the process generating the structure actually has the character of the chaotic attractor, although quite probably it is in a 2-dimensional mechanical and chemical space of low number of dimensions.

In our practical approach, we calculated the Renyi entropy contribution of each of the points in the image. In practice our resolution is limited by the data point. We calculate the Renyi entropy for the data set containing the examined point and the dataset in which the examined point was excluded. This is the Point Information Gain ($\gamma_\alpha(x,y)$) for given entropy of the order α:

$$\gamma_\alpha(x,y) = \frac{1}{1-\alpha} ln\left(\sum_{i=1}^{n} p_{i,x,y}^{\alpha}\right) - \frac{1}{1-\alpha} ln\left(\sum_{i=1}^{n} p_i^{\alpha}\right), \qquad (10)$$

where $\rho_{i,x,y}$ and ρ_i are probabilities of occurrence of given intensity for given point/*x, y* coordinate of the camera pixel at a given α in the image without and with the examined point.

The question remains how large the dataset used for calculation of the $\gamma_\alpha(x,y)$ should be.

In the next step, the number of points of given intensity is summed and normalized to obtain Point Information Gain Entropy (H_α):

$$H_\alpha = \sum_{x=1}^{x=n} \sum_{y=1}^{y=m} \gamma_\alpha(x,y) \tag{11}$$

For a given dataset, i.e. image, the ordered tuple of dimensionless α coefficient and H_α is a unique characteristic of the image, i.e. each image will have a different set to the extent of the precision of the digital imaging. As seen from comparing the equations (9) and (10), respectively (11), H_α is a measure of the same characteristics of the object as the generalized dimension D_α. Detailed reasoning why this simplification was chosen for practical reasons is beyond the scope of this article. Nevertheless, it is beyond doubt that with a given technical setup, the set of H_α for a sufficiently high number of α values is uniquely characteristic of the image. Indeed, we may explore whether the H_α values could be used as phenomenological coordinates for construction of the phenomenological phase space of the multifractal image of the BZ reaction.

The $\Gamma_\alpha(i)$ occurrence histogram of images obtained for different α values indicates that the set of cumulative variables H_α is a unique identifyier of the image. We may construct a provisional phase space based solely on H_α values. There is, however, no guarantee that $H_\alpha$values are linearly independent; quite the contrary, they probably are not orthogonal for many reasons both fundamental and technical in scope. Using statistical approaches such as principal component analysis (PCA), we may construct orthogonal spaces which best fit the observed dataset [3,4].

The probability density function may be calculated for the whole object/image intensity distribution or for some kind of local surrounding. These two approaches differ in principle. In the case of using the whole image intensity distribution/approximate probability density function, we consider only the "meaning" of the point. This is the whole image approach, indicated by the subscript *w,* which gives semantic information. However, when we define some context, we place the "meaning" into a certain "context". This is partly syntactic information. We decided to define context by using intensity distribution in the cross intersecting the image whose shanks intersect in examined point, with the cross approach indicated by the subscript *c*. Thus, we have two algorithms of calculation. For a detailed description, we refer the reader to our previous work [7].

The probability density functions' approximations, which we define in previous paragraphs, are reflections of the multifractal nature of the observed object. We consider them phenomenological variables in the same way as, for example, in chemistry the absorbance at a given wavelength is used instead of the activity/chemical potential of given compound. We do not have any information on the probability density function of the processes contribution to observed phenomena in experimental self-organizing systems equally well as we do not have any information on intensity and nature of molecular interactions which determine activity of given compound. In the case of a chemical clock, this analogy is very relevant. A discussion of this aspect deserves a separate paper. The only thing which will be done here is to use a statistical approach to best approximate variables of the system.

When nothing is known about the appropriate distribution, the best choice is to assume the action of the central limit theorem, and expect that the normal distribution will be the best choice. We were guided by this assumption by choosing the principal component analysis (PCA) as the method of multivariate analysis for our system proceeding [4]. Adequate expression of the system behavior in the phase space depends on coordinates' transformations and could not be mapped in a way that will skew normal distribution. The principal component analysis application consists of three steps: (1) normalization of each data-set, (2) calculation of the covariance matrix and (3) calculation of principal components, i.e. orthogonal coordinates which determine directions of

the main variance in the data. The resulting variables, called principal components, may be assumed merely as practical descriptors of the system. However, the principal components are also the best approximation to internal orthogonal coordinates in state space approximate to stochastic (macroscopic) variables of which each has normal distribution. Thus, we construct a coordinate system in which the state function is a plane in multidimensional space.

4. Analysis of the obtained BZ reaction state trajectory

After all the transformations above are done for a given image, we obtain a complex system in the 39-dimensional space (13 variations of α parameter in 3 different color filters). One of the advantages of the method which we use for multivariate analysis is that this method – Principal Component Analysis (PCA) –allows us to not only reduce the dimensionality of the space to a 5-dimensional space, but also transform a set of our data in orthogonal coordinates which generally fits with the theory we use. Special arrangement of the data-points in the space of PCA-components creates the phenomenological state trajectory of the BZ reaction in the phenomenological phase space defined by statistically well-defined orthogonal coordinates (Figure 2).

One of the drawbacks of PCA is that, due to the nature of mathematical apparatuses working at the base of the method, we get a distorted multidimensional space for the realization of experimental data: each of the positions of points in state trajectory is projected onto a plane. This can distort the spatial structure of the discovered model. An important criterion is that, in the processing of data by the PCA-method, the noise is filtered out and the important data signal stays unchanged (sometimes useful signal intensity is largely inferior to noise ratio). These correlations between each of the PC-components to the original data should be found in successful analysis. Total residual and explained variances provided by PCA show how well the model fits to the data (in our case we analyzed the second one).

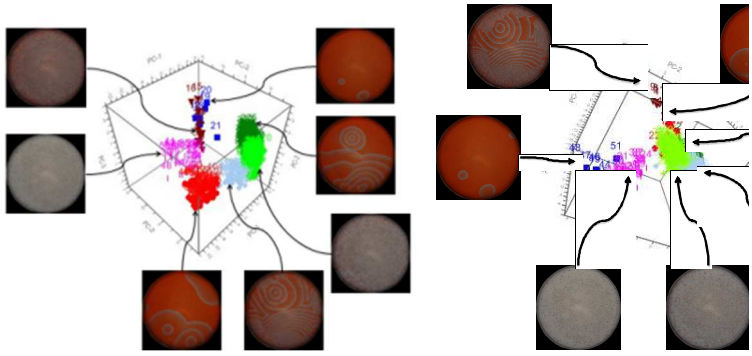

Figure 2. The state trajectory of the BZ reaction performed in the Petri dish. Principle component analysis of the $H_{\alpha,w}$ calculated by the whole image method is presented on the left, and principle component analysis of the $H_{\alpha,c}$ calculated by cross method is presented on the right. It is possible to notice the differenced caused by the method of entropy calculation when you compare syntactic–cross method and semantic–whole image method information.

First, we section the state trajectory into clusters. They should reflect the change in the overall character of the observed image structure as it is clearly observed during the time evolution of the reaction. With respect to the inner structure of the phase space, which is only reflected in the image, we believe that the state space is partitioned into basins of attraction of individual asymptotically stable structures. In the real BZ reaction, it is possible to observe several observable typical states of the reaction following each other as the reaction proceeds: first the formation of colored spots in the reaction medium, then their growth into a series of expanding concentric rings or spirals, the development of dense waves, then development of an oscillating pattern, and at last the disappearance of the structure. For a more detailed analysis of the structure of the system we have conducted nonhierarchical type of clustering (k-means clustering analysis) based on certain specific distance measurements between the components of the system. We used our state trajectory obtained by the principal component analysis. Each of the clusters should present a certain state of the system and have its own spectrum of values that characterizes it [5].

In this practically focused article, we show that in our new phenomenological orthogonal space we are able, using k-mean clustering method and with the assumption that nearby points belong to

the same stage of evolution of the system, to discriminate between states. As we do not have any independent measure of the identity of the state, the only measure for us was that clusters in the phase space have to logically follow each other with only certain possible overlaps in intermediate cases, i.e. that they lay on state trajectory of the system.

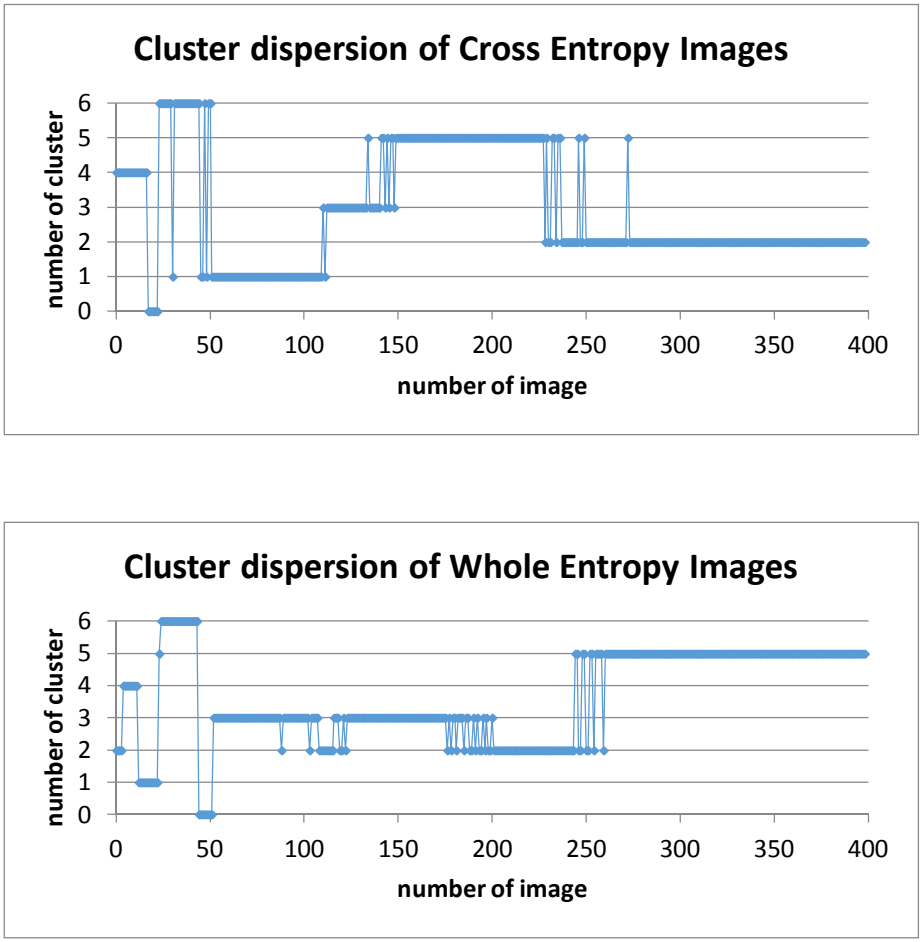

Figure 3. The developed method of calculating the entropy with the exception of one pixel allows us to successfully carry out a cluster analysis of the obtained state trajectory and to separate the individual clusters (in this example there are 7) corresponding to certain phases of the reaction.

We started with two clusters and increased their number and found that the minimum number of clusters which satisfies this assumption is seven and that using the $H_{\alpha,\,c}$ values is more feasible than using $H_{\alpha,\,w}$ (see the annex 1 for details of the procedure) value. Using this logic, we may say that it was experimentally proved that the division of the state trajectory into seven states most adequately describes the behavior of the system. There are some obvious problems in this analysis. They come mainly from the smooth transitions between different states which results in the existence of mixed states. Nevertheless, we were able, for example, to identify three different states in the late oscillating phase of the reaction which were obvious after following expert examination. This is shown in the diagrams (Figure 3 and 4) of cluster distribution --- even in the course of successfully chosen number of clusters in the distribution, it is impossible to avoid some points which may not be assigned to a particular cluster.

The important question is what the origin of this success of data classification is. For that we must examine contribution of individual components. The result is given in Figure 5, where the spatial distribution of $\Gamma_{0.1,w}$ is depicted. In this way, rare points are emphasized. We may analyze the result as a three channel spatially resolved colorimetric assay. Obviously, there is a big difference between information carried by different channels. The $\Gamma_{0.1,w}$ mainly emphasizes rare points. In the blue channel, these points are located at the contours of the object; in the green channels, we see contributions of "smears" behind travelling waves; while in the red channel, we see a strong contribution of structures inside the objects. From the first sight, it is clear that there is nothing like "sick", "healthy" and "infected" cells which are considered in the cellular automata model of the chemical clock.

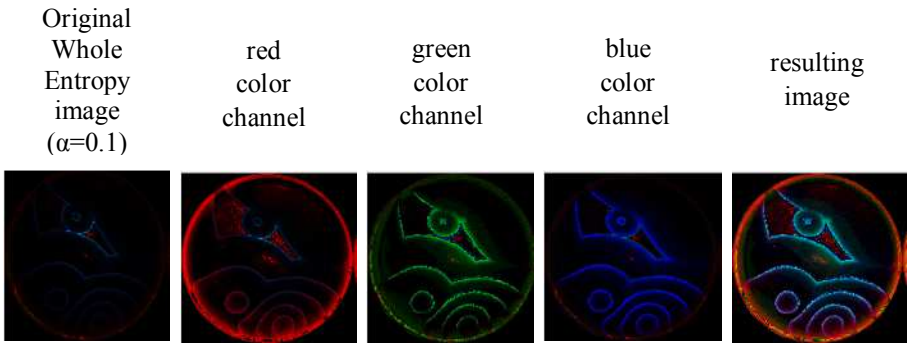

Figure 4. Color filter apportionment used not only for plotting 3D construction for further computer analysis and model plotting, but also to make more visible some details in our image that are sensitive to light wave length. The image processing was performed by the software tool CellMarkerSci [9], which permits us to separate a RGB image into three components according to three image color channels and change the span of observed intensity levels.

The image below (in Figure 5) represents $\Gamma_{2.0,c}$ by which each particular point contributes to the overall information in the image of the reaction dynamics. The blue channel carries most structural information and was thus chosen as an example image. The upper image represents the full information about the blue channel for which $\Gamma_{2.0}$ was calculated using cross sampling of the image. The central and bottom images show how sections from the original image in one blue color channel are represented in the image. Large areas, with low $\Gamma_{2.0}$, represent the noise; medium $\Gamma_{2.0}$ highlights edges of the image; and rare, high entropy points, represent stripes of chemically different regions in the medium.

The image represents the $\Gamma_{2.0,c}$ value by which each particular point contributes to overall information in the image of the reaction dynamics. As the main changes are observed in the blue channel, it carries the most information about the shapes of spreading waves (which also have blue color), which may be shown by its contribution to discrimination between clusters. Thus, as we mentioned earlier, the blue channel was chosen as an example image.

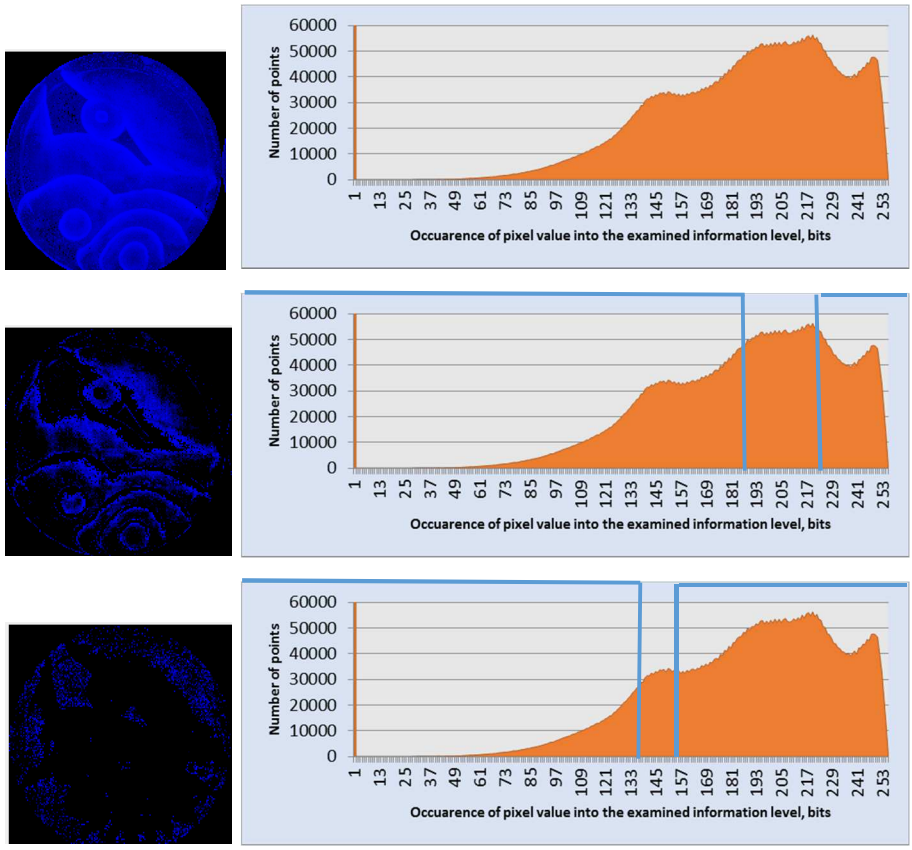

Figure 5. Selected regions of different $\Gamma_{2.0,c}$ value. Here, as we utilize a circular vessel, the number of relevant points changes, which causes the peak-like appearance of individual signals. Points of similar types in similar locations contribute to individual peaks. Lines may be separated into groups and examined selectively.

The whole method is prone to technical errors caused mainly by signal digitization, image compression, etc. These problems could not be discussed here. The success of grouping of image sequence into logical states indicates that many of these potential problems are not critical for analysis of the complexity of the images with the point information gain entropy method.

5. Conclusions

Based on the obtained data, we can conclude that using the proposed method point information gain entropy it is possible to classify images of dynamic, complex systems. We may construct statistically relevant approximations of the trajectory of the observed system through phenomenological phase space. It is usually advantageous to utilize this approach for considering the context of the point in the image for many reasons. There may be "intelligent smoothing" caused by the grouping of individual points combined with inaccuracies caused by numerical precision. There may also be real differences between the use of semantic and syntactic information. In any case, this method allows us to automate image classification in a series of evolving or similar images which is would be extremely labor-intensive to do manually.

The application shown here was performed using a prominent example of the complex, self-organizing system which, due to natural change of parameters, also jumps between two distinct regions of the chaotic attractor or even between different attractor types. Principal component analysis using a set of $H_{\alpha,w}$ component analysis is possible for the clustering of similar states, but it does not give any information about the possible models.

In particular, we may say that the phenomenological state trajectory of the Belousov-Zhabotinsky reaction may be distinguished into several rather clearly separable states. The validity of the observation of one image for the calculation of statistical variables, which is behind the calculation of generalized dimension D_α, remains an open question. Therefore, it is not possible yet to derive any conclusions about the internal structure of the observed self-organizing system. The proposed approach requires numerous technical improvements before we may be able to draw more in-depth conclusions about the origin of the system observation.

References:

[1] B. Belousov, Periodic processes of malonic acid oxidation in a liquid phase, Biophysics 9 (1959), pp. 306–311.

[2] J. Cohen, Belousov–Zhabotinski Reaction Do-it-Yourself Kit, 2010. Available at http://drjackcohen.com/BZ01.html (accessed 2 September 2010).

[3] D. Stys, HCTFOOD; software available at http://www.expertomica.eu/software.php.

[4] D. Stys, J.Vanek, T. Nahlik, J. Urban, and P. Cisar, The cell monolayer trajectory from the system state point of view, J. Mol. BioSyst. 7(10) (2011), pp. 2824–2833.

[5] D. Stys, P. Jizba, S. Papacek, T. Nahlik, and P. Cizar, On measurement of internal variables of complex self-organized system and their relation to multifractal spectra, Sixth InternationalWorkshop on Self-Organizing Systems, IWSOS 2012, Delft, The Netherlands, 2012.

[6] D. Stys, P. Jizba, T. Nahlik, K. Romanova, A. Zhyrova, and P. Cisar, Practical approach to construction of internal variables of complex self-organized systems and its theoretical foundation, European Conference on Complex Systems, ECCS'2012, Belgium, 2012 (To be published online by Springer Complexity).

[7] J. Theiler, Estimating fractal dimension, J. Opt. Soc. Am. A 7(6) (1990), pp. 1055–1073.

[8] J. Urban, J.Vanék, and D. Stys, Preprocessing of microscopy images via Shannon's entropy, Proceedings of Pattern Recognition and Information Processing, Minsk, Belarus, 2009, pp. 283–287.

[9] P. Zampa and R. Arnost, Alternative approach to continuous-time stochastic systems definition, Proceeding of the 4th WSEAS International Conference on System Theory and Society,Wisconsin, USA, 2004.

3.3. Effect of Spatial Constraints on the Self-Organizing Behavior of the Belousov-Zhabotinsky Reaction

---

This chapter is based on Paper III:

Zhyrova, A., Rychtáriková, R., Náhlík, T., 2016. Effect of Spatial Constrain on the Self-Organizing Behavior of the Belousov-Zhabotinsky Reaction*, IWBBIO 2016: Proceedings Extended Abstracts on Bioinformatics and Biomedical Engineering*, pp. 246-258, ISBN: 978-84-16478-75-0 (Print). (Book series, conference paper).

ABSTRACT

The effect of the deformation by the available space's limitations on the self-organizing system evolution space was observed. The common-known oscillating Belousov-Zhabotinsky reaction was chosen as an example of a primitive self-organizing system. As the pattern detection method was used, point information gain entropy density calculations could be made, which allowed us to determine subtle changes in pattern geometry and system states' identification. Upon the change of geometry, we observed changes in duration of reaction initiation phases and intrusions in the traveling wave period and shape when the BZ system was performed in the space constriction conditions. Transfer of the reaction mixture from a circular vessel to the square vessel induces the generation of atypical wave evolution. Results indicate that pattern formation is independent from actual concentration of chemicals in a broad range of concentrations. Structure dilution occurs at the end of the process when the reaction mixture is exhausted of the organic substrate and bromine oxidant.

INRODUCTION

The Belousov-Zhabotinsky (BZ) reaction, discovered more than half century ago [1, 2] is the most well-known representative of chemical self-organization in nature. The chemical system was chosen as an object of investigation due to analogues of organizational dynamics

provided by the reaction pattern phenomena with ones found in biological systems [3]. The result of the chemical oscillation in the thin (less than 3 mm) layer of reagents mixture, spread in Petri dish (2D space model), is manifested as pattern (chemical waves) formation whose geometry changes significantly during the system evolution. There is a great variety of shapes' geometry and their dynamics. The literature [4] distinguishes three main states of the BZ system: target patterns, travelling waves, and spiral waves. The transitions between these states are very blurred and there is as of yet no consensus on a logical explanation in the scientific community. There is also no general agreement on factors influencing the formation of wave generation centers. According to some researchers [5, 6], the initial concentrations of the reagents constituting the BZ system play a leading role in the pattern dynamic. The most famous model of the BZ dynamics – the Field-Koros-Noyes model [7] - reflects these works. From the other point of view [8, 9], the diffusion and convection of the reaction volume play the dominant role in the pattern shape definition. From the point of view of other authors [10], the network connectivity between oscillating space groups and its interaction with other waves forms a unique picture of the BZ patterns. Results in this paper fit with another popular model reaction, the cellular automata [11].

Only a few works, like [12], explored the influence of space geometry on pattern formation, reporting an experiment when decreasing the reaction cuvette width caused a change of the chemical oscillation regimen from chaotic to periodic behavior. According to the inverse Ruelle-Takens-Newhouse scenario [13], the system's behavior corresponds to the sequence period-1 → quasiperiodicity → chaos, or, as far as the attractors in the phase space are concerned, limit cycle → torus → strange attractor.

This paper aims to shed light on the above questions and on the importance of the geometry of space as a guiding factor for the predetermination of states of the BZ system pattern dynamic. Based on the results of previous research [14, 15, 16], we are using the information entropy changes---in particular the point information gain entropy density---as the parameter for characterizing the system structure. By consequent multivariate statistical analysis, we are able to define system states to the best technically achievable precision. We

believe that the work algorithm could be used as a tool for characterizing, designing, modeling, and understanding oscillation dynamics in nature and may find it to be applicable to such fields as bio-medical signal analysis, simulation and visualization of biological systems, or medical image processing.

MATERIALS AND METHODS

The oscillating bromated-ferroin-bromomalonic acid reaction was chosen for experiments (Belousov-Zhabotinsky reaction recipe provided by Dr. Jack Cohen) [17]. The reaction mixture includes 0.34 M sodium bromate (Penta), 0.2 M sulphuric acid (Penta), 0.057 M sodium bromide (Penta), 0.11 M malonic acid (Sigma-Aldrich) as substrate and redox indicator and catalyst 0.12 M 1,10 phenantroline ferrous complex (Penta). All reagents were mixed in the previously mentioned sequence. Experiments were performed in a specially constructed thermostat which included: an aquarium from Plexiglas and built-in aquarium base heated by the Low Temperature Circulating Water Bath-Chiller. The construction allowed us to adjust the needed temperature with inaccuracy of 0.1 °C. During the experiments described here, the temperature was 26 °C.

To create spaces of different sizes and geometry, different experimental dishes were used. These Petri dishes included: those with a circular shape with diameters of 35 mm, 90 mm, 120 mm and 200 mm (further referred as 35 mm Petri dish etc.) and square-shaped dishes of the size 75 x 75 mm and 30 x 30 mm. The mixing of all reagents was performed directly in the dish of the predetermined shape by hand for 1 minute.

The chemical waves were recorded by Nikon D90 camera in Time lapse shooting mode with an interval of 10 seconds between snapshots with Exposure compensation $+\frac{2}{3}$ EV, ISO 320, Aperture $\frac{f}{18}$ and Shutter speed $\frac{1}{10}$ second. Image quality was of the NEF 12-bit raw-format provided by the camera manufacturing company. As a result of subsequent image processing, the original RAW data format was transferred to the 12-bit PNG image format without losing data.

The experiments' recording of each particular dish shape and size were performed three times. Since the analyzed data showed the same pattern dynamics, and to prevent from overflowing this paper with redundant information, the results from one experiment for each particular case were presented.

The analytic tool invented by our work team is based on calculation of the Renyi entropy gain/loss for each pixel in single image [15]:

$$I_\alpha(p_i) = \frac{1}{1-\alpha}\ln\sum_{i=1}^{N} p_i^\alpha \tag{1}$$

where parameter α – the Renyi coefficient -- indicates the information cost with regards of the of the anticipated and examined probability distribution. Renyi entropy provides information characteristic of the multifractal system and is included in the generalized dimension measure $D_q = \lim_{l\to 0}\frac{I_\alpha(p(l))}{\ln(l)}$, which represents the information needed to specify a point on the set of accuracy p_i. Renyi entropy, unlike Shannon information entropy, has a measure that is much more flexible due to the parameter α. From the practical point of view for measurements in any multifractal structure, we may use $\gamma_{\alpha,x,y}$ to gain multiple parameters (i.e. measures) representing uncertainty corresponding to a given reference distribution.

To examine the point information contribution, we calculate the point information gain $\gamma_{\alpha,x,y}$ as a difference between the information content of a given distribution with and without the examined point:

$$\gamma_{\alpha,i}(x,y) = \frac{1}{1-\alpha}\ln\sum_{i=1}^{k} p_{i,x,y}^\alpha - \frac{1}{1-\alpha}\ln\sum_{i=1}^{k} p_i^\alpha \tag{2}$$

where k is number of elements in the discrete distribution, p_i^α and $p_{i,x,y}^\alpha$ are the probabilities of occurrence of given intensity for given point *x, y* coordinate of camera pixel without and with the examined point. By changing the α parameter we focused on the probability distribution of one type of the events of interest while suppressing the other. Just to have a general overview of the examined event, we used thirteen α values: 0.1; 0.3; 0.5; 0.7; 1.0 (Shannon information entropy case); 1.3;

1.5; 1.7; 2.0; 2.5; 3.0; 3.5. To collect the total information from a connected series of events, we determine point information entropy H_α as a sum of all $\gamma_\alpha(x,y)$, and point information entropy density Ξ_α as a sum of all $\gamma_\alpha(x,y)$ levels found in the image:

$$H_\alpha = \sum_{i=1}^{k} n_i \gamma_{\alpha,i}(x,y) \tag{3}$$

$$\Xi_\alpha = \sum_{i=1}^{k} \gamma_{\alpha,i}(x,y) \tag{4}$$

where n_i is number of points in the examined distribution. The H_α may be understood as a multiple of the average of $\gamma_\alpha(x,y)$, while the Ξ_α could be interpret as average gain of the phenomenon. From a practical point of view, Ξ_α gives the same emphasis to each different element of the distribution, is more sensitive to changes, and is thus more useful. It is also a principally different concept from standard entropy while H_α is merely its variation.

Obtained spectra Ξ_α vs. α were used to draw the BZ system state trajectory. We obtained a point in 13-dimensional space in which the structure of examined image is defined by Ξ_α values. The original space is in general not orthogonal. From these values, we did principal component analysis and obtained an orthogonal coordinate space whose first three principal components are reported on Figs. 2-7. The different states of the chemical system evolution were recognized by k-mean clustering analysis performed for each experiment separately. Since the patterns in the chemical system evolve in the strict order: target patterns → travelling waves → spiral waves, the sequence number of the cluster ought to associate with certain reaction stages for the different experiments and the charted state trajectory time synchronization was obtained for all of the performed experiments due to this experimental object properties.

In the selection of the optimal number of clusters, we were guided by knowledge from literature [4], according to which at least three different states should be presented in the BZ system (the case of smaller dish shapes we had used in experiments) and also by our assumption that in case of increasing the reaction space, the proper conditions for co-

existence of the intermediate system stages where both of the pattern regimes could be present in the same time on the reaction surface (the case of a bigger size experimental dishes) will be discovered. However, the crucial role in the number of *k* centers definition was played by the experimental image series time separation on the cluster dispersion histogram: for seven cluster domains, it presented the most logical scene. Therefore, the number of clusters in our method was adjusted empirically and for the majority of our experiments (with the exclusion of the smallest Petri dish with diameter 35 mm, and the square dish with side 30 mm, where the area limitation came into effect) was chosen to be seven. The clustering separation picture mentioned above was repeated with negligible variation for all repetitions of the experiments from the same dish shape and size cases.

RESULTS AND DISCUSSIONS

Circular reaction vessel

The space geometry and area size effect on pattern formation during BZ reaction performance could be observed by the naked eye (see Fig. 1). The presented reaction images demonstrate the simple logic: the more space available for the developing system, the more pattern diversity is observed in the system. The number of repeated experiments showed that in the cases of the smallest Petri dish and smallest square dish, the spaces were not sufficient for long-term generation of circular expanding waves (target patterns). The space-limited oscillation system couldn't persist in a travelling wave's state for a long time and jumped immediately to the next state (spiral wave formation). The calculation results below give numerical values for each case of geometrical organization. With space area increasing, there is space and time for the formation of a higher number of wave initiation centers' formation caused by the fact that the next phase does not start only in the vessel interior but predominantly at its curvy borders. For example, in the biggest Petri dish (200 mm), more than five target pattern centers could exist. Another case is the pattern formation in the dish of 'non-standard' square geometry constrictions. The corners play the role of wave

initiation centers from which the waves proceed to the centroid of the dish (cross point of the square diagonals).

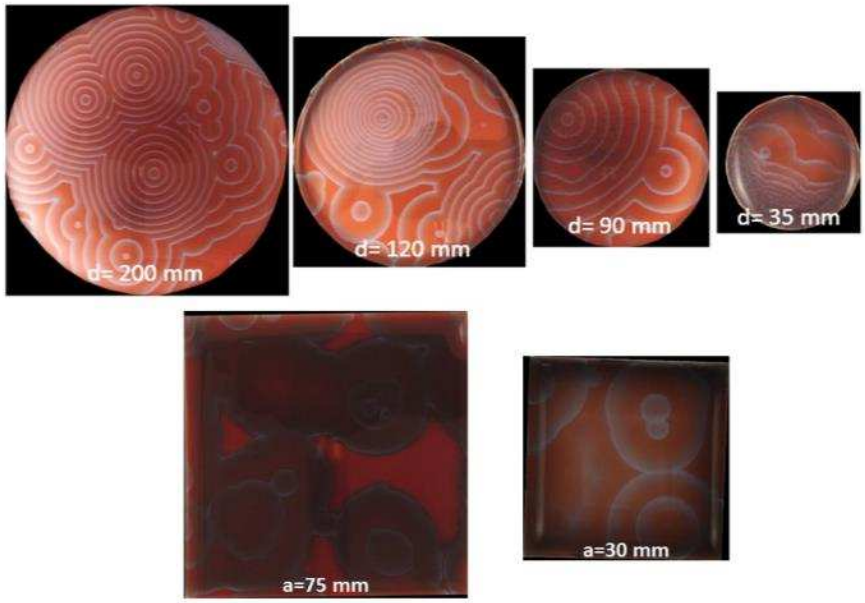

Figure 1. BZ reaction pattern formation response to the change of space geometry circle → square and area: extended Petri dish (upper row), extended square dish (lower row).

Using the point information gain entropy density, Ξ_α, spectrum it is possible to classify the state evolution of the structure formation. In comparison with the 'classical' size Petri dish, the one with the smaller diameter (35 mm) produced the smaller number of clusters in the Cluster dispersion plot (see Fig. 2 and Fig. 3). This indicates that some of the states did not evolve to the extent detectable by the analysis and were overcome by the next state.

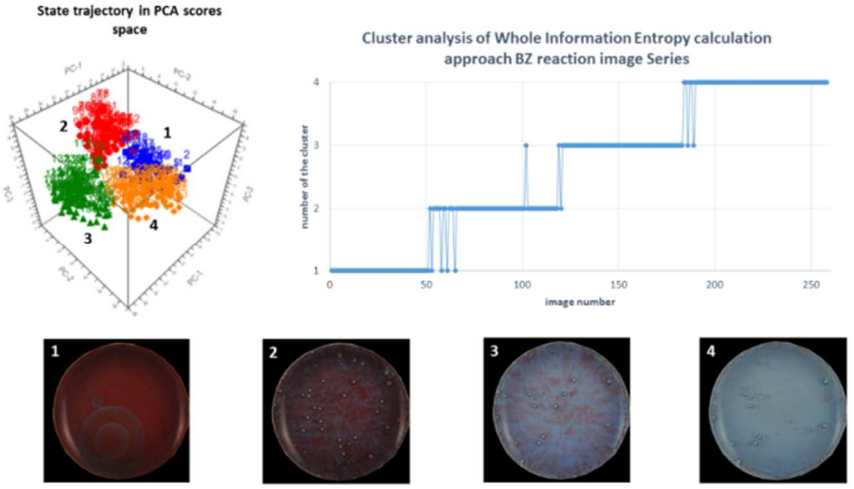

Figure 2. Ξ_α three major components of the principal component analysis of spectral values calculated from images captured on the trajectory BZ wave evolution in circle Petri dish with diameter of 35 mm (left), cluster dispersion of the presented data series (right) and corresponding characteristic images (bottom, numbered).

The reaction phase in which the target pattern evolves through the available space (recorded on Fig. 3, image 2) is absent in the small 35 mm Petri dish. Also, the relative length of different phases is different. In the smallest 35 mm Petri dish, 19% of evolution time accounts for wave initiation whereas in the 'classical' 90 mm one it is only 8%. The length of the spiral wave phase in 90 mm dish is much longer than in 35 mm Petri dish (50% versus 38%). Both these values are, however, obscured by potentially incorrect cluster assignments, respectively cluster merging in the 35 mm Petri dish. In the 35-mm dish, the chemical oscillation damping phase takes a longer time: 30% of the whole reaction time in contrast to 21% for the 90 mm Petri dish.

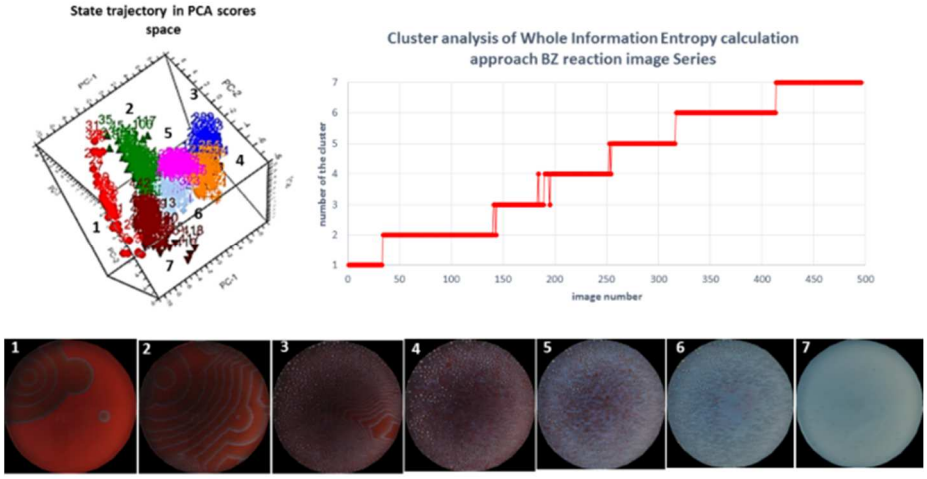

Figure 3. Ξ_α three major components of the principal component analysis of spectral values calculated from images captured on the trajectory BZ wave evolution in circle Petri dish with diameter 90 mm (left), cluster dispersion of the presented data series (right) and corresponding characteristic images (bottom, numbered).

Upon increasing in size from a standard Petri dish (90 mm) to that of 120 mm in diameter (Fig. 4), the phase for the target pattern formation was further elongated (22% vs. 20% of the whole reaction time in the "classical" Petri dish). The effect is obviously caused by the placement of centers far enough from each other and from the dish border to allow longer evolution until the fronts reach each other, merge, and eventually give rise to spiral waves. Spiral waves arise from wave front fractures which result in traveling waves' overlap. The bigger area offers more suitable conditions for the intermediate BZ reaction state elongation, where there coexist target patterns and spiral waves (18% vs. 9% for 90 mm case). The minor decrease of the oscillation damping time (18% vs. "classical" 21%) could be explained by the consumption of chemicals which, in the Petri dish, is independent from the wave evolution phase--- and the longer the waves evolve, the shorter the observation of the "dilution" effect only.

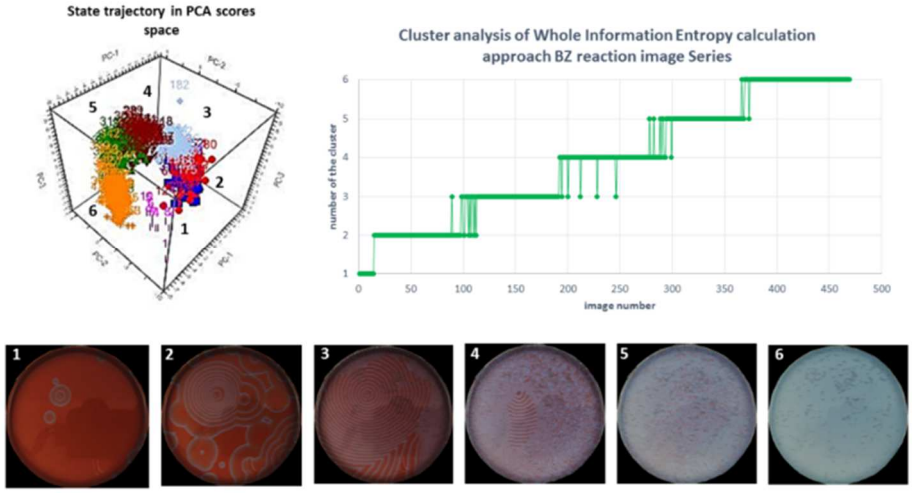

Figure 4. Ξ_α three major components of the principal component analysis of spectral values calculated from images captured on the trajectory BZ wave evolution in circle Petri dish with diameter 120 mm (left), cluster dispersion of the presented data series (right) and corresponding characteristic images (bottom, numbered).

The trend of elongation of the initial period continued in the 200 mm Petri dish (see Fig. 5) (19% in comparison to 8% resp. 3%), as did the traveling waves/spiral waves phase: 34% vs. 18% resp. 9% for 11304. The cluster analysis allowed us to separate the later stage into two clusters: 20% of the total reaction time was with travelling wave domination over the spiral wave and 14% for the spiral wave prevalence. The wave initiation phases, in this case, are equal to the smallest Petri dish results (19% of total reaction time), but the reason is different: in the 35 mm Petri dish, the wave initiation foci were suppressed by the space limitation, namely the border effects, and the cluster is merged with the next state. The biggest reaction area (200 mm) provided the free space for centers' generation. Then it took more time to fill the provided space until the dense waves begin to evolve at borders. In other words, in the 200 mm Petri dish, the target pattern generation was freely evolving while in the 35 mm it was not observed and merged with the next phase. The resulting longer evolution indeed resulted in higher consumption of chemicals before the final phase was reached and the damping phase was correspondingly shorter, 16% vs. 18% resp. 21% for smaller dishes.

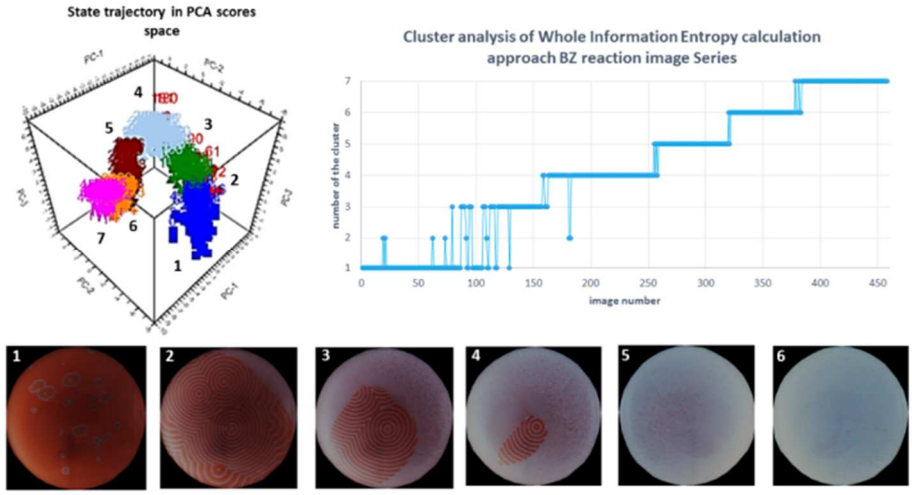

Figure 5. Ξ_α three major components of the principal component analysis of spectral values calculated from images captured on the trajectory BZ wave evolution in circle Petri dish with diameter 200 mm (left), cluster dispersion of the presented data series (right) and corresponding characteristic images (bottom, numbered).

Square reaction vessel

The BZ waves' behavior changed even more dramatically when we went from the circular to the square dish (see Fig. 6 and Fig. 7). Space restriction led to wave formation at dish corners. As shown in Fig. 6 image 1, in the bigger 75 x 75 mm area at least four centers of wave foci could co-exist, while the smaller 30 x 30 mm space provided space for only two wave initiation centers (on Fig. 7 image 1). Also, it should be noted, that waves from foci in the square dish did not produce perfectly circular target patterns, but rather ellipses with curly borders. This circular geometry collapse is obviously an effect of the square corners but the nature of the border effect does not have any simple description. Also, in the circular dish, there is an observable effect of the borders, in particular for the dense waves' evolution, but it is much less dramatic since the dish is circularly symmetric. The presence of additional geometric constraints in the reaction medium pushes the system to evolve to the spiral wave phase faster than in the circular dish, accounting for 22% of the whole reaction time in the 90 mm Petri dish

and 13% in 30 x 30 mm. In the 75 x 75 mm square dish, the spiral phase was completely absent.

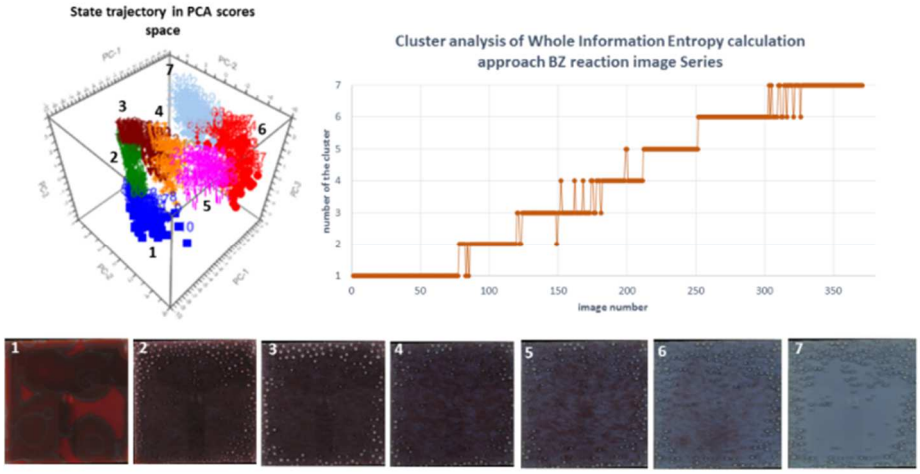

Figure 6. Ξ_α three major components of the principal component analysis of spectral values calculated from images captured on the trajectory BZ wave evolution in square square area 75 x 75 mm (left), cluster dispersion of the presented data series (right) and corresponding characteristic images (bottom, numbered).

Like with the circular-shaped dishes, in the smaller square dish we could not detect several stages of the wave formation (the algorithm identified only four clusters for 30 x 30 mm dish, see Fig. 7). The wave initiation phase took almost the same time for the both cases: 20% of the whole reaction time for the 35 mm Petri dish and 21% for the 30 x 30 mm square dish. The early phase travelling waves were present for 13% of all reaction time; their fronts meet along the diagonal of the square. For the 75 x 75 mm dish, we observed elongation of the spiral wave phase: 62% compared to 32% for 30 x 30 mm dish. The algorithm determined five different clusters for spiral wave phases in the 75 x 75 mm square dish (image 2, 3, 4. 5 and 6 in Fig. 6). The damping phase of the BZ reaction took place in the 75 x 75 mm dish for 18% from the whole reaction time, whereas in the 30 x 30 mm dish it took 34% of the total reaction time.

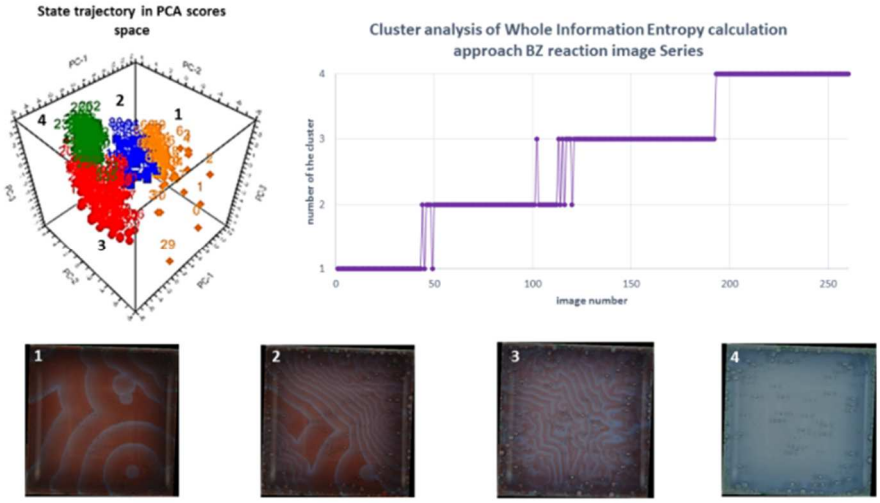

Figure 7. Ξ_α three major components of the principal component analysis of spectral values calculated from images captured on the trajectory BZ wave evolution in square area 30 x 30 mm (left), cluster dispersion of the presented data series (right) and corresponding characteristic images (bottom, numbered).

CONCLUSIONS

Presented results are detailed analyses of one experimental series of the BZ reaction upon space constraints. In order to judge the free evolution of the system, we must examine the first the Petri dish of 200mm in diameter. In this case, there were 6 different stages of the evolution of structures: (1) phase of formation of centers, (2) phase of free evolution of concentric target patterns, (3) merging of target patterns, (4) coexistence of dense waves with target patterns, (5) breakage of dense waves into spirals, and (6) the wave damping phase. In the smaller circular vessels, some of the phases were overcome. In the smallest Petri dish of 35 mm in diameter, we detected only four phases and the last phase (damping phase) was the longest. The damping phase seems to be caused by the decay of the chemical energy while the other phases seem to be independent of the time of chemical decay. In the square dish, there was an undulation of the wave front and an evolution of waves from corners.

One obvious observation is the strong influence of borders. The more the border is curved, the more it initiates evolution of waves. In the circular dish, dense waves evolve; in the square dish the border seems to influence the whole dish. The narrower and more curved the borders are, the more the early phase of isolated target patterns is shortened and overcome by dense waves and spirals. The shortening of early phase results in elongation of the dampening phase. It thus seems that structure formation is to a large extent independent of the chemical composition of the vessel. This conclusion is supported by the observation of the possibility to re-start the structure formation form the early phase by re-shaking the vessel [17].

Certain explanations may be given by comparing these results with those of the multilevel cellular automata model [11]. In this case, it is anticipated that the existence of a firm rectangular structure of cells in which the reaction occurs. Formation of such structures in non-linear dynamic systems such as Bénard cells [18] is rather well known. In the case of the BZ reaction, we only anticipate that a regular waves' structures is maintained by chemical energy. In a large circular Petri dish, this structure is nearly ideal. The narrower the space is and the more curved the edges are, the more this ideal structure is compromised. The cellular automata concept supports the opinion that even the trajectories undergoing very unnatural intermediate structures end in a limited set of a mixture of spirals and waves like that of phase 5 in the experiment. The limited set is a very stable structure with a rather broad zone of attraction.

We thus propose that the proper model of the BZ reaction which explains qualitatively all observations is the excitable media / multilevel cellular automaton operating on a regular structure induced by chemical energy. The spatial constraints induce numerous ignition points, namely at vessel borders. The resulting quickly evolving dense waves overcome the free evolving target patterns and shorten the time of the system evolution to the limit set. The regular structure is maintained as long as the chemical energy is sufficient and its collapse is to a large extent independent from the excitable media operation. For this reason, the wave damping phase is longer in cases in which the evolution is shorter.

REFERENCES

1. Belousov, B. P.: Periodically acting reaction and its mechanism, Collection of abstracts on radiation medicine, pp. 145-147 (1959)
2. Zhabotinsky, A. M.: Periodical process of oxidation of malonic acid solution. Biophysics 9, 306-311 (1964)
3. Ball, P.: Pattern Formation in Nature: Physical Constraints and Self-Organising Characteristics. Special Issue: Material Computation: Higher Integration in Morphogenetic Design, Volume 82, 22-27 (2012)
4. Cross, M. C., Hohenberg, P. S.: Pattern formation outside of equilibrium. Rew. Mod. Phys. Vol. 65, No. 3, 851-1112 (1993)
5. Biosa, G., Masia, M., Marchettini, N., Rustici, M.: A ternary nonequilibrium phase diagram for a closed unstirred Belousov–Zhabotinsky system. J. Chem. Phys., 308, 7-12 (2005)
6. Belmonte, A. L., Ouyang, Qi, Flesselles, J-M.: Experimental Survey of Spiral Dynamics in the Belousov-Zhabotinsky Reaction. J. Phys. II France 7, No. 10, 1425-1468 (1997)
7. Field, R. J., Korös, E., Noyes, R. M.: Oscillations in Chemical Systems II. Thorough analysis of temporal oscillations in the Ce-BrO_3^-- malonic acid system. J. Am. Chem. Soc. 94, 8649-64 (1972)
8. Kitahata, Hiroyuki: Spatio-temporal pattern formation in reaction-diffusion systems coupled with convection and geometrical effect. Open Access Thesis and Dissertation, available at: http://hdl.handle.net/2433/64953 (2006)
9. Budroni, M. A., Rustici, M., Tiezzi, E.: On the Origin of Chaos in the Belousov-Zhabotinsky Reaction in Closed and Unstirred Reactors. Math. Model. Nat. Phenom. Vol. 6, No. 1, 226-242 (2011)
10. Holley, J., Adamatzky A., Bull, L., Costello, B., Jahan, I.: Computational Modalities of Belousov-Zhabotinsky Encapsulated Vesicles, available at: http://arxiv.org/pdf/1009.2044.pdf (2010)
11. John von Neumann: The general and logical theory of automata. L.A. Jeffress, ed., Cerebral Mechanisms in Behavior – The Hixon Symposium, 1-31 (1951)
12. Liveri, M. L. T., Lombardo, R., Masia, M., Calvaruso, G., Rustici, M.: Role of the reactor Geometry in the Onset of Transient Chaos in an Unstirred Belousov-Zhabotinsky System. J. Phys. Chem. A, 107, 4834-4837 (2003)

13. Rustici, M., Branca, M., Brunetti, A., Caravati, C., Marchettini, N.: Inverse Ruelle-Takens-Newhouse scenario in a closed unstirred cerium catalyzed Belousov-Zhabotinsky System. Chem. Phys. Lett. 293, 145-151 (1998)
14. Stys, D., Urban, J., Rychtarikova, R., Zhyrova, A., Cisar, P.: Measurement in Biological Systems from the Self-organisation Point of View. Springer International Publishing Switzerland, Lecture Notes in Computer Science Volume 9044, Bioinformatics and Biomedical Engineering, 431-443, (2015)
15. Rychtarikova, R., Korbel, J., Machacek, P., Cısar, P., Urban, J., Soloviov, D., Stys, D.: Point information gain, point information gain entropy and point information gain entropy density as measures of semantic and syntactic information of multidimensional discrete phenomena, available at: http://arxiv.org/pdf/1501.02891.pdf (2015)
16. Zhyrova, A., Stys, D.: Construction of the phenomenological model of Belousov – Zhabotinsky reaction state trajectory. International Journal of Computer Mathematics, 91(1), 4-13 (2014)
17. Cohen, J. Belousov-Zhabotinski Reaction Do-it-Yourself Kit, available at: http://drjackcohen.com/BZ01.html (2009)
18. Bénard, H.: Les Tourbillons Cellulaires Dans Une Nappe Liquide (Cellular Eddies in a Horizontal Liquid Layer), PhD dissertation, University of Paris (1900)

3.4. Recognition of Stages in the Belousov-Zhabotinsky Reaction Using Information Entropy: Implications for Cell Biology

This chapter is based on Paper IV:

Zhyrova A., Rychtáriková R., Štys D., 2017. Recognition of Stages in the Belousov-Zhabotinsky Reaction Using Information Entropy. *IWBBIO 2017, Proceedings, Part I, Lecture Notes in Computer Science*, 10208, Springer, Switzerland, 2017, pp. 335–346, ISBN: 978-3-319-56147-9 (Print) (SJR 2016 = 0.315).

ABSTRACT

A common property of a living organism as a non-equilibrium dynamic system is self-organization, including the evolution of this self-organized system through distinct consecutive stages. In this article, the properties of dynamic self-organization are examined on a primitive model of life -- the oscillating Belousov-Zhabotinsky (BZ) reaction. This system is sensitive to the changes of external conditions by dynamic reorganization of chemical waves. The generated patterns bring the information on history of the reaction evolution. We performed the pattern classification using calculation of the point information gain entropy density followed by multivariate statistical analysis. It was proved by numerous experiments that each obtained cluster is related to a unique reaction stage with characteristic concentrations of the reactants. The reliability makes this method promising for application to the recognition of stages in variety of complex systems. The results obtained via visual inspection of 6 parallel image series of the BZ reaction together with their statistical analysis approximate cell physiology during development and differentiation of tissues - a small change in the initial conditions leads to a different development of the cell population. This finding also explains a low reproducibility of measurements of biological systems.

INRODUCTION

The Belousov-Zhabotinsky (BZ) reaction, which is named after the scientists who discovered it [1, 2], is a cascade of more than 80 chemical reactions whose starting mechanism and relationship between its components remain still unknown. The hallmark of this chemical process is its ability to change the direction of reaction in the precise frequency which leads to a periodic oscillation. When a thin layer of the reaction mixture is placed onto a vessel, the BZ reaction gives color patterns (chemical waves). These patterns have a complex geometry that changes over time in a distinct order (first analyzed by Winfree [3]) and their shape and duration depend on the actual composition of the reaction mixture and shape of the reaction vessel [4, 5]. The time evolution of chemical waves [6, 7] proceeds in the sequence from circular target patterns to the variety of spirals (a simply rotating spiral, a meandering spiral, a renascent stable spiral, a convectional unstable spiral, etc.). At the end of the reaction process, when the main reagents are exhausted, chemical structures are diluted (waves bleach and disappear at all).

The choice of the BZ reaction as the object of investigation was not accidental, since the observed chemical reaction flows have all initial properties of life objects, such as: dissipative structure [8], ability to self-organization [9] and regimes of periodicity [10]. Many processes in nature could be understand from the point of wave transformation view, e.g., spiral patterns of *Dictyostelium molds* [11], cardiac muscle [12] or chicken retina [13].

That make the BZ reaction an extremely valuable pilot object for studying the properties of life [14]. In terms of bio-engineering, it means that cause-effect models explaining the core processes pushing the BZ system to change its states could be used for the interpretation of the transformation circumstances underlying the more complex forms of life, like cells or biological species.

In this paper, we describe the BZ system using a variable point information gain entropy density [15], which classifies multifractal scaling properties of a complex structured system. The found pattern

sequence as well as the duration of individual stages are similar but not identical to properties of living organisms [16].

MATERIALS AND METHODS

Experiment Setup

The experiments were performed with oscillating bromate-ferroin-bromomalonic acid reaction (a recipe of the Belousov-Zhabotinsky reaction provided by Dr. Jack Cohen [17]). The reaction mixture includes 0.34-M sodium bromate, 0.2-M sulphuric acid, 0.057-M sodium bromide (all from Penta), 0.11-M malonic acid (Sigma-Aldrich) as substrates and a redox indicator and 0.12-M 1,10-phenanthroline ferrous complex (Penta) as a catalyst. All reagents were mixed in the above-mentioned sequence. The experiments were performed in a specially constructed thermostat which consists of a Plexiglas aquarium and a low-temperature circulating water bath-chiller. The temperature during the experiments was kept at 27 °C.

The reaction mixture was placed onto a circular Petri dish with the diameter of 90 mm (this type of vessel was chosen because the majority of experiments described in the literature were performed in it) and mixed using a laboratory three-dimensional orbital shaker TL 10 - Edmund Bühler GmbH (Fisher Scientific) under 14 rot/min and angle of tilt equal 5° counterclockwise for 2 minutes. The experiment was repeated six times.

Image Processing and Data Calculation Performance

The chemical waves were recorded by a Nikon D90 camera (setting up: Time-lapse shooting 10 s/snapshot, Exposure compensation $+1\frac{1}{2}$ EV, ISO 320, Aperture $\frac{f}{8}$, Shutter speed $\frac{1}{80}$ s). The original 12-bit NEF raw image format was losslessly transformed to an 8-bit PNG format (using a Least Information Loss Converter [18]) and a non-informative image background was cropped using a MATLAB software [19].

Such-treated images were further processed using an Image Info Extractor Professional software [20]. The analytic tool for classification of image series was derived from the Rényi entropy:

$$I_\alpha = \frac{1}{1-\alpha}\ln\sum_{i=1}^{m} p_i^\alpha \quad (1)$$

where the parameter α -- the Rényi coefficient – $\alpha \geq 0$, $\alpha \neq 1$, indicates the information cost with regards to the examined probability distribution $f(p_i)$. Variable p_i denotes a discrete probability of a given phenomenon *i*, i.e., in our case, a probability of occurrence of a given intensity in the center of the intersection of the row and column pixel grid of an image (so-called cross type of information surroundings). The total number of intensity levels in the histogram which was created from the intensities on this cross is marked as *m*. The Rényi entropy provides information characteristics for the multifractal system and is included in the measure of the generalized dimension:

$$D_q = \lim_{l\to 0}\frac{I_\alpha(l)}{\ln(l)} \quad (2)$$

where *l* is a measure of a spatial element. In the case of an image, the spatial element is a camera pixel and is fixed.

To examine the point information contribution, we calculate the point information gain $\gamma_{\alpha,x,y}$ as a difference between the information content of a probability distribution of occurrence of the intensity *i* in the histogram which was created from pixels around the point at the coordinate *(x, y)* without $p_{i,x,y}$ and with p_i a point at the coordinate *(x,y)*:

$$\gamma_{\alpha,x,y} = I_\alpha - I_{\alpha,x,y} = \frac{1}{1-\alpha}\ln\sum_{i=1}^{k} p_{i,x,y}^\alpha - \frac{1}{1-\alpha}\ln\sum_{i=1}^{k} p_i^\alpha = \ln\left(\frac{\sum_{i=1}^{k} p_{i,x,y}^\alpha}{\sum_{i=1}^{k} p_i^\alpha}\right) \quad (3)$$

In the Image Info Extractor Professional software, the natural logarithm *ln* is supplied by the binary logarithm $\log_2$ which gives the information contribution of the given pixel *(x, y)* in bits.

Unlike the Shannon information entropy (which is a special case of the Rényi entropy for α = 1 and is derived for the normal distribution), the α-parameterized Rényi entropy in the computation of $\gamma_{\alpha,x,y}$ enables to

specify multifractal structure of the distribution (the intensity histogram) unambiguously via usage of a multiple of the Rényi coefficients α which gives spectra $\gamma_{\alpha,x,y}$ vs. α. By changing the parameter α, we can focus on the probability distribution of one event of interest while suppressing the other. In order to have a general overview on the multifractality of the examined point, we calculated the $\gamma_{\alpha,x,y}$ for thirteen α: 0.1, 0.3, 0.5, 0.7, 1.0 (the Shannon information entropy), 1.3, 1.5, 1.7, 2.0, 2.5, 3.0, 3.5, and 4.0.

To collect the total information of the image, we determine a point information entropy H_α as a sum of all $\gamma_{\alpha,x,y}$:

$$H_\alpha = \sum_{x=1}^{s} \sum_{y=1}^{r} \gamma_{\alpha,x,y} \tag{4}$$

where *s* and *r* are dimensions of the image (i.e., numbers of pixels in the rows and columns, respectively). The H_α may be understood as a multiple of the average $\gamma_{\alpha,x,y}$ by the total number of pixels. The full specification of each series image was achieved via calculation of the vectors H_α for each color image channel.

The following cluster analysis (k-means algorithm, squared Euclidian distance) of the obtained spectra H_α vs. α using the Unscrambler X software [21] recognized different evolution states in the chemical system. The optimal number of $k = 7$ clusters was defined empirically by the comparison of the cluster dispersion histogram for different numbers of clusters with the visual inspection of the image series. Based on the calculation by the cluster analysis of the duration time of the unique BZ reaction phases, the correlation analysis of the examined six experiments was performed.

RESULTS AND DISCUSSIONS

The course of reaction was very similar for all experiments:

1. a short latent period, no longer than 400 s, in which no wave exists;
2. formation of (usually no more than two) wave foci, which further spread over the available reaction surface;
3. frequent growth of drifting waves;
4. interaction of wave fronts followed by initiation of formation of spiral waves in the points of wave breaks;
5. evolution of the spiral waves, which occupy the two-thirds of total reaction time;
6. damping of chemical oscillation, which manifests itself in bleaching of waves and turning the reaction system into the transparent blue color;
7. the end of the reaction, when it is not able to register any change of color of the reaction medium (it is homogeneously blue).

The damping phase seems to be a result of the decay of the chemical energy, while the other phases seem to be independent of the time of chemical decay. Mainly in Experiment 1 and 4, the waves started to propagate as concentric structures of irregular geometry at the borders of the dish and further converged into the center of the dish. The border effect also led to the formation of radial patterns with sprained waves at the edges of the vessels followed by their compaction at the center of the dish. The used type of mixing of reagents (Sect. 2) formed a force vector which caused the drift of spiral centers in a counterclockwise direction. Also, it should be noted that bleaching of waves started in the center of the reaction space, where the processes such as evaporation of the organic substrate and bromide oxidant (formation of bubbles) were more intensive. This prolonged the attenuation of formation of waves placed near the dish boundaries. Indeed, the reaction process itself represents a transition from one (red reaction surface) to another (complete blue surface) state through many quasi-states (target patterns, circular waves, spiral waves, etc.). The samples of photos from 6 parallel experiments are shown in Fig. 1 (the latent reaction period and the end of the BZ reaction is not shown).

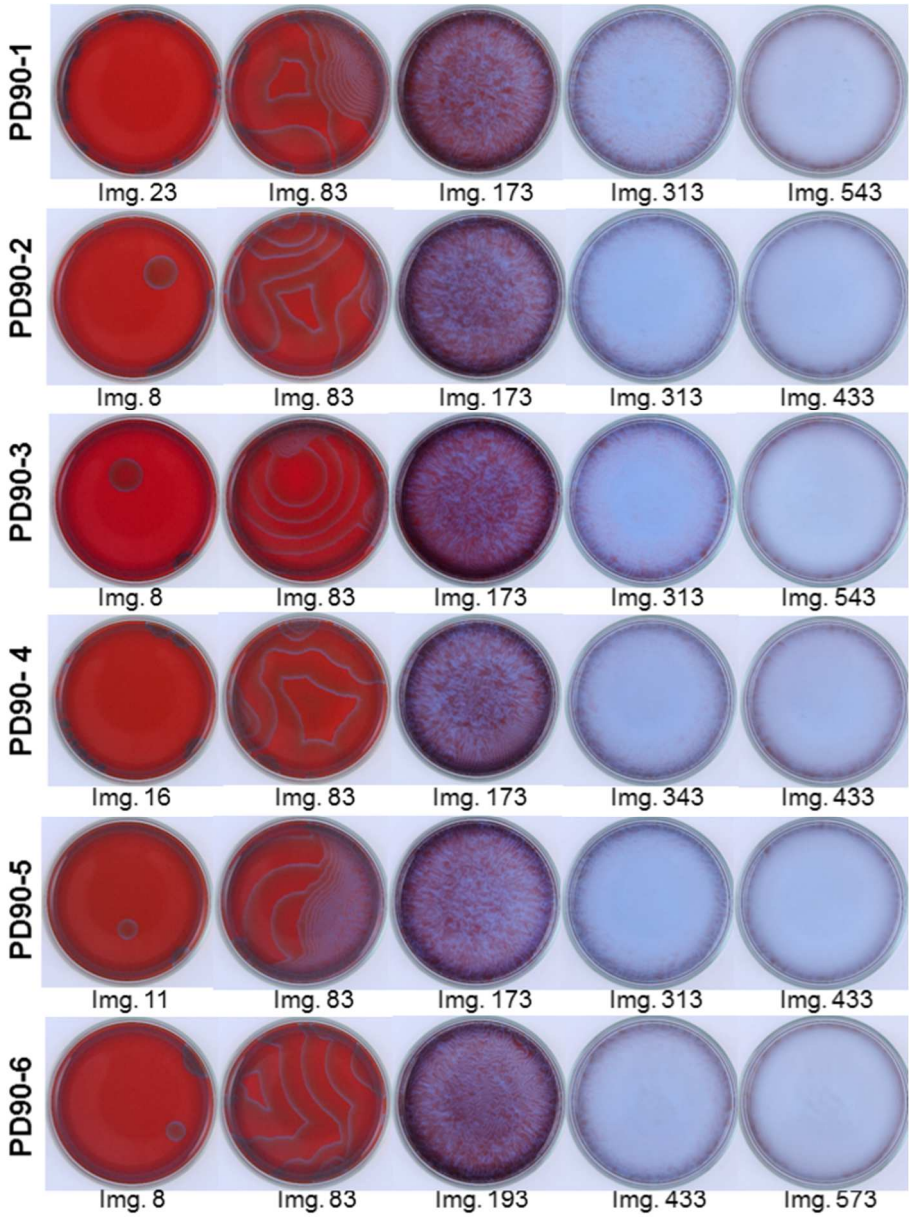

Fig. 1. Key moments in the dynamics of pattern formation in the course of the Belousov-Zhabotinsky reaction (6 experimental repetitions). The serial number of the image indicates the remoteness of the recorded picture on the initial reaction time. All reaction courses exhibit a general law of wave formation from organized circular waves to chaotically oriented spiral waves (*from left to right*).

Experiment 1: Experiment 1 had the longest latent period from all experiments (200 s). The waves started to be formed at the dish borders (Img. 23) and spread along the perimeter to the dish center (Img. 83). In agreement with literature [6], due to the spatial constrains, the spirals started at the place of interaction of wave fronts (Img. 173). Diffusion processes in the reaction medium promoted rotation of waves, whose centers also drifted anticlockwise through the reaction system under the influence of mixing. After ca. 3000 s, the oscillation damping started (Img. 313) and blue waves broadened till the end of reaction. Even after 5000 s, some weak oscillations were still observed at the dish border (Img. 543). It took the reaction system 2000 s to come to totally blue stage, when no waves were observed.

Experiment 2: In contrast to Experiment 1, Experiment 2 started after a very short latent period (10 s), when a circular wave center appeared relatively far from the border (Img. 8). The circular wave fronts from this initiation center merged (Img. 83) with those generated at the dish border. In the same ways as in Experiment 1, two waves of different zones of package (more dense and less dense) were formed followed by the phase of spiral waves (Img. 173), the phase of degradation of pattern structures (Img. 313) and the complete attenuation of the reaction due to the exhaustion of the main components (Img. 433). It took 3300 s until the reaction was completely finished.

Experiment 3: As in Experiment 2, the first wave focus appeared far from the dish border (Img. 8), whereas the second one was set at the border. After that, both circular wave fronts spread towards each other. The oscillation center was very stable and kept generating the waves (Img. 83) for more than 900 s. More and more wave fronts were evolving and interacted each with other which resulted in their breakage and generation of spiral waves (Img. 173). Spiral waves have more force to shift traveling waves when concurring in the space. The spiral waves evolved to chaotic patterns (Img. 313), which finally ended with the oscillation attenuating (Img. 543). The time of damping phase was equal to Experiment 1 (ca. 200 s).

Experiment 4: As in Experiment 1, Experiment 4 exhibited a long latent period (130 s), when the patterns started to form from the dish border (Img. 16). After that, generated circular waves converged into the center

of the dish (Img. 83). As in the previous observations, the spiral waves appeared as a result of the interactions of wave fronts (Img. 173). The following transformation of spirals to the offensive of the chaotic reaction (Img. 343) was finished by the damping of the chemical oscillation (Img. 433). Like Experiment 2, the reaction was completely finished after 330 s.

Experiment 5: The course of Experiment 5 almost copied Experiments 2-3: after a 70-s latent period, two wave foci appeared --- one focus near the center of the dish and the second focus at the dish border (Img. 11). Such a distribution of the wave centers (Img. 83) led to the wave fronts forming two equivalent spatial cluster with more densely packed waves and less dense ones. The following phase of spiral waves (Img. 173) was replaced by the phase of chaotically oriented patterns (Img. 313). As registered in Experiments 2 and 4, the oscillations finished in 330 s when the first manifestations of the reaction damping were observed (Img. 433).

Experiment 6: The initial period in Experiment 6 took only 30 s, when two wave foci appeared --- one of them near the dish border and the second one at the dish border (Img. 8). Due to their short distance, these waves merged soon into a wave front which was further propagated from one edge of the reaction vessel to the opposite one (Img. 83). Spreading of the joint wave fronts avoided the breakage of waves for a long time and delayed the occurrence of the phase of spiral waves (Img. 193). Compared with the previous experiments, the onset of the chaotically oriented patterns (Img. 433) as well as the beginning of the oscillation damping (Img. 573) were observed later. This reaction exhibited the shortest period of oscillation damping (1730 s).

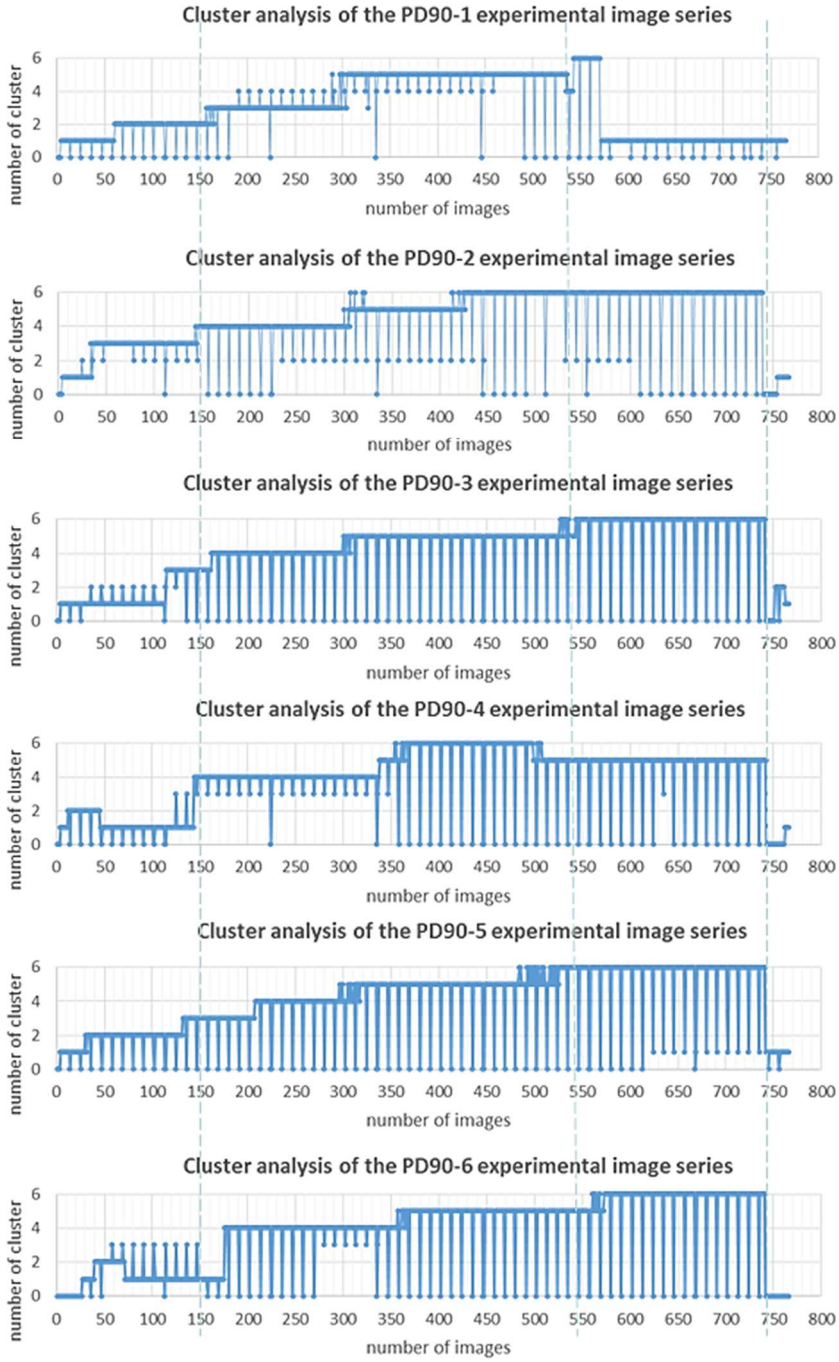

Fig. 2. Time distribution of the reaction phases in the Belousov-Zhabotinsky reaction determined using cluster analysis of vectors of point information gain entropy (6 experimental repetitions).

In most observed cases (four from six), initial reaction centers were placed far from the dish border. In these cases, after a short latent period, circular waves were smoothly developed. However, if the chemical waves started at the dish border, the course of the BZ reaction underwent significant changes. These "outlying" experiments did not correlate with the others as well as between each other. It thus seems that the formation of structures is to a large extent independent of the chemical composition in the vessel. This conclusion is supported by the observation of (1) re-formation of structures after re-starting a finished experiment by re-shaking the vessel [17] or (2) the change of the course of the BZ reaction in dishes of different geometry or size. For instance, compared with experiments in a 200-mm P. dish [25, 26] in which waves are generated mainly from the center of the dish, the results described here are more strongly influenced by borders and initial reaction centers are created more often at the dish border.

The experimental observations of the stages of the BZ reaction are consistent with cluster analysis received from information-entropic data (Fig. 2). The plots of cluster dispersions show clear division of reaction patterns into stages as follows:

1. wave initiation, which is dependent on the length of the latent period (Imgs. 1-30),
2. target waves, which completely fill the whole reaction space (Imgs. 31-150),
3. the spiral waves' onset, which is the same for most of the experiments, regardless of the position of the initial point of reaction (Imgs. 150-200, the beginning of this cluster is marked by a dashed line),
4. spreading of the spiral waves across the reaction space (Imgs. 200-550), and
5. the final stage of reaction oscillation damping, which occurs in the same time for all experiments as well (Imgs. 550-766, the beginning of this cluster is marked by a dash line).

The distinction in the initiation chemical waves observed in the experiments (Fig. 1) is also reflected in the plots of clusters (Fig. 2). When waves started from the dish border (Experiments 1 and 4), the latent period took a longer time, but phases of mixture of spirals and waves came faster - this is presented by two clusters. If the wave foci appeared far from the dish border, the variety of evolved patterns created several (up to four in Experiment 6) clusters. Anyhow, as noticed in the experiments as well as in the clustering of experimental data, in all experiments, the stage of spirals and waves began at the same time irrespectively of the position of the reaction initiation centers - in all plots, the beginning of a new cluster took place in Img. 150 (Fig. 2). Cluster analysis allocated evolution of spiral waves to several groups: The first cluster is associated with spiral wave deployment and diffusion between the BZ patterns, when the second cluster corresponds to the time of switching the phase of spirals and waves to chaotic structures (cf. Imgs. 173 and 313 in Fig. 1). The phase of oscillation damping is the longest stage in all examined experiments. It occupies the biggest cluster in the plots of clusters (Fig. 2) and started approximately at the same time after beginning of the reaction (dash line through Img. 550 in Fig. 2). The end of the reaction, when no waves were detected, was assigned to the same cluster as the latent period (Experiments 2, 3, 5, and 6). Due to the used calculation approach (i.e., cross point information gain), the distribution of the clusters does not depend on the predominance of blue or red color in the images, but on the presence and shape of the investigated patterns.

The similarities between all six experiments were assessed by correlation analysis of the lengths of each reaction stage that was estimated by the k-mean clustering (Tab. 1). All experiments showed mutual significant correlation at the significance level $p < 0.05$ with Pearson's coefficients from 0.4585 (experiments 1 and 2) up to 0.9636 (experiments 3 and 5). Obtained correlations as well as the visual inspection of the recorded data confirm our expectation: the way how the chemical waves started to spread change the course of the BZ reaction drastically.

The features detected in the experiments can be interpreted in terms of a proper model of the BZ reaction -- an excitable medium of multilevel cellular automaton, which explains qualitatively all observations and simulates an increase/decrease of chemical energy of regular structures [26]. The regular structure is maintained as long as the chemical energy is sufficient and its collapse is to a large extent independent of the operation of the excitable medium.

Tab. 1. Pearson's correlation coefficient for 6 image series of the Belousov-Zhabotinsky reaction (evaluated for vectors of clusters obtained using vectors of point information gain entropy)

Experiment	**1**	**2**	**3**	**4**	**5**	**6**
1	1.000					
2	0.4585	1.000				
3	0.6049	0.5615	1.000			
4	0.6098	0.5742	0.9241	1.000		
5	0.5412	0.5574	0.9636	0.9051	1.000	
6	0.6160	0.5284	0.9440	0.9140	0.9538	1.000

For this reason, the wave damping phase is longer in cases in which the evolution of waves is shorter. In the simulation, the limit set (the last phase) of mixture of spirals and waves is very similar to phase 5 in the experiments. The limit set is a very stable structure with a rather broad zone of attraction.

CONCLUSIONS

The paper proposed a new approach for a non-invasive detection of developmental phases followed by modeling of the state trajectory of a complex biological object. The transformation of the α-dependent variables point information gain entropy, which correspond to the visible structure of the investigated object, into the space of orthogonal principal components describes macroscopic behavior of a self-organizing system and identifies each development state by a cluster on the charting state trajectory. This mathematical tool for image processing was tested on the series of photographs of the BZ reaction as a primitive simulation of life, with further plans to adopt the method for a wide range of biological phenomena. The obtained models of different modifications of the BZ reaction lead to the conclusion that application of the information-entropic approach to the image processing gives enough specific characteristics for plotting clear mathematical model of the self-developing system and for the automatic recognition of unique states of the investigated process.

The developed procedure with necessary future updates can be used for, e.g., an inexpensive, automatic, contactless recognition of the cell cycle states [23, 24, 27, 28]. This will bring a major contribution to understanding of the reasons of cell cycle abnormalities that lead to malignization and genesis of cancer, which is a key objective of modern medicine, biology, and related sciences. Under the comparison with other methods, which are traditionally used in cell biology, the data processing using the information-entropic approach is much faster and precise than monitoring of cell growth by a human operator.

Structures which are similar to the final mixture of spirals and waves were observed in many free-evolving self-organized objects. This fact indicates that these structures are results of many - qualitatively similar - processes. When a structure is mechanically constrained, the pattern is changed significantly and the evolution of the structure can be changed up to the level that some stages do not exist. In other words, the properties normally attributed solely to the living systems can be observed in simple chemical mixtures.

Based on the correlations of repetitions of the simple self-organizing BZ reaction, the results discussed in the paper also demonstrate a relatively low level of reproducibility of measurements in biological systems.

REFERENCES

19. Belousov, B. P.: Periodically acting reaction and its mechanism. Collection of abstracts on radiation medicine, 147-145 (1959)
20. Zhabotinsky, A.M.: Periodic processes of malonic acid oxidation in a liquid phase. Biophys., 9, 306–311 (1964)
21. Winfree, A. T.: The Geometry of Biological Time. Biomath., v. 8. Springer-Verlag, Berlin-Heidelberg-New York (1980)
22. Zhyrova, A., Štys, D.: Construction of the phenomenological model of Belousov–Zhabotinsky reaction state trajectory. Int. J. Comp. Math., 91(1), 4-13 (2014)
23. Zhyrova, A., Stys, D., Cisar, P.: Information entropy approach as a method of analysing Belousov-Zhabotinsky reaction wave formation. Chem. L., 107 (Suppl. 3), S341-S342 (2013)
24. Cross, M. C., Hohenberg, P. C.: Pattern formation outside of equilibrium, Rev. Mod. Phys., 65, 851-1124 (1993)
25. Jian, Liu, Zhen-Su, She: Hierarchical structure description of spatiotemporal chaos, available from: http://arxiv.org/pdf/nlin/0408024.pdf (2008)
26. Prigogine, I., Nicolis, G.: Self-Organization in Nonequilibrium Systems: From Dissipative Structures to Order through Fluctuations, Wiley-Interscience, New York, 1-st edition, 512 pp. (1977)
27. Camazine, S., Deneubourg, J.-L., Franks, N. R., Sneyd, J., Theraulaz, G., Bonabeau, E.: Self-Organization in Biological Systems, Princeton University Press, 560 pp. (2003)
28. Hines, T. M.: Comprehensive Review of Biorhythm Theory, Psychological Reports 83 (1): pp. 19 - 64 (1998)
29. Siegert, F., Weijer, C. J.: Spiral and concentric waves organize multicellular *Dictyostelium* mounds. Current Biology 5(8), 937–943 (1995)
30. Davidenko, J. M., Pertsov, A. V., Salomonsz, R., Baxter, W., Jalife, J.: Stationary and drifting spiral waves of excitation in isolated cardiac muscle. Nature 355(6358), 349–351 (1992)

31. Gorelova, N. A., Bures, J.: Spiral waves of spreading depression in the isolated chicken retina. J. Neurobiol. 14(5), 353-63 (1983)
32. Shanks, N.: Modelling the Biological Systems: the Belousov-Zhabotinsky Reaction, Foundations of Chemistry 3: pp. 33 - 53 (2001)
33. Rychtáriková, R.: Clustering of multi-image sets using Rényi information entropy. LNCS, vol. 9656, pp. 517–526. Springer, Heidelberg (2016)
34. Štys, D., Urban, J., Rychtáriková, R., Zhyrova, A., Císař, P.: Measurement in Biological Systems from the Self-organization Point of View. LNCS, vol. 9044, pp. 431–433. Springer, Heidelberg (2015)
35. Cohen, J. Belousov-Zhabotinski Reaction Do-it-Yourself Kit, available at: http://drjackcohen.com/BZ01.html (2009)
36. Stys, D., Nahlik, T., Machacek, P., Rychtarikova, R., Saberioon, M.: Least Information Loss (LIL) conversion of digital images and lessons learned for scientific image inspection. LNCS, vol. 9656, pp. 527–536. Springer, Heidelberg (2016)
37. MATLAB version 7.10.0. Natick, Massachusetts: The MathWorks Inc. (2010)
38. Císař, P., Urban, J., Náhlík, T., Rychtáriková, R., Štys, D.: Image Info Extractor Professional, v. b9, available at: http://www.auc.cz/software/index5.htm (2015)
39. The Unscrambler X version 10.1. Oslo, Norway: CAMO Software. (2011)
40. Rychtarikova, R., Korbel, J., Machacek, P., Cisar, P., Urban, J., Soloviov, D., Stys, D.: Point Information Gain, Point Information Gain Entropy and Point Information Gain Entropy Density as Measures of Semantic and Syntactic Information of Multidimensional Discrete Phenomena, archived at https://arxiv.org/abs/1501.02891 (2015)
41. Stys, D., Urban, J., Vanek, J., Cisar, P.: Analysis of biological time-lapse microscopic experiment from the point of view of the information theory. Micron 42, pp. 360-365 (2011)
42. Stys, D., Vanek, J., Nahlik, T., Urban, J., Cisar, P.: The cell monolayer trajectory from the system state point of view. Mol. Biosys. 7, pp. 2824-2833 (2011)

43. Zhyrova, A., Rychtáriková, R., Náhlík, T.: Effect of Spatial Constrain on the Self-Organizing Behavior of the Belousov-Zhabotinsky Reaction, IWBBIO 2016, Proceedings Extended Abstracts, Bioinformatics and Biomedical Engineering, pp. 246-258 (2016)
44. Štys, D., Náhlík, T., Zhyrova, A., Rychtáriková, R., Papáček, Š., Císař, P.: Model of the Belousov-Zhabotinsky Reaction. LNCS, vol. 9611, pp. 171-185. Springer, Heidelberg (2016)
45. Náhlík, T., Urban, J., Císař, P., Vaněk, J., Štys, D.: Entropy based approximation to cell monolayer development, IFMBE Proceedings, v. 37(1), pp. 563-- 566 (2012)
46. Rychtáriková R., Náhlík T., Smaha R., Urban J., Štys D. Jr., Císař, P., Štys D.,. Multifractality in imaging: application of information entropy for observation of inner dynamics inside of an unlabeled living cell in bright-field microscopy, ISCS14, pp. 261 - 267. Springer, Switzerland, (2015)

CONCLUSIONS

The oscillating Belousov-Zhabotinsky chemical reaction is an easily performable example of self-organization. It manifests in the form of colored chemical patterns which could be straightforwardly recorded and estimated by available photographic technology. A series of reaction transformations leading to the formation of chemical waves have been investigated by scientists for more than 50 years. As I had shown in the Introduction, self-organization of the BZ system and its adaptation to the changing parameters of the external environment is still not fully understood.

The purpose of this PhD thesis is to measure and to capture the pattern evolution in the B-Z reaction using the modern digital imaging technology and to analyze the chemical waves without a-priori assumptions using the most general approaches: Rényi entropy, multifractality – whose measure the Rényi entropy is, and multivariate statistics.

The correct structural datasets may be analyzed with an *a priori* assumption, which is a deductive scientific method, or the data may be analyzed inasmuch without assumption. For an internally structured dataset, i.e. when the Gaussian statistics or, in other words, the central limit theorem may not be applied, the most general assumption is that the dataset is multifractal. This assumption is also technically advantageous because the dataset may be inspected for its generalized dimension spectrum (*Theiler, 1989*).

$$D_\alpha(p_i) = \frac{1}{\alpha - 1}\lim_{r\to 0}\frac{\ln\sum_i p_i^\alpha}{\ln r} = \lim_{r\to 0}\frac{-I_\alpha(p_i)}{\ln r} \qquad (21)$$

The Rényi entropy (I_α) is key for the calculation of the generalized dimension spectrum. For discrete datasets, our team has developed local variable point information gain (PIG) and summary variables point information gain entropy (PIE) and point information gain entropy density (PIED) (*Rychtáriková et. al., 2016*). In the BZ reaction case, when the dimension is given by the grid of the camera pixel, we have used PIG_α, PIE_α and $PIED_\alpha$ as operational variables replacing the generalized dimension (*Zhyrova and Štys, 2014*).

Our work team (Císař, Macháček, Náhlík, Rychtáriková, Štys, Urban, Vaněk, Zhyrova,) developed the PIG, PIE and PIED calculation software "Image Info Extractor" and tested it on solution of a wide range of scientific problems where the results come in the form of digital camera datasets form the BZ reaction through microscopic images (*Rychtáriková et al., 2017*) down to the ethological observations *(Štys et al., 2015b)*.

The calculation of PIG, PIE and PIED thus may be used for the analysis and classification of trajectories of all self-organized systems due to their unavoidable multifractal nature (*Štys et al., 2015*).

I applied the "Image Info Extractor Professional" for the investigation the oscillation process in BZ reaction. Estimated from experimental image series PIG, PIE ad PIED values I used for creation the state-trajectory of the reaction course. Typically, I used 13 α coefficient values to sample the Rényi entropy spectrum. As a result, it was typically obtained 36 PIE and PIED values calculated by the whole and cross methods, i.e. up to 144 variables. I used the principal component analysis (PCA) to reduce the dimensionality of the problem and it was found in majority of the experiments that three principal components explain more than 90% of the variance and that a logical trajectory of the BZ reaction state-trajectory is found in this three-dimensional space (*Zhyrova et. al., 2013; 2014*). In other words, there are likely three main components (i.e. chemical self-organizing processes leading to observable multifractality) which dominate the formation of patterns (*Zhyrova et al., 2017*). Identification of these processes is not in the range of the experiment for the moment but emerging technologies such as MALDI – TOF imaging (*Spragginse et. al., 2011*) may bring the answer in the future.

See Fig. 2-7 in Result and Discussion section (subsection 3.3.) for example of BZ reaction stage-trajectory plot.

I also found out that segmentation of the trajectory into 7 clusters gives a separation of the trajectory into phases which reasonably resemble the segmentation which would be made by manual analysis of the reaction performed in the P. dish of 90 mm in diameter (*Zhyrova et. al., 2014; 2015; 2016; 2017*). We may conclude that the each of the BZ system oscillation state (wave formation, stage of the circular waves, spiral waves generation stage, etc.) has its own characteristic values of PIE and PIED, i.e. that it has got its own multifractal spectrum.

I employed the information entropy method on the modified BZ reaction. By changing chemical vessel geometry (circular, squared or even triangular) and area (from 200 mm in diameter to 35 mm), I achieved the changes into reaction oscillation course. Even more significant were the changes caused by the method of mixing. The vigorous mixing by magnetic stirrer resulted in fast prevalence of dense waves emanating from vessel borders in circular vessels and whole vessel oscillation accompanied by stable patterns in the square vessel.

These results have not been reported before and have important implications to the search of the B-Z reaction mechanism as well as in the less complicated chemical self-organization cases such as living cells. Namely, it is obvious that geometry of the vessel determines the pattern structure as well as the method of mixing. When the analogy to living cells is made, we propose that just the constriction of the cells by the surrounding tissue may change its chemistry. Similarly, the chemistry, and, perhaps, the duration of lifetime, may be affected by shaking. A complicated intracellular signaling is in many cases not needed. This analogy is further expanded in the article *(Štys et al., 2015)*.

Large amount of experimental material still undergoes analysis and remains unpublished. *It is made available to the scientific public at the ftp: http://160.217.215.250/protocol/head/1169.*

The experiments done in years 2009-2015 suffered many technical non-idealities. In the spring 2016 the Institute of Complex Systems in Nové Hrady installed the illumination box providing very homogeneous illumination *(see Fig. 2.4. in Materials and Methods section)* equipped by the JAI Spark SP-5000-USB rapid camera. In this set-up majority of the non-idealities of the image capture were eliminated. The summerschool students Martin Němec, Kateřina Tučková and later Pavel Souček developed the camera calibration software which enabled us to correct for most remaining problems. The main advantage of the new camera is acquisition of the 16-bit RAW image format in the rate of 30 frames/second. The image series was corrected using the calibration tool which enabled us to fully compare coloration in various parts of the image. It was found that the trajectory in the space of the first three components of the multivariate analysis is much smoother and even doublets reflecting that arose from a new wave were observed (Fig. 2.9.1.*)*. Also the separation into clusters was more logical and smooth (Fig. 2.9.2.).

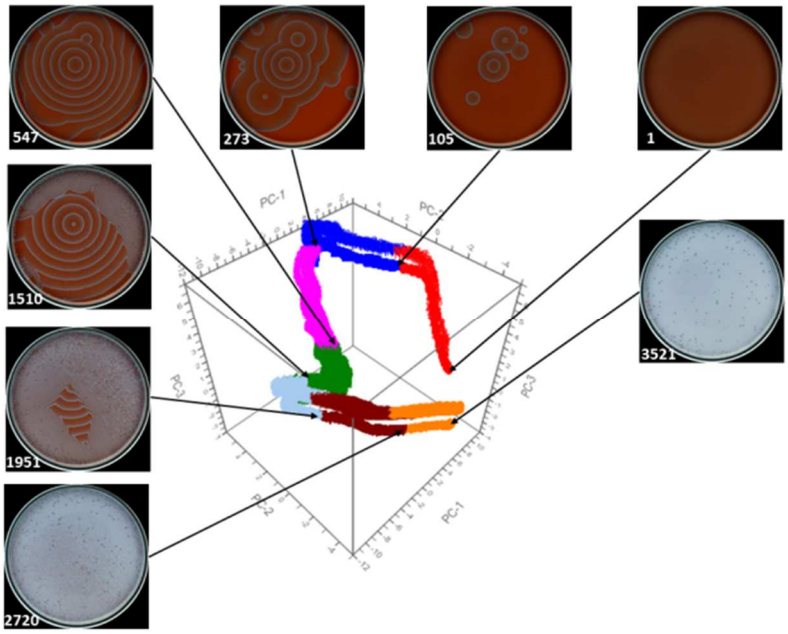

Figure 2.9.1. The BZ model by the JAI SP-5000-USB rapid. It is clear identification of the unique states of the reaction highlighted by the different colors in BZ reaction state trajectory with corresponding characteristic image of the current system state.

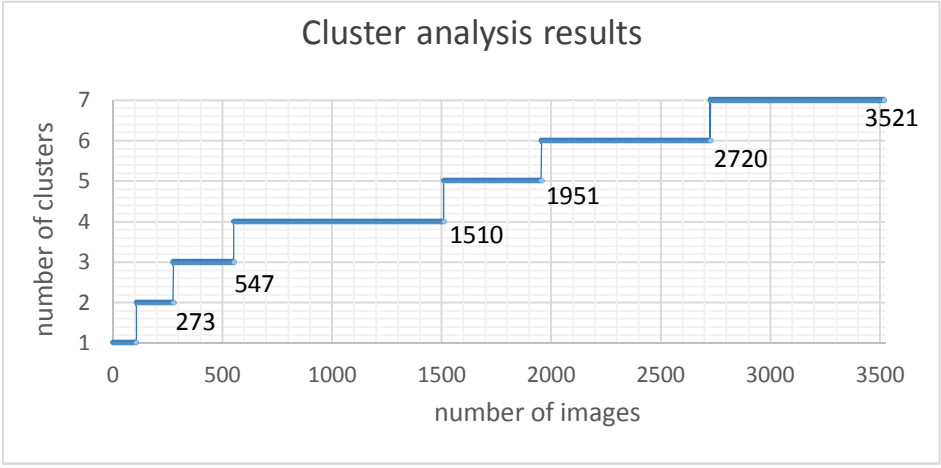

Figure 2.9.2. Cluster analysis of the BZ reaction recorded by JAI SP-5000-USB rapid camera. Since the equipment allowed to record more intermediate states in BZ wave transformation course, the obtained state separation is look more precise than for slower camera analogues (like /Nikon D90).

We may conclude that all questions about the validity of our approach were neglected by optimization of the technical set-up. We have repeated all key experiments and open them to the scientific public for discussions and analysis.

Comments on articles with candidate co-authorship not included in the thesis.

A few articles dealing with the subject of the B-Z reaction contributed by myself were not included in the thesis. These were namely the articles dealing with the model of the B-Z reaction using cellular automata *(Štys et al. 2016, Štys et al. Arxive .. Štys et al Arxive.., also part 1.4.3. of the introduction of this thesis)*. We found that starting from a small number of points and inducing asymmetry in the starting unit makes a trajectory more similar to that observed in the experiment than any of the models obtained so-far. On that basis, we introduced a simple chemical model which, however, induced a lot of controversies among the reviewers. The article is still in the review process. Thus the, in our opinion, simplest, elementary correct and assumption-free explanation of the BZ reaction pattern is still under the scrutiny of the academic society and I decided not to include it as part of the thesis.

REFERENCES

Abdi. H., Williams, L.J. (2010). Principal component analysis, *Wiley Interdisciplinary Reviews: Computational Statistics*, 2 (4): 433–459. DOI:10.1002/wics.101.

Aczel, J., Daroczy, Z. (1975). On Measures of Information and their Characterizations, Academic Press, *New York*, 115 pp. DOI: 10.1002/zamm.19780581215.

Adobe Systems Inc. (2004). Introducing the Digital Negative Specification: Information for Manufacturers, 5 pp. Available from: http://wwwimages.adobe.com/content/dam/Adobe/en/products/photoshop/pdfs/DNG_primer_manufacturers.pdf.

Adobe Systems Inc. (2012). Digital Negative (DNG) Specification, 101 pp. Available from: http://wwwimages.adobe.com/content/dam/Adobe/en/products/photoshop/pdfs/dng_spec_1.4.0.0.pdf.

Adobe Systems Inc. (2015). Adobe Camera Raw and DNG Converter version 8.7.1.311 as of March 2015. Downloads: https://www.adobe.com/support/downloads/thankyou.jsp?ftpID=5864&fileID=5905.

Barragan D., Agreda J., Parra W. (2015). Entropy production in the Oregonator model perturbed in a calorimeter with a chemical pulse, *J. Therm. Anal. Calorim*., 119: 705–713. DOI: 10.1007/s10973-014-4129-0.

CAMO Software (2011). The Unscrambler X 10.1. Official site: www.camo.com/rt/Products/Unscrambler/unscrambler.html.

Císař P., Štys D. (2011). Expertomica CellMarker (*software*). Link: http://auc.cz/software/index1.htm#Expertomica Cell Marker.

Císař, P., Náhlík, T., Rychtáriková, R., Macháček, P. (2016). Visual Exploration of Principles of Microscopic Image Intensities Formation using Image Explorer Software, *Lecture Notes in Computer Science*, 9656: 537–544. DOI: 10.1007/978-3-319-31744-1_48.

Císař, P., Urban, J., Náhlík, T., Rychtáriková, R., Štys, D. (2015). Image Info Extractor Professional b9. (*software*), Link: http://www.auc.cz/software/index5.htm.

Císař, P., Vaněk, J., Urban, J., Štys, D., (2011). Expertomica Entropy Calculator. (software), Link: http://auc.cz/software/index.html#Expertomica Entropy Calculator.

Cohen, J. (2009). Belousov-Zhabotinski Reaction [Web source]. Link: http://drjackcohen.com/BZ01.html

Ding, C., He, X. (2004). K-means Clustering via Principal Component Analysis, *Proc. of 21-th Int. Conf. Machine Learning*, pp. 225-232. DOI: 10.1145/1015330.1015408.

Eddins, S. (2011). Tips for reading a camera raw file into MATLAB [Web log post]. Retrieved from: http://blogs.mathworks.com/steve/2011/03/08/tips-for-reading-a-camera-raw-file-into-matlab/

Forgy E.W. (1965). Cluster analysis of multivariate data: efficiency versus interpretability of classifications, *Biometrics*. 21: 768–769.

Hasley, T., Jense,n M., Kadanoff, L., Procaccia, I., Shraiman, B. (1986). Fractal measures and their singularities: The characterization of strange sets, *Phys. Review A*, 33: 1141 - 1151. DOI:http://dx.doi.org/10.1103/PhysRevA.33.1141.

JAI Spark SP-5000-USB rapid camera specification. Available at website: http://www.stemmer-imaging.co.uk/media/uploads/cameras/jai/en/en-JAI-SP-5000-USB-5-Megapixel-CMOS-Global-Shutter-Camera-KJAIO50-201501.pdf

Kinoshita, S. (2013). Pattern Formations and Oscillatory Phenomena, 1st Edition, *Print book*, 280 pp.

Linsker, R. (1988). Self-organization in a perceptual network, *IEEE Computer*, 21 (3): 105–117. DOI:10.1109/2.36.

Martinec, E. (2010). The Consequences of Noise [Web log post]. Retrieved from: http://theory.uchicago.edu/~ejm/pix/20d/tests/noise/noise-p3.html.

Náhlík T., Rychtáriková R., Štys D., 2015. LIL Convertor (2012). (*software*), Available from: http://www.auc.cz/software/index5.htm.

Náhlík, T., Urban, J., Císař, P., Vaněk, J., Štys, D. (2012). Entropy based approximation to cell monolayer development, *IFMBE Proceedings*, 37(1): 563-566. DOI: 10.1007/978-3-642-23508-5_146.

Nikon Inc., 2014. Nikon D90 Specification [Web source]. Link: http://imaging.nikon.com/lineup/dslr/d90/spec.htm.

Nikon Inc. (2016). Nikon Electronic Format (NEF), Nikon Learn & Explore article. Available from: http://www.nikonusa.com/en/learn-and-explore/article/ftlzi4ri/nikon-electronic-format-nef.html.

Pearson, K. (1901). On Lines and Planes of Closest Fit to Systems of Points in Space, *Philosophical Magazine*. 2 (11): 559–572. DOI: 10.1080/14786440109462720.

Rychtáriková R., Malečková D., Urban J., Bárta A., Novotná M., Zhyrova A., Náhlík T., Štys D. (2015). Study of Human Perception with the Usage of Information Entropy Analysis of Patterns, *PURPLSOC: Pursuit of Pattern Language for Societal Challenges*: 366–384. ISBN 978-3-7375-5458-9.

Rychtáriková R., Náhlík T., Smaha R., Urban J., Štys D. Jr., Císař P., Štys D. (2015). Multifractality in imaging: application of information entropy for observation of inner dynamics inside of an unlabeled living cell in bright-field microscopy, *ISCS14: Interdisciplinary Symposium on Complex Systems*, 14: 261–267. ISBN: 978-3-319-10758-5.

Rychtáriková R., Zhyrova A., Štys D. (2017). Comparison of information-entropic clustering of image information on evolution of real dynamic systems, *HPCSE 2015 Proceedings, Lecture Notes in Computer Science,* Springer. (in press).

Rychtáriková, R. (2016). Clustering of multi-image sets using Rényi information entropy, *Lecture Notes in Computer Science*, 9656: 517–526. DOI: 10.1007/978-3-319-31744-1_46.

Rychtáriková, R., Korbel, J., Macháček, P., Císař, P., Urban, J., Soloviov, D., Štys, D. (2015). Point information gain, point information gain entropy and point information gain entropy density as measures of semantic and syntactic information of multidimensional discrete phenomena, *preprint arxiv*, 17pp. arXiv DOI:1501.02891 [physics.data-an].

Rychtáriková, R., Náhlík, T., Smaha, R., Urban, J., Štys, D. Jr., Císař, P., Štys, D. (2015). Multifractality in imaging: application of information entropy for observation of inner dynamics inside of an unlabeled living cell in bright-field microscopy, ISCS14, Springer, Switzerland, pp. 261–267. DOI: 10.1007/978-3-319-10759-2.

Shannon, C. E. (1948). A Mathematical Theory of Communication, *Bell System Technical Journal*, 27 (3): 379-423.

Sporring, J., Weickert, J. (2005). On generalized entropies and scale-space Scale-Space, *Theory in Computer Vision*, 1252: 51-64.

Spraggins, J., Caprioli, R. (2011). High-Speed MALDI-TOF Imaging Mass Spectrometry: Rapid Ion Image Acquisition and Considerations for Next Generation Instrumentation, *J. Am. Soc. Mass Spectrom. 22: 1022–1031*. DOI:10.1007/s13361-011-0121-0.

Štys, D., Jizba, P., Papáček, Š., Náhlík, T., Císař, P. (2012). On Measurement of Internal Variables of Complex Self-Organized Systems and Their Relation to Multifractal Spectra, *Lecture Notes in Computer Science, Self-Organizing Systems*, 7166: 36-47. DOI: 10.1007/978-3-642-28583-7_4.

Štys, D., Náhlík, T., Macháček, P., Rychtáriková, R., Saberioon, M., (2016). Least Information Loss (LIL) conversion of digital images and lessons learned for scientific image inspection, *Lecture Notes in Computer Science,* IWBBIO 2016, LNBI 9656: 527–536, 2016. DOI: 10.1007/978-3-319-31744-1 47.

Štys, D., Urban, J., Rychtáriková, R., Zhyrova, A., Císař, P. (2015). Measurement in Biological Systems from the Self-organization Point of View, *Springer International Publishing, Switzerland, Lecture Notes in Computer Science*, 9044: 431-443. DOI: 10.1007/978-3-319-16480-9_43.

Štys, D., Urban, J., Vaněk, J., Císař, P. (2011). Analysis of biological time-lapse microscopic experiment from the point of view of the information theory, *Micron*, 42: 360-365. DOI: 10.1016/j.micron.2010.01.012.

Štys, D., Vaněk, J., Náhlík, T., Urban, J., Císař, P. (2011). The cell monolayer trajectory from the system state point of view, *Molecular Biosystems,* 7: 2824-2833. DOI: 10.1039/c1mb05083d.

The MathWorks Inc., 2014. MATLAB 2014b, The MathWorks – MATLAB and Simulink for technical computing. Official site: http://www.mathworks.com/products/matlab.

Theiler, J. (1990). Estimating fractal dimension, *J. Opt. Soc. Am. A*, 7 (6): 1055-1073. DOI: 10.1364/JOSAA.7.001055.

Urban, J., Vaněk, J., Štys, D. (2009). Preprocessing of microscopy images via Shannon's entropy, *Proceedings of Pattern Recognition and Information Processing*, Minsk, Belarus: 183–187.

Vitabin, (2013). Spectral response of Nikon DSLRs (D90 and D300s), [Web log post]. Retrieved from: http://vitabin.blogspot.cz/2013/04/spectral-response-of-nikon-dslrs-d90.html.

Zhyrova, A., Rychtáriková, R., Náhlík, T. (2016). Effect of Spatial Constraint on the Self-Organizing Behavior of the Belousov-Zhabotinsky Reaction, IWBBIO 2016 Proceedings, *Bioinformatics and Biomedical Engineering*: 246-258. ISBN: 978-84-16478-75-0.

Zhyrova, A., Štys, D. (2014). Construction of the phenomenological model of Belousov–Zhabotinsky reaction state trajectory, *Int. J. Comp. Math.*, 91(1): 4-13. DOI: 10.1080/00207160.2013.766332.

Zhyrova, A., Štys, D., Císař, P. (2013). Information entropy approach as a method of analysing Belousov-Zhabotinsky reaction wave formation, *Chemicke Listy*, 107 (Suppl. 3): S341-S342.

azhyrova@frov.jcu.cz

State trajectory approach for the interpretation of the self-organization in the Belousov-Zhabotinsky reaction
Ph.D. Thesis Series, 2017, No. 14, 127 pp.

Printed in the Czech Republic by Typodesign
Edition of 20 copies

University of South Bohemia in České Budějovice
Faculty of Science
Branišovská 1760
CZ-37005 České Budějovice, Czech Republic

Phone: +420 387 776 201
www.prf.jcu.cz, e-mail: sekret-fpr@prf.jcu.cz